Max-Planck-Institut für Meteorologie
Max Planck Institute for Meteorology

Report No. 337

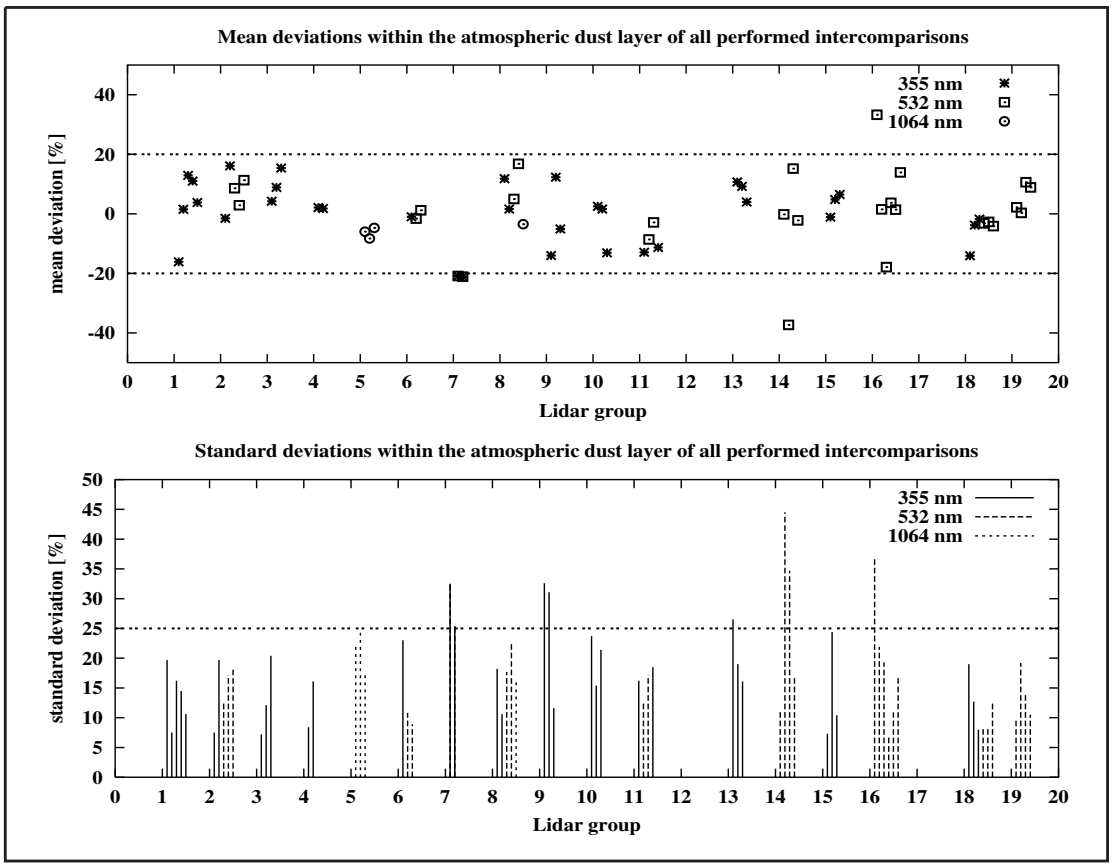

Lidar intercomparisons on algorithm and system level in the frame of EARLINET

by

Volker Matthias et al.

Hamburg, May 2002

Authors

J. Bösenberg, H. Linné, V. Matthias	Max-Planck-Institut für Meteorologie
C. Böckmann	Universität Potsdam, Institut für Mathematik, Potsdam, Germany
V. Freudenthaler, M. Wiegner	Meteorologisches Institut der Maximilians-Universität, München, Germany
G. Pappalardo, A. Amodeo	Istituto di Metodologie per l'Analisi Ambientale - C.N.R., Tito Scalo (Potenza), Italy
V. Amiridis, D. Balis, C. Zerefos	Aristotele University of Thessaloniki, Laboratory of Atmospheric Physics, Thessaloniki, Greece
A. Ansmann, I. Mattis, U. Wandinger	Institut für Troposphärenforschung, Leipzig, Germany
A. Boselli, X. Wang	Istituto Nazionale per la Fisica della Materia, Complesso Universitario di Monte S. Angelo, Napoli, Italy
A. Chaykovski, V. Shcherbakov	Institute of Physics, National Academy of Sciences of Belarus, Minsk, Belarus
G. Chourdakis, A. Papayannis	National Technical University of Athens, Lasers & Applications Group (LAG-LIDAR Group), Zografou, Greece
A. Comeron, F. Rocadenbosch	Universitat Politécnica de Catalunya, Dept. TSC, Barcelona, Spain
A. Delaval, J. Pelon, L. Sauvage	Institut Pierre Simon Laplace, Laboratoire de la Météorologie Dynamique, Palaiseau cedex, France
F. DeTomasi, R. M. Perrone	Istituto Nazionale per la Fisica della Materia, Dipartimento di Fisica - Universit di Lecce, Lecce, Italy
R. Eixmann, J. Schneider	Leibniz-Institut für Atmosphärenphysik, Kühlungsborn, Germany
M. Frioud, R. Matthey	Observatoire de Neuchâtel, Neuchâtel, Switzerland
A. Hågård, R. Persson	FOI, Swedish Defence Research Agency, Division of Sensor Technology, Linköping, Sweden
M. Iarlori, V. Rizi	Universit Degli Studi - L'Aqulia, Dipartimento di Fisica, L'Aqulia, Italy
L. Konguem	Physics Department of the University of Wales, Aberystwyth Ceredigion, United Kingdom
S. Kreipl	Fraunhofer Institut für Atmosphärische Umweltforschung, Garmisch Partenkirchen, Germany
G. Larchevêque, V. Simeonov	Ecole Polytechnique Fédérale de Lausanne, Lausanne, Switzerland
J. A. Rodriguez, D. P. Resendes	Centro de Fisica de Plasmas - I.S.T., Lisboa, Portugal
R. Schumacher	Alfred Wegener Institut für Polar- und Meeresforschung, Potsdam, Germany

Max-Planck-Institut für Meteorologie
Bundesstrasse 55
D - 20146 Hamburg
Germany

Tel.: +49-(0)40-4 11 73-0
Fax: +49-(0)40-4 11 73-298
e-mail: <name>@dkrz.de
Web: www.mpimet.mpg.de

Lidar intercomparisons on algorithm and system level in the frame of EARLINET

V. Matthias, C. Böckmann, V. Freudenthaler, G. Pappalardo, J. Bösenberg, V. Amiridis, A. Amodeo, A. Ansmann, D. Balis, A. Boselli, A. Chaykovski, G. Chourdakis, A. Comeron, A. Delaval, F. De Tomasi, R. Eixmann, M. Frioud, A. Hågård, M. Iarlori, L. Komguem, S. Kreipl, G. Larchevêque, H. Linné, R. Matthey, I. Mattis, A. Papayannis, J. Pelon, R. M. Perrone, R. Persson, D. P. Resendes, V. Rizi, F. Rocadenbosch, J. A. Rodriguez, L. Sauvage, J. Schneider, R. Schumacher, V. Shcherbakov, V. Simeonov, U. Wandinger, X. Wang, M. Wiegner, and C. Zerefos

ISSN 0937 1060

Contents

Chapter 1

Introduction

EARLINET (European Aerosol Research Lidar Network to Establish an Aerosol Climatology) is a joint project of 19 lidar groups operating aerosol lidar systems at 21 stations over a large part of Europe, plus one group focussing on mathematical problems associated with the retrieval of aerosol properties from lidar observations. The main goal of EARLINET is to establish a comprehensive statistically representative data set of the aerosol vertical distribution. For this purpose, each lidar group performs vertical aerosol soundings on a routine basis three times a week on preselected days and times. Additionally several special measurements (e.g. on Saharan dust, temporal cycles, rural and urban differences, long and medium range transport) are part of the project.
Most of the lidar systems transmit at least two wavelengths between the ultraviolet (UV) and the near infrared (NIR) spectral region. A large number of systems is also equipped with Raman channels to detect the inelastic Raman backscattering from nitrogen molecules to derive quantitative aerosol extinction profiles. The participating groups are (acronyms in brackets):

- Max-Planck-Institut für Meteorologie, Hamburg, Germany (MPI)
- Meteorologisches Institut der Ludwig-Maximilians-Universität München, Germany (MIM)
- Physics Department of the University of Wales, Aberystwyth, United Kingdom (UABER)
- National Technical University of Athens, Greece (NTUA)
- Universitat Politécnica de Catalunya, Barcelona, Spain (UPC)
- Fraunhofer Institut für Umweltforschung, Garmisch-Partenkirchen, Germany (IFU)
- Ecole Polytechnique Fédérale de Lausanne, Switzerland (EPFL)
- Institut für Atmosphärenphysik, Kühlungsborn, Germany (IAP)
- Universit Degli Studi, Dipartimento di Fisica, L'Aqulia, Italy (ULAQ)
- Istituto Nazionale per la Fisica della Materia, Lecce, Italy (INFM(L))
- Institut für Troposphärenforschung, Leipzig, Germany (IFT)
- Istituto Superior Tecnico, Lisboa, Portugal (IST)
- Försvarets Forsknings Anstalt, Linköping, Sweden (FOA)
- Institute of Physics, Academy of Sciences of Belarus, Minsk, Belarus (IPNANB)

- Istituto Nazionale per la Fisica della Materia, Napoli, Italy (INFM(N))
- Observatoire Cantonal Neuchâtel, Switzerland (OCN)
- Institute Pierre Simon Laplace, Laboratoire de la Météorologie Dynamique, Palaiseau, France (LMD)
- Istituto Nazionale per la Fisica della Materia (INFM(P)) and Istituto di Metodologie per l'Analisi Ambientale, Potenza, Italy (IMAA-CNR)
- Aristoteles University of Thessaloniki, Greece (AUTH)
- Institut für Mathematik der Universität Potsdam (UPIM)

Homogeneous and well established data quality is one of the key conditions for the combined use of data originating from different systems. Because the establishment of a joint dataset and its use in comparative studies are major objectives of EARLINET, specific attention is given to data quality assurance. The quality control workpackage of the EARLINET was split into two parts: the algorithm intercomparison and the system intercomparison. In the first part, the algorithms used for the evaluation of the lidar data have been tested using synthetic lidar data. For the system intercomparisons, simultaneous measurements of at least two lidar systems at one site have been performed and the calculated aerosol backscatter and extinction profiles have been compared. If available, also intercomparisons of the aerosol optical depth with sunphotometers have been made.

Chapter 2

Methods

The basis of any lidar signal analysis is the lidar equation which describes the receiver signal as a function of atmospheric and system parameters. The lidar equation in its simplest form is valid for quasimonochromatic emission of the laser light, instantaneous scattering, and negligible multiple scattering and coherence:

$$P(\lambda, z) = P_0(\lambda) C \frac{O(z)}{z^2} \beta(\lambda, z) \exp\left(-2 \int_0^z \alpha(\lambda, \zeta)\, d\zeta \right) \tag{2.1}$$

where $P(\lambda, z)$ is the backscattered laser power at wavelength λ from range z and $P_0(\lambda)$ is the emitted laser power at wavelength λ. C is the range independent system constant and $O(z)$ the overlap function. $\beta(\lambda, z)$ stands for the backscatter coefficient and $\alpha(\lambda, \zeta)$ for the total extinction coefficient. $C = \eta A \frac{c\tau_L}{2}$ depends on the efficiency η of the detector system, the receiving telescope area A and the pulsewidth of the laser τ_L. c is the velocity of light.

Different methods can be applied to derive aerosol vertical profiles from lidar measurements. If only elastically backscattered light at one laser wavelength is available, aerosol backscatter profiles can only be calculated when assumptions are made about the relation between aerosol extinction and backscatter coefficients (lidar ratio) and for the backscatter coefficient at a calibration range. Because in particular the lidar ratio generally is not sufficiently well known, this method is not really quantitative. However, it is widely used because single wavelength backscatter lidars are the systems that are easiest to operate, and because it is at least a by-product of any lidar measurement.

Raman measurements, that rely on pure molecular scattered signals at Raman shifted longer wavelengths, can be used to get independent information on the aerosol extinction profile. With this information and the additional elastic return signal, backscatter profiles can be derived which depend only on the calibration which in many cases can be done with good accuracy. Since one of the major goals of EARLINET is to derive aerosol vertical profiles on a quantitative basis, many groups use Raman channels to get really quantitative measurements of the aerosol extinction and backscatter.

Lidar measurements under different zenith angles (scanning lidar) are also used for the determination of aerosol extinction profiles in the atmospheric boundary layer, but only few groups use this technique. Additionally, it requires horizontal homogeneity of the aerosol distribution which is not given in many cases.

2.1 Backscatter lidar

To solve the lidar equation for one wavelength in the simplest case of no gaseous absorption, it is useful to split the backscatter and extinction in their molecular and aerosol parts and use only that part of the profile where the laser beam fully overlaps with the field of view of the receiving telescope ($O(z) = 1$):

$$P(\lambda, z) = P_0(\lambda) C \frac{\beta_{aer}(\lambda, z) + \beta_{mol}(\lambda, z)}{z^2} \exp\left(-2 \int_0^z \left(\alpha_{aer}(\lambda, \zeta) + \alpha_{mol}(\lambda, \zeta) \right) d\zeta \right) \quad (2.2)$$

with the extinction coefficient

$$\alpha(\lambda, z) = \alpha_{mol}(\lambda, z) + \alpha_{aer}(\lambda, z) = \alpha_{mol}^{abs}(\lambda, z) + \alpha_{mol}^{sca}(\lambda, z) + \alpha_{aer}^{abs}(\lambda, z) + \alpha_{aer}^{sca}(\lambda, z) \; . \quad (2.3)$$

Assuming the molecular part of this equation can be calculated using standard atmosphere conditions or an atmospheric density profile from nearby launched radiosondes, $\alpha_{aer}(z)$ and $\beta_{aer}(z)$ remain as two height dependent unknowns while one signal has been measured. This problem is usually solved by assuming a (a priori unknown) relationship between aerosol backscatter and extinction. $S_{aer}(\lambda, z) = \alpha_{aer}(\lambda, z)/\beta_{aer}(\lambda, z)$ is usually called the lidar ratio. It is wavelength and height dependent. The determination of $\beta_{aer}(z)$ for one wavelength from 2.2 requires the additional assumption of an unknown constant, representing the height independent system parameters. To solve the equation for $\beta_{aer}(z)$, usually a so called calibration or reference value $\beta_{aer}(\lambda, z_0)$ is chosen which prescribes the aerosol backscatter in a certain height z_0.
Under these assumptions, the equation for $\beta_{aer}(z)$ can be solved following Klett (1981, 1985) and Fernald et al. (1972); Fernald (1984). One gets for all heights where $z_0 > z$ (calibration in the far range)

$$\beta_{aer}(z) = -\beta_{mol}(z) + \frac{P(z) z^2 \exp\left(-2(S_{aer} - S_{mol}) \int_0^z \beta_{mol}(\zeta) d\zeta \right)}{P_0 C - 2 S_{aer} \int_0^z P(\zeta) \zeta^2 \exp[-2(S_{aer} - S_{mol}) \int_0^\zeta \beta_{mol}(z') dz'] d\zeta} \; . \quad (2.4)$$

where $S_{mol} = \alpha_{mol}(\lambda, z)/\beta_{mol}(\lambda, z) = \frac{8\pi}{3}$. Calibration in height z_0 gives the system constants $P_0(\lambda)C$. Writing $X(z) = P(z)z^2$ gives

$$\beta_{aer}(z) = -\beta_{mol}(z) + \frac{X(z) \exp\left(-2(S_{aer} - S_{mol}) \int_{z_0}^z \beta_{mol}(\zeta) d\zeta \right)}{\frac{X(z_0)}{\beta_{aer}(z_0) + \beta_{mol}(z_0)} - 2 S_{aer} \int_{z_0}^z X(\zeta) \exp[-2(S_{aer} - S_{mol}) \int_{z_0}^\zeta \beta_{mol}(z') dz'] d\zeta} \; . \quad (2.5)$$

This equation can then be solved iteratively down- or upward from z_0. Molecular absorption is neglected here. Molecular scattering can be calculated from

$$\alpha_{mol}^{sca}(z, \lambda; p, T) = \frac{8\pi^3 (m_{air}^2 - 1)^2}{3\lambda^4 N_S^2} \frac{6 + 3\gamma}{6 - 7\gamma} N_S \frac{T_0}{p_0} \frac{p(z)}{T(z)} \quad (2.6)$$

with the refractive index of the air m_{air}, the depolarization factor γ (γ is 0.0301, 0.0284 and 0.0273 for 350, 550 and 1000 nm, respectively), and the molecular number density N_s= 2.547·10^{19}cm^{-3} for standard atmospheric conditions at ground level (p_0=1013.25 hPa, T_0=15°C, 0.03% CO_2). Profiles of temperature $T(z)$ and pressure $p(z)$ are taken from actual radiosonde measurements or from a

standard atmosphere with actual ground values of temperature and pressure (Edlen, 1953; Elterman, 1968; Bodhaine et al., 1999). We emphasize once again that two unknown quantities, the particle lidar ratio and the particle backscatter coefficient $\beta_{aer}(z_0)$ at a suitable reference height z_0, have to be estimated in the determination of the particle backscatter-coefficient profile after Eq. (2.5). The numerical application of Eq. (2.5) has been discussed in the literature as Fernald or Klett algorithm for more than 20 years. Contributions to the problem are also given by Sasano et al. (1985), Kovalev and Moosmüller (1994), Matsumoto and Takeuchi (1994) and Bösenberg et al. (1997). They are usually considered in the algorithms.

2.2 Raman lidar

Raman scattering is an inelastic pure molecular scattering with a shift of the emitted laser wavelength λ_0 to the scattered laser wavelength λ_R which depends only on the scattering molecule. Detecting the Raman scattering of a gas with known atmospheric density like nitrogen or oxygen, the backscatter coefficient in the Raman lidar equation is known and only the aerosol extinction and its wavelength dependence remain as unknowns:

$$P(\lambda_0, \lambda_R, z) = P_0(\lambda_0) C_R \cdot \frac{\beta_R(\lambda_0, z)}{z^2} \exp\left(- \int_0^z \big(\alpha(\lambda_0, \zeta) + \alpha(\lambda_R, \zeta)\big) d\zeta \right), \tag{2.7}$$

where $\beta_R(\lambda_0, z) = N(z)\sigma_R(\lambda_0)$ is the Raman backscatter coefficient, with $N(z)$ the atmospheric density of the Raman scatterer and $\sigma_R(\lambda_0)$ the Raman backscatter cross section. C_R contains all range independent system constants of the Raman detection channel. Writing the differential form of this equation

$$\frac{d}{dz} \ln\left(P(\lambda_0, \lambda_R, z) \cdot z^2 \right) = \frac{d}{dz} \ln \beta_R(\lambda_0, z) - \alpha(\lambda_0, z) - \alpha(\lambda_R, z) \tag{2.8}$$

and assuming an Ångstrøm law for the wavelength dependence of the aerosol extinction $\alpha_{aer} \propto \lambda^{-k}$, the Raman lidar equation can be solved for the aerosol extinction at the emitted laser wavelength:

$$\alpha_{aer,z}(\lambda_0) = \frac{1}{1 + \left(\frac{\lambda_0}{\lambda_R}\right)^k} \frac{d}{dz} \ln\left(\frac{N(z)}{P_R(z) z^2} \right) - \alpha_{mol}(\lambda_0, z) - \alpha_{mol}(\lambda_R, z) \tag{2.9}$$

Here $d/dz\, \sigma_R(\lambda_0) = 0$ has been used. Again the molecular extinction is well known from Rayleigh scattering coefficients and standard atmospheric density profiles.
In the analysis of Raman lidar measurements of aerosol extinction it is necessary to calculate the derivative of the logarithm of the ratio of the atmospheric number density and the range corrected lidar-received power. The application of this formula is not straightforward since both aerosol extinction coefficient and its error can be miscalculated if data acquisition and analysis are not correctly accomplished. For this reason, great care is necessary in handling data in order to retrieve the extinction coefficient profile starting from Raman signals. In particular, it is important to consider the sources of uncertainties in the estimate of the aerosol extinction coefficient that are listed in the following:

(a) the statistical error due to signal detection (Bösenberg and Theopold, 1988);

(b) the systematic error associated with the estimate of temperature and pressure profiles (Ansmann et al., 1992);

(c) the systematic error associated with the estimate of the ozone profiles in the UV (Ansmann et al., 1992);

(d) the systematic error associated with the wavelength dependence parameter k (Ansmann et al., 1992; Whiteman, 1999);

(e) the systematic error associated with the multiple scattering (Ansmann et al., 1992; Wandinger, 1998; Whiteman, 1999);

(f) the error introduced by operational procedures such as signal averaging during varying atmospheric extinction and scattering conditions (Ansmann et al., 1992; Bösenberg, 1998).

With the detection of the Raman scattered light, independent aerosol extinction profiles can be determined. This information can be used to derive also the aerosol backscatter without assuming a lidar ratio. More than that, the lidar ratio can be calculated if an accurate calibration of the backscatter profile can be made in a height region with negligible aerosol backscatter. The backscatter profile is either calculated by forming the ratio of the elastic and the Raman backscattered signals in height z and calibration height z_0, as Ansmann et al. (1992) propose, or by directly solving eq. (2.2) for the aerosol backscatter when the aerosol extinction is known. Again the system constants are eliminated by chosing a calibration value $\beta_{aer}(z_0)$ for the aerosol backscatter in height z_0.

Chapter 3

Algorithm intercomparisons

Besides the system intercomparison (see Chapter 4), a basic exercise to assure the quality of network measurements is the comparison of the algorithms used to calculate the optical parameters from lidar signals. The importance of such comparisons was shown and is proven by similar publications of other networks (Bösenberg et al., 2001; Godin et al., 1999; Steinbrecht et al., 1996). Therefore, intercomparisons of algorithms applied by different lidar groups for retrieving the particle backscatter-coefficient profile of a backscatter lidar and the particle extinction-coefficient profile of a Raman lidar were organized as part of the European Lidar Network (EARLINET).

3.1 Algorithm intercomparison of the backscatter lidar

edited by C. Böckmann (UP-IM)

with contributions from U. Wandinger (IFT), A. Ansmann (IFT), J. Bösenberg (MPI), V. Amiridis (AUTH), A. Boselli (INFM(N)), A. Delaval (LMD), F. De Tomasi (INFM(L)), M. Frioud (OCN), M. Iarlori (ULAQ), L. Komguem (UABER), S. Kreipl (IFU), G. Larchevêque (EPFL), V. Matthias (MPI), A. Papayannis (NTUA), R. Persson (FOA), F. Rocadenbosch (UPC), J. Schneider (IAP), V. Shcherbakov (IPNANB), and M. Wiegner (MIM)

The determination of the particle backscatter coefficient from a single elastic backscatter signal was investigated in the first part of the algorithm intercomparison. All participating groups processed three sets of synthetic lidar data using their individual algorithms. Some specific details of the groups' individual algorithms are presented in Table 3.1. Finally the results of the intercomparison study are discussed.

3.1.1 Data simulation and evaluation procedure

Synthetic lidar signals were used to test the numerical correctness and accuracy of the algorithms as well as the experience of the groups and the limits of the method itself. Three examples with different degree of difficulty were calculated with the IfT lidar simulation model.[1] This software permits to simulate and to evaluate elastically and inelastically backscattered lidar signals at arbitrary wavelengths in dependence of a variety of system parameters for a variable model atmosphere with

[1] The simulations were performed by a person who was not involved in the evaluation of these data for the intercomparison study and the input data were not known to other persons.

(a)

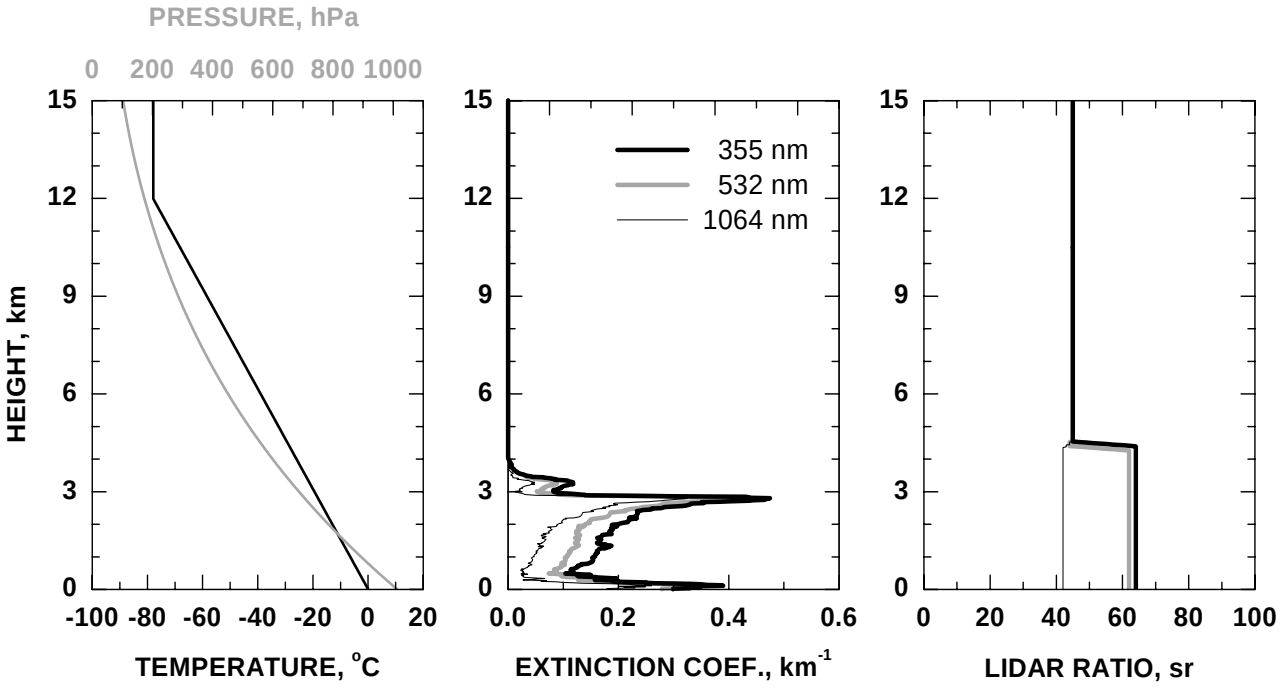

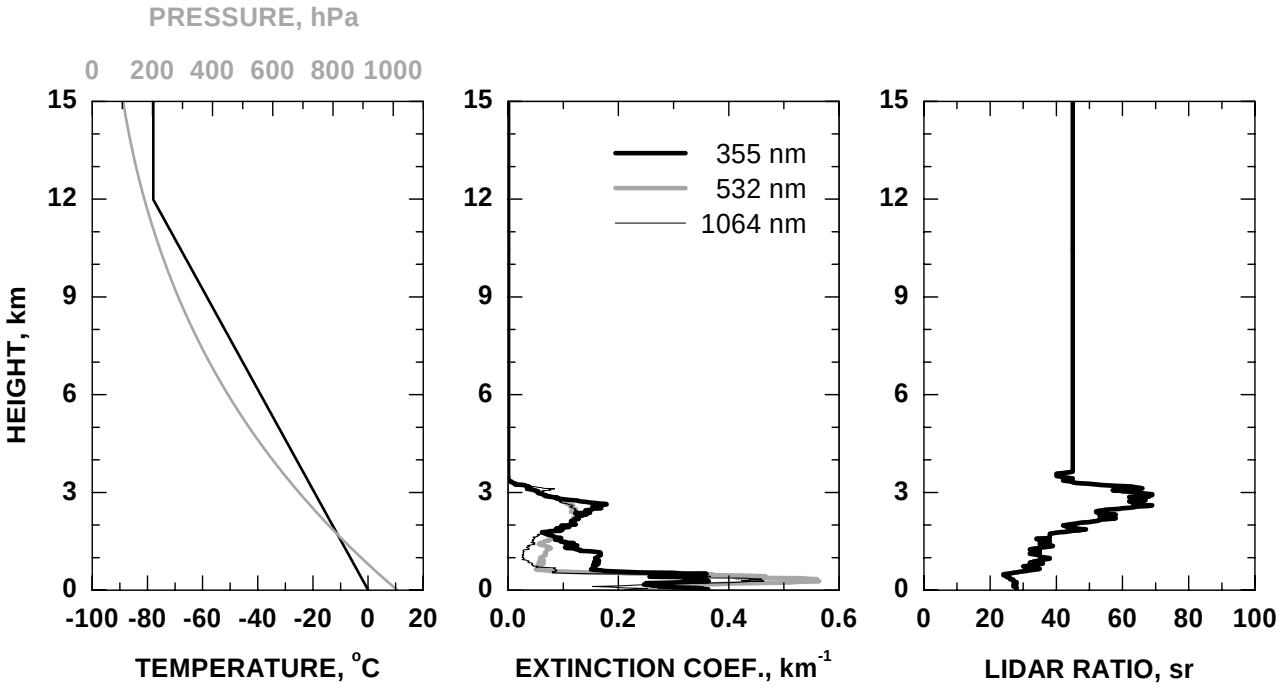

(b)

Figure 3.1: Input data for (a) simulation case 2 and (b) simulation case 3.

arbitrary aerosol and cloud layers. Sky background, background noise, and signal noise are considered as well. Atmospheric input parameters are profiles of temperature and pressure to calculate Rayleigh scattering and profiles of extinction coefficients and lidar ratios for the simulation of aerosol and cloud layers.

For the algorithm intercomparison three different data sets of elastic backscatter signals at wavelengths of 355, 532, and 1064 nm were simulated. A US standard atmosphere (United States Committee on Extension to the Standard Atmosphere, 1976) with a ground pressure of 1013 hPa and a ground temperature of 0 °C, a tropopause height of 12.0 km, and isothermal conditions above was assumed. The signal profiles were simulated without signal noise. An incomplete overlap of laser beam and receiver field of view below 250 m was introduced. Typical system parameters (laser power, telescope diameter, etc.) were used for the calculations. However, they are not of importance for the algorithm intercomparison.

In all cases, only boundary-layer aerosols in heights below 4.5 km were simulated. Minor particle scattering in the free troposphere and the stratosphere was introduced and no clouds were considered. The three simulation cases represent different atmospheric conditions with increasing degree of difficulty in data evaluation:

Case 1: The first case did not represent realistic atmospheric conditions. The extinction coefficient was independent of wavelength and changed stepwise from $3 \cdot 10^{-4}$ m^{-1} below 1500 m to $3.5 \cdot 10^{-4}$ m^{-1} between 1500 and 2000 m and $4 \cdot 10^{-4}$ m^{-1} between 2000 and 2440 m, and decreased to values below 10^{-6} m^{-1} above. The lidar ratio had a constant value of 50 sr for all heights and all wavelengths.

Case 2: In the second case, significant aerosol load up to 4000 m was simulated, see Fig. (3.1) (a). A more realistic, height-dependent extinction coefficient was assumed. In addition, the extinction coefficient changed with wavelength, with highest values for the shortest wavelength and lowest values for the longest wavelength. The lidar ratio was height-independent in the aerosol layer, but took different values of 64 sr for 355 nm, 62 sr for 532 nm, and 42 sr for 1064 nm. Above 4500 m the lidar ratio was 45 sr for all wavelengths.

Case 3: In case 3, significant aerosol load up to 3300 m was simulated, see Fig. (3.1) (b). Realistic, height-dependent extinction coefficients and lidar ratios were introduced. The extinction coefficient varied quite differently with wavelength in different heights. The lidar ratio took values between 24 and 69 sr, but did not vary with wavelength. Above 3600 m the lidar ratio was set to 45 sr for all wavelengths.

For the first case (not shown here) the input profiles of extinction coefficient and lidar ratio were provided to the participants to allow an exercise with known solutions. Cases 2 and 3 were used for the intercomparison. The results are discussed here. The procedure of the algorithm intercomparison was as follows.

Stage 1: The simulated signals were distributed to all groups without any information on the input parameters, except the used standard atmosphere. Each group calculated particle backscatter coefficient profiles using their own algorithm.

Stage 2: The prescribed lidar ratio profile was provided to all groups. Evaluation was repeated.

Stage 3: The reference value at calibration height was also provided. Evaluation was repeated.

Table 3.1: Participating groups and capabilities of their processing algorithms: height dependent lidar ratio, both integration directions from the calibration point and possibility to include radiosonde data.

	Lidar group	lidar ratio	integration direction	radio-sonde
A1	Lidar Group, École Polytechnique Fédérale de Lausanne, Switzerland	yes	yes	yes
A2	Observatory of Neuchâtel, Switzerland	yes	yes	yes
A3	Institut für Troposphärenforschung, Leipzig, Germany	yes	yes	yes
A4	Physics Department, National Technical University of Athens, Greece	yes	no	no
A5	Max-Planck-Institut für Meteorologie, Hamburg, Germany	yes	yes	yes
A6	Leibniz-Institut Kühlungsborn der Universität Rostock, Germany	yes	yes	yes
A7	Department of Physics, Università degli Studi, L'Aquila, Italy	yes	yes	yes
A8	Institute of Physics, National Academy of Sciences, Belarus	yes	yes	yes
A9	Laboratory of Atmospheric Physics, Aristotelian University of Thessaloniki, Greece	yes	yes	yes
A10	Meteorologisches Institut der Universität München, Germany	yes	yes	yes
A11	I.N.F.M. Napoli and Dipartimento di Scienze Fisiche Università di Napoli, Italy	yes	yes	yes
A12	Dipartimento di Fisica and I.N.F.M. Unità di Lecce, Italy	yes	yes	yes
A13	Fraunhofer-Institut für Atmosphärische Umweltforschung, Garmisch-Partenkirchen, Germany	yes	yes	no
A14	Universitat Politecnica de Catalunya, Barcelona, Spain	yes	no	no
A15	Institute Pierre Simone Laplace, Paris-Jussieu, France	yes	yes	yes
A16	Physics Department, University of Wales, Aberystwyth, United Kingdom	yes	yes	yes
A17	Istituto Nazionale per la Fisica della Materia and Istituto di Metodologie per l'Analisi Ambientale, Potenza, Italy	yes	yes	yes
A18	Försvarets Forskninganstalt, Linköping, Sweden	yes	yes	yes

For each stage the results were collected by UPIM because this group is not involved in experimental lidar work and acted as the referee. The first stage was the most difficult and most realistic one, because lidar-ratio profiles and reference values were unknown. Therefore, not only the correctness and accuracy of the algorithms was proven but also the dependence of the solution on estimates of the lidar ratio and the reference value. In the third and final stage all parameters were known. So the numerical correctness and stability of the algorithms was definitely tested. The results of each group from each step were compared with the input data in order to determine the systematic errors. They are discussed at the end of the next subsection.

3.1.2 Intercomparison results

The numerical schemes differ from each other only in some details. Before eq. (2.5) can be applied to measured lidar signals, the signals are averaged over the time interval of interest, corrected for background, and usually spatially averaged (smoothed). For the synthetic data used here, this procedure was not necessary. In Table 3.1, three details of the individual algorithms concerning the following questions are given.

Table 3.2: Mean errors of cases 2 and 3 for the wavelength 355 nm in stage 3

Stage 3: 355 nm				
	Case 2		Case 3	
Group	mean relative error [%] 0.3075-3.4875km	mean absolute error [1/(km*sr)] 3.5025-15.0675km	mean relative error [%] 0.3075-3.0075km	mean absolute error [1/(km*sr)] 3.0225-15.0675km
A1	1.54±0.91	1.72e-5±1.28e-5	1.01±0.85	1.85e-5±1.41e-5
A2	0.46±0.40	1.43e-7±5.42e-7	0.63±0.29	2.38e-7±1.24e-6
A3	0.45±0.38	3.94e-7±5.42e-7	0.60±0.30	4.94e-7±1.14e-6
A4	3.73±5.65	8.76e-7±2.56e-6	1.39±1.45	1.92e-6±4.73e-6
A5	1.84±2.14	3.91e-6±2.59e-6	1.51±0.79	4.14e-6±3.15e-6
A6	0.46±0.40	2.59e-7±5.20e-7	0.63±0.28	3.43e-7±1.22e-6
A7	0.46±0.40	1.41e-7±5.36e-7	0.63±0.28	2.34e-7±1.22e-6
A8	0.45±0.41	4.27e-7±6.52e-7	0.68±0.47	5.41e-7±1.34e-6
A9	5.57±3.25	2.18e-5±4.62e-5	5.34±3.86	2.89e-5±5.67e-5
A10	2.45±1.56	2.79e-5±2.08e-5	1.58±1.32	2.99e-5±2.26e-5
A11/A17	2.25±1.21	2.28e-5±1.71e-5	1.86±1.21	2.44e-5±1.86e-5
A12	0.45±0.40	2.95e-7±5.76e-7	0.63±0.28	9.31e-7±2.17e-6
A13	4.82±1.85	4.41e-5±1.71e-5	3.76±2.14	3.15e-5±2.58e-5
A14	0.90±0.80	6.73e-5±3.76e-5	0.96±0.72	6.53e-5±3.81e-5
A15	0.48±0.42	2.32e-6±1.42e-6	12.88±8.27	7.44e-6±1.40e-5
A16	1.76±1.05	5.01e-6±4.27e-6	0.72±0.47	5.07e-6±3.81e-6
A18	3.66±0.62	6.65e-6±4.85e-6	3.11±0.72	6.46e-6±5.64e-6
mean values	1.87	1.30e-5	2.23	1.33e-5

- Is the determination of the backscatter-coefficient profile with height-dependent lidar-ratio S_{aer} possible?
- Is the integration in Eq. (2.5) in forward and backward direction possible?
- Is it possible to use temperature and pressure values from radiosonde ascent?

Tables 3.2 to 3.4 and Fig. 3.2 to 3.5 summarize the results of the algorithm intercomparison.
The results for case 2 are shown in detail in the six parts of Fig. 3.2 and 3.3 as well as in columns 2 and 3 of Tables 3.2-3.4. In the first stage, the mean deviations from the correct solution (see Fig. 3.2 first column) were between 0% and 120%. Especially for the wavelength 355 nm the deviations are very large whereas with increasing wavelength the mean errors become smaller. The mean errors over all groups for the wavelengths of 355, 532, and 1064 nm are about 65%, 30%, and 15%, respectively. In the second stage with known lidar-ratio profile but still unknown reference value the mean deviations from the correct solution (see Fig. 3.2 second column) become visibly smaller and were approximately between 0%, and 30% only. The mean errors over all groups for the wavelengths of 355, 532, and 1064 nm are about 7%, 5%, and 8%, respectively.
The final stage is shown in Fig. 3.3 in more detail including relative error profiles. First, with increasing knowledge on the input parameters (stages 2 and 3), the errors decreased to a few percent, in almost all individual algorithms well below 5% for all wavelengths in the range between 0.3075 and 3.4875 km (see Fig. 3.3 and Tables 3.2-3.4). The mean error over all groups stays well below 2% for all wavelengths. Second, in the range from 3.5025 to 15.0675 km the mean absolute error over all groups is smaller than $1 \cdot 10^{-5}(\mathrm{km} \cdot \mathrm{sr})^{-1}$. Both facts indicate that all algorithms work well and can generally reproduce the simulated profiles of case 2 if all input parameters are known.

Table 3.3: Mean errors of both cases for the wavelenth 532 nm in stage 3

Stage 3: 532 nm				
	Case 2		Case 3	
Group	mean relative error [%] 0.3075-3.4875km	mean absolute error [1/(km*sr)] 3.5025-15.0675km	mean relative error [%] 0.3075-3.0075km	mean absolute error [1/(km*sr)] 3.0225-15.0675km
A1	0.91±0.72	9.68e-7±1.00e-6	1.36±0.39	1.24e-6±1.80e-6
A2	0.71±0.46	1.16e-7±6.13e-7	0.97±0.23	2.12e-7±1.33e-6
A3	0.62±0.47	2.24e-7±4.92e-7	0.88±0.28	3.32e-7±1.14e-6
A4	0.71±0.48	1.80e-7±5.69e-7	1.17±3.35	2.97e-7±1.28e-6
A5	2.34±1.07	9.97e-7±1.39e-6	2.24±0.66	1.29e-6±2.96e-6
A6	0.72±0.46	1.75e-7±6.20e-7	0.98±0.24	2.74e-7±1.36e-6
A7	0.71±0.46	1.13e-7±6.12e-7	0.97±0.23	2.11e-7±1.34e-6
A8	0.68±0.43	1.23e-7±5.92e-7	0.94±0.23	2.16e-7±1.28e-6
A9	2.90±1.59	5.54e-6±1.22e-5	2.88±3.41	7.31e-6±5.30e-6
A10	0.16±0.14	4.90e-7±4.61e-7	0.19±0.08	5.34e-7±5.04e-7
A11/A17	1.36±0.82	3.98e-7±1.24e-6	1.84±0.44	5.95e-7±2.57e-6
A12	0.70±0.44	1.27e-7±6.04e-7	0.95±0.23	2.14e-7±1.31e-6
A13	5.22±2.73	1.92e-5±1.15e-5	6.39±1.73	1.45e-5±1.65e-5
A14	4.54±2.78	3.44e-5±1.53e-5	5.45±1.78	3.49e-5±1.67e-5
A15	0.81±0.52	2.28e-6±1.91e-6	8.18±2.88	4.36e-6±7.19e-6
A16	0.63±0.46	1.98e-7±7.77e-7	0.90±0.25	3.57e-7±1.70e-6
A18	-	-	-	-
mean values	1.48	4.10e-6	2.27	4.18e-6

Finally, it has to be stated that the retrieval of the backscatter coefficient profile in the range between 0 and 250 m is impossible for these simulations, because an incomplete overlap between the laser beam and the receiver field of view was included in the model. The overlap function was not known by the groups, hence, it could not be corrected for. The simulation of the incomplete overlap should remind the groups that one has to take great care in the near range (100 to several 100 m), where the overlap function is generally not known.

The results for case 3, which is a more realistic one with a height dependent lidar ratio but still without statistical noise and without clouds, are shown in Fig. 3.4, 3.5 and at Tables 3.2-3.4 in columns 4 and 5. For the stages 1 and 2 the mean errors are more or less in the same range as for case 2. In detail, the mean errors over all groups for the first stage for the wavelengths of 355, 532, and 1064 nm are approximately 40%, 20%, and 17%, respectively. Moreover, for stage 2 the respective errors are about 10%, 8%, and 7%. For the third stage, the errors are somewhat larger than for case 2, which is mainly caused by the height-dependent lidar ratio. In the range between 0.3075 and 3.0075 km (see Fig. 3.5 and Tables 3.2-3.4) the mean error over all groups stays well below 3% for all wavelengths. Only the group A15 has still some problems, especially for the wavelength 355 nm, which have to be improved in the future. In the range from 3.0225 to 15.0675 km the mean absolute error over all groups is smaller than $1 \cdot 10^{-5}(km \cdot sr)^{-1}$. Finally, in the range between 0 and 250 m the retrieval of the backscatter coefficient again is impossible because of the unknown overlap function.

The algorithm intercomparison shows that in general the data evaluation schemes of the different groups work well. Differences in the solutions can mainly be attributed to differences in the estimation of input parameters. If the input parameters are known, remaining errors are in the order of a few percent. The unknown height-dependent lidar ratio had the largest influence on the solutions, which

Table 3.4: Mean errors of both cases for the wavelength 1064 nm in stage 3

Stage 3: 1064 nm				
	Case 2		Case 3	
Group	mean relative error [%] 0.3075-3.4875km	mean absolute error [1/(km*sr)] 3.5025-15.0675km	mean relative error [%] 0.3075-3.0075km	mean absolute error [1/(km*sr)] 3.0225-15.0675km
A1	2.88±0.60	1.18e-7±7.29e-7	3.05±0.39	7.02e-7±5.10e-6
A2	0.21±0.04	8.89e-9±5.31e-8	0.22±0.03	5.29e-8±3.75e-7
A3	0.15±0.11	1.54e-8±4.81e-8	0.17±0.12	4.95e-8±3.99e-7
A4	-	-	-	-
A5	1.94±0.85	1.01e-7±3.29e-7	1.57±0.55	3.57e-7±2.16e-6
A6	0.22±0.05	1.36e-8±5.59e-8	0.23±0.03	5.80e-8±3.86e-7
A7	0.22±0.04	8.89e-9±5.35e-8	0.22±0.03	5.13e-8±3.72e-7
A8	0.19±0.04	9.86e-9±4.63e-8	0.21±0.04	4.95e-8±3.51e-7
A9	-	-	-	-
A10	1.29±0.27	5.25e-8±3.19e-7	1.38±0.15	3.08e-7±2.23e-6
A11/A17	3.44±0.74	1.37e-7±8.64e-7	3.56±0.50	8.31e-7±6.03e-6
A12	0.23±0.05	9.25e-9±5.61e-8	0.23±0.03	5.42e-8±3.93e-7
A13	0.66±0.27	1.19e-6±7.53e-7	0.83±1.72	1.14e-6±3.33e-6
A14	6.42±1.48	3.05e-6±2.40e-6	6.25±0.87	4.21e-6±1.05e-5
A15	1.31±0.28	1.51e-6±9.12e-7	8.33±5.22	4.35e-6±6.35e-6
A16	0.19±0.04	1.34e-8±6.28e-8	0.19±0.03	7.77e-8±4.28e-7
A18	-	-	-	-
mean values	1.38	4.46e-7	1.89	8.78e-7

demonstrates the need for independent measurements of the particle extinction coefficient, e.g., with the Raman method. To overcome this problem, independent measurements of the particle extinction coefficient with the Raman method are or will be performed at most of the network stations.

The unknown reference value was of minor importance for the examples presented here, because height regions with dominating Rayleigh scattering were present in all cases. It should be mentioned, however, that this is not necessarily the case under realistic atmospheric conditions. Especially at 1064 nm, particle scattering often dominates the signals in the entire measurement range, which may cause additional errors that were not discussed here.

Some additional remarks will be given now. Firstly, during the algorithm intercomparison some groups developed or improved their algorithms so that a few groups are not present in stages 1 and 2 (see Fig. 3.2) 3.4. Secondly, the groups A4 and A9 use only at the wavelengths 355 nm and 532 nm at their lidar stations and group A18 emits only at 355 nm. Therefore they did not perform evaluations at 1064 nm and 532 nm, respectively. Thirdly, the groups A17 and A11 used the same algorithm. Finally, group A19 did not participate in the algorithm intercomparison. They are still working on the development of a suitable algorithm. Their algorithm will be tested against the simulated data very soon.

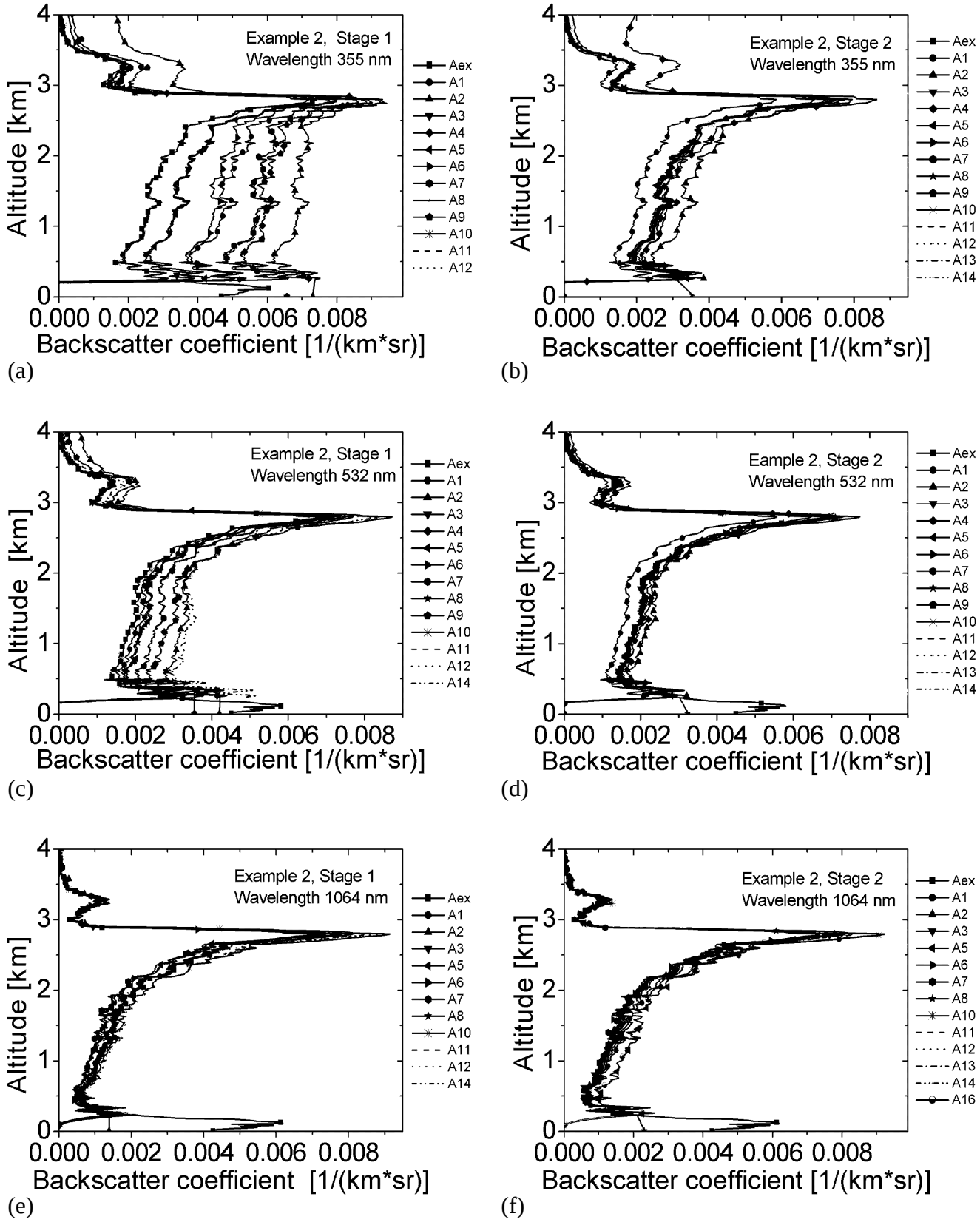

Figure 3.2: Retrieved particle backscatter-coefficient profiles at all three wavelengths in comparison to the simulation input profiles of case 2 concerning the first stage (a),(c),(e), and the second one (b),(d),(f).

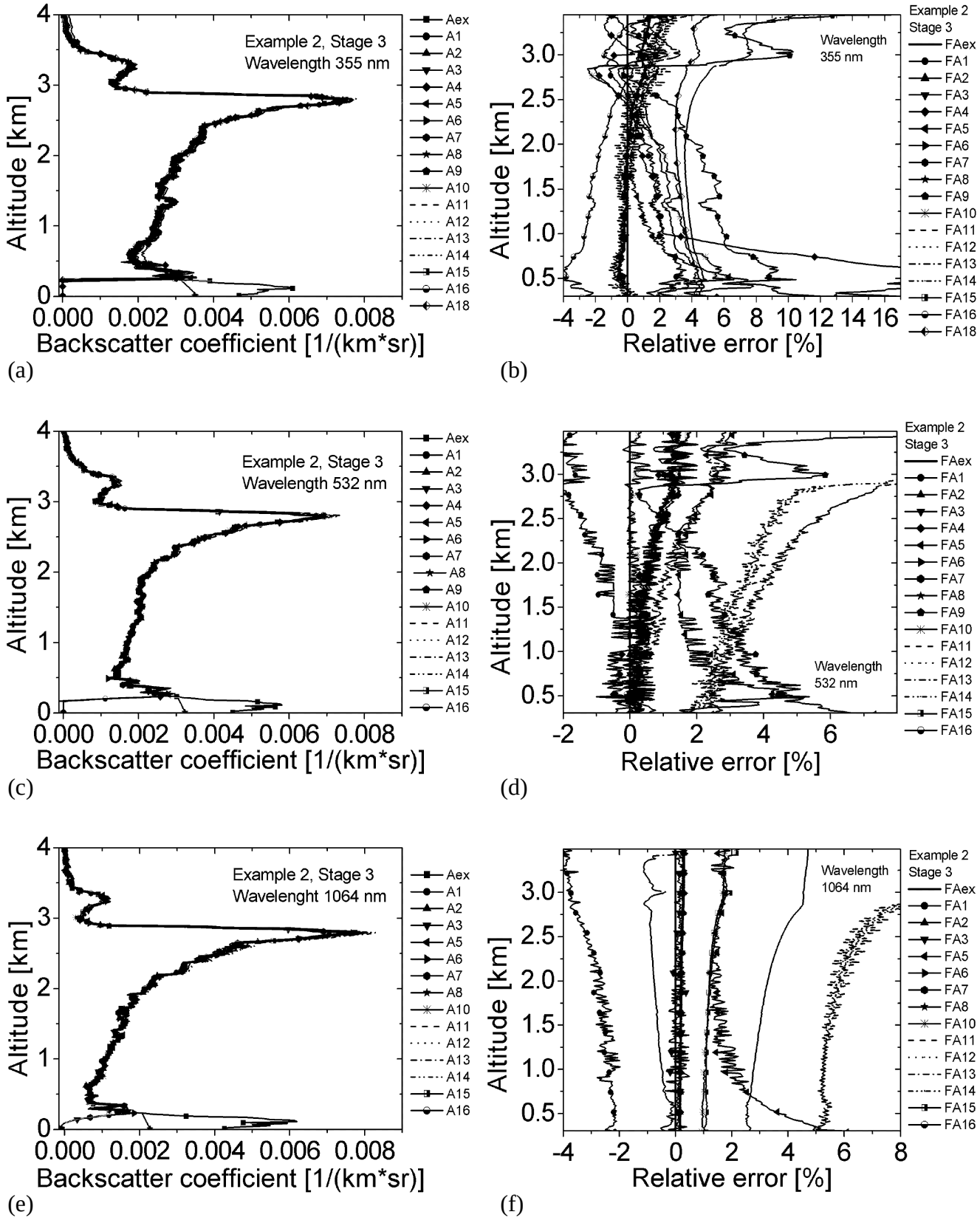

Figure 3.3: Retrieved particle backscatter-coefficient profiles at all three wavelengths in comparison to the simulation input profiles (a),(c),(e), and respective relative errors (b),(d),(f) of case 2 for the third stage.

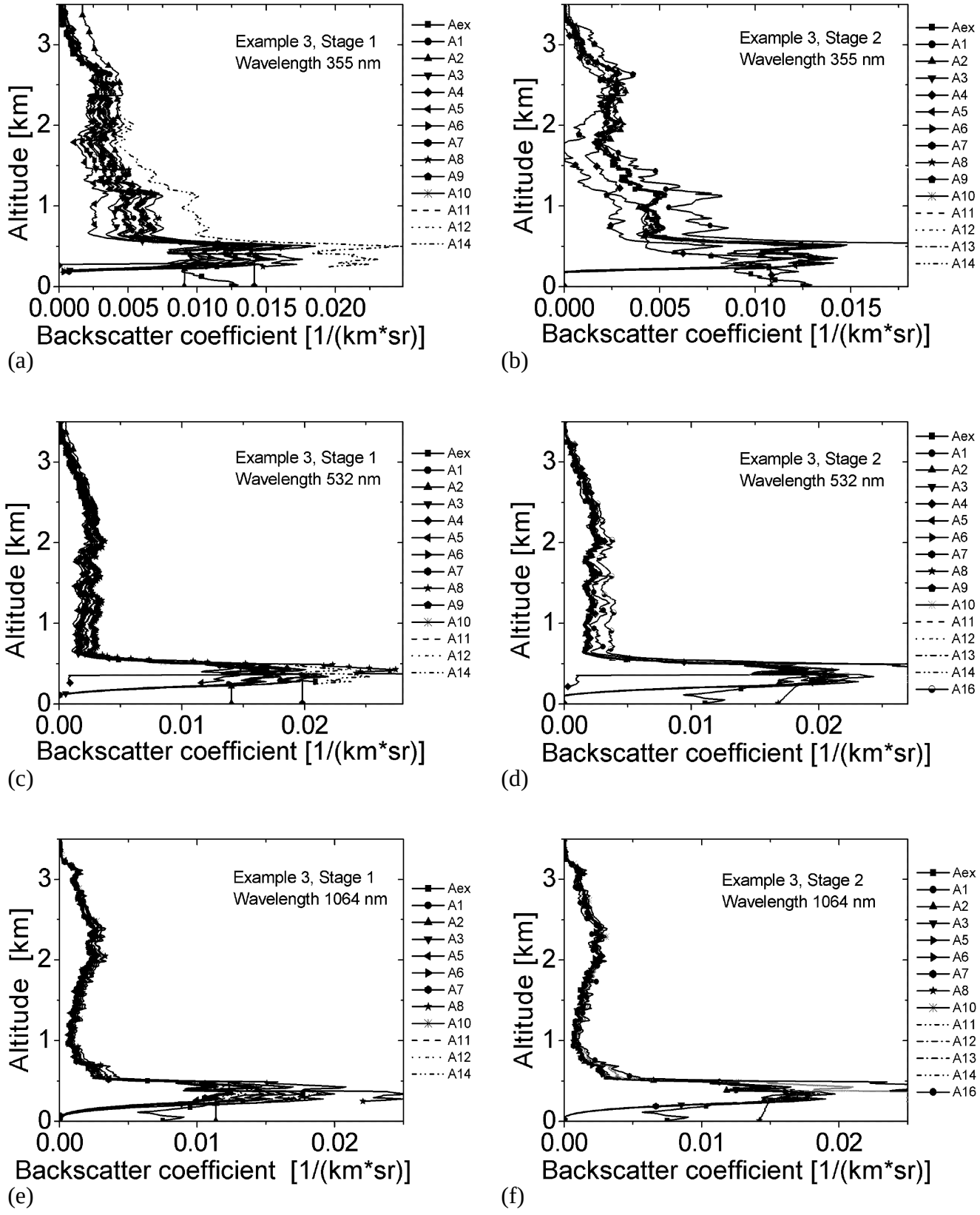

Figure 3.4: Retrieved particle backscatter-coefficient profiles at all three wavelengths in comparison to the simulation input profiles of case 3 concerning the first stage (a),(c),(e), and the second one (b),(d),(f).

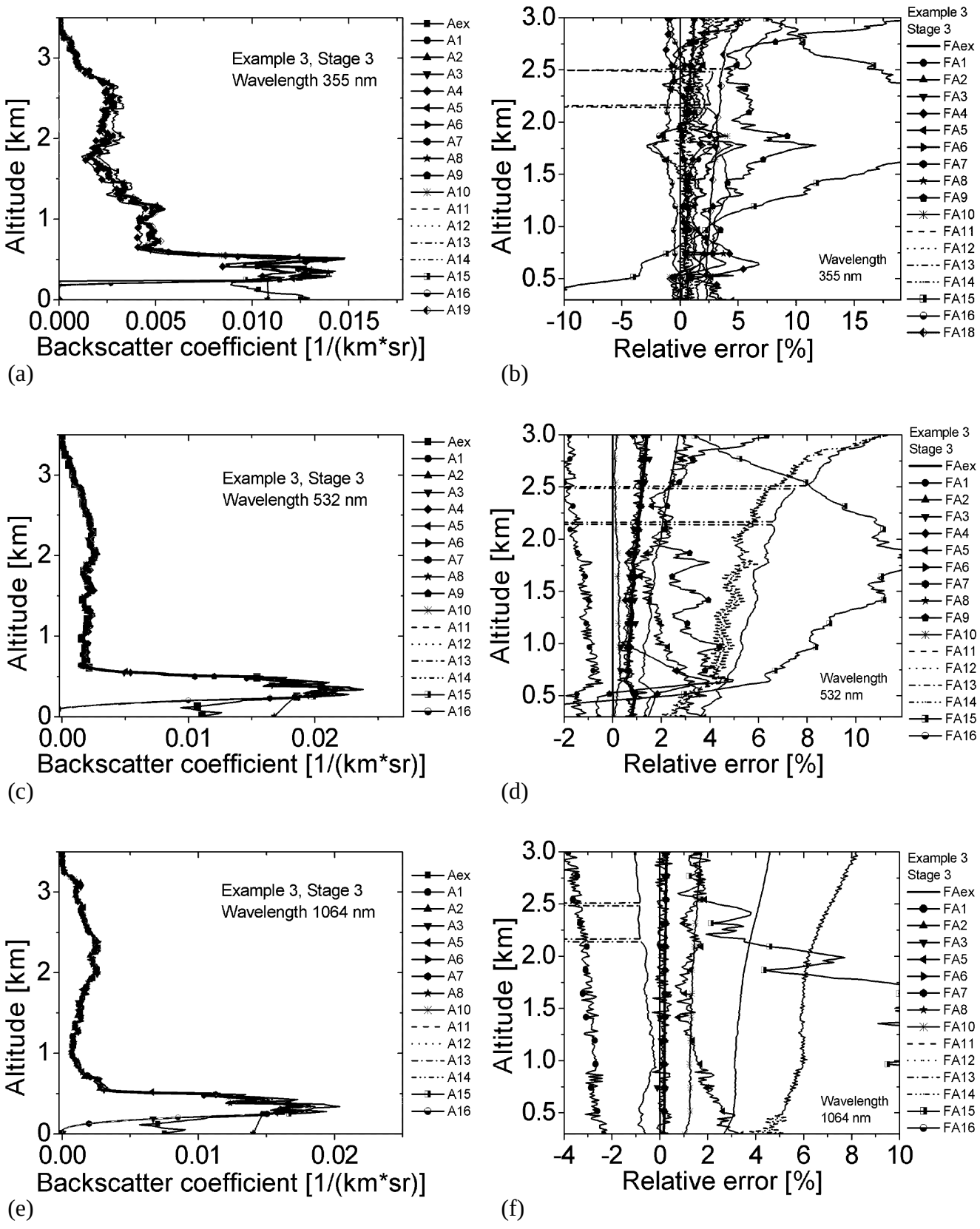

Figure 3.5: Retrieved particle backscatter-coefficient profiles at all three wavelengths in comparison to the simulation input profiles (a),(c),(e), and respective relative errors (b),(d),(f) of case 3 for the third stage.

3.2 Algorithm intercomparison of the Raman lidar

edited by G. Pappalardo (IMAA-CNR)

with contributions from U. Wandinger (IFT), M. Alpers (IAP), V. Amiridis (AUTH), F. De Tomasi (INFM(L)), M. Frioud (OCN), M. Iarlori (ULAQ), L. Komguem (UABER), G. Larchevêque (EPFL), V. Matthias (MPI), A. Papayannis (NTUA), R. Schumacher (AWI) [2] , and X. Wang (INFM(N))

One of the main objectives of EARLINET is to provide quantitative aerosol measurements on a regular basis. Generally this is not possible with the standard backscatter lidar, because two sets of unknown parameters, aerosol backscatter and extinction, determine the received power. However, different methods have been demonstrated to provide independent aerosol extinction measurements: high spectral resolution lidar (HSRL) (Shipley et al., 1983), Raman lidar (Ansmann et al., 1990) and multiple zenith angle measurements (Gutkowicz-Krusin, 1993; Wiegner and Freudenthaler, 1998).

Table 3.5: Participating groups and their processing algorithms for Raman algorithm intercomparison

A1	EPFL	Sliding average
A2	OCN	Binning with variable resolution
A3	IFT	Sliding linear least-squares fit
A4	NTUA	Sliding average filter and polynomial fit
A5	MPI	Sliding average
A6	IAP	Binning
A7	ULAQ	2^{nd} order digital filter Savitzky-Golay
A9	AUTH	Least-square fit
A11	INFM(N)	Sliding linear fit
A12	INFM(L)	Sliding linear least-squares fit
A16	UABER	Linear and quadratic fit
A17	INFM(P)	Sliding linear least-squares fit
A20	AWI	Kaiser filter for data smoothing

Because most lidars are only vertically pointing and multiple zenith angle measurements additionally require horizontal homogeneity of the aerosol distribution, this method only is applied by one group within EARLINET (the MIM). The Raman and the HSRL technique both rely on the detection of a pure molecular backscatter signal, but the HSRL requires much higher technical effort to suppress the aerosol scattering. So for reasons of technical practicability the preferred method within the network is the combination of Raman and elastic scattering at one wavelength around 355 nm. Therefore, within the EARLINET community a big effort has been devoted to upgrade the Raman capability. At the moment, nine lidar stations are able to perform measurements of nitrogen Raman scattering in the UV simultaneously with the elastic backscatter; two of these can also measure nitrogen Raman scattering in the visible domain (Kühlungsborn and Leipzig). An increasing number of stations is going to be equipped with Raman channels and 15 among the 21 stations of the network will have the capability to operate in this mode until the end of 2002. Therefore also groups who are not yet operating Raman channels have participated in the algorithm intercomparison.

[2]The Alfred Wegener Institut für Polar- und Meeresforschung (AWI), Potsdam, Germany, has participated in this intercomparison although it is not involved in the EARLINET project.

3.2.1 Raman data simulation

The main goal of the Raman algorithm intercomparison experiment is to test the correctness and accuracy of the algorithms used by each group for the retrieval of the aerosol extinction profile starting from nitrogen Raman lidar signals. For this purpose, synthetic lidar signals at a wavelength of 532 nm were calculated with the IfT lidar simulation model. All algorithms are suitable for Raman signals in the UV and the visible. Three different cases with different degrees of difficulty have been prepared:

Case 1: The first case represents a simple step-wise changing extinction profile. Two different signals, one with a shot noise for 10000 and the other with a shot noise for 1000 laser pulses, were simulated.

Case 2: The second case represents the same simple step-wise changing extinction profile as the previous one, but in this case a series of 15 profiles, with 3600 laser shots each, were simulated.

Case 3: In the third case, a series of 20 profiles corresponding to 3600 laser shots each, with an abrupt change of aerosol properties after the first 10 profiles, were simulated.

For case 1, simulated Raman signals were distributed together with results (input extinction profile) as a training case for the intercomparison of Raman algorithms. Data were simulated for a simple step-wise changing extinction profile with the values 0.3 km^{-1} below 1500 m, 0.35 km^{-1} between 1500 and 2000 m, 0.4 km^{-1} between 2000 and 2445 m, and a decrease to $2{\cdot}10^{-4}$ km^{-1} above 2500 m, $2{\cdot}10^{-5}$ km^{-1} above 7500 m and $2{\cdot}10^{-6}$ km^{-1} above 10000 m. The parameter k, characterising a wavelength dependence of the extinction coefficient proportional to λ^{-k} between the emitted light at 532 nm and the received Raman nitrogen light at 607 nm, was set to k = 1.5. Two different signals, one with a shot noise for 10000 laser pulses and one with a shot noise for 1000 laser pulses were simulated. A US standard atmosphere with a ground pressure of 1013 hPa and a ground temperature of 0°C, a tropopause height of 12.0 km, and isothermal conditions above were assumed. An incomplete overlap of laser beam and receiver field of view below 250 m was introduced.

Table 3.6: Altitude resolution for case 1

Group	**Altitude resolution**
A1	60 m for 10000 shots and 90 m for 1000 shots
A3	150 m
A4	180 m up to 500 m and 1350 up to 9000 m (10000 shots), 200 m up to 500 m and 1500 m up to 9000 m (1000 shots)
A5	150 m up to 3000 m and 510 m above
A6	200 m (1-5 km), 500 m (5-10 km), 1000 m (10-20 km)
A7	105 m (10000 shots) 180 m (1000 shots)
A9	75 m
A11	135 m
A12	150 m up to 3000 m and 450 m above
A16	15 m up to 2.5 km
A17	135 m
A20	15 m

In case 2, simulated Raman signal profiles were also distributed together with the solution for the extinction coefficient. The extinction profile, used as input for the simulation, was the same as for case 1 with the same wavelength dependence, atmospheric parameters, and overlap function. Here, 15 different lidar signals with 3600 shots each, corresponding to 2-min averages with a 30-Hz system, were provided. Each group has been asked to provide solutions and error values for three different temporal averages of 10, 20, and 30 minutes with a maximum statistical error of 10% in the 500-2000 m height range. Hence, all participating groups had the opportunity to test their own algorithm in terms of different averaging in time and space and of error evaluation.
For case 3, simulated data were provided without any solution; this was a real blind intercomparison. In this case, 20 profiles with 3600 laser shots each, corresponding to 40 minutes time period, were simulated. The wavelength dependence parameter was set again to k = 1.5. Standard atmosphere conditions were used as in the cases 1 and 2 and an incomplete overlap function below 250 m was introduced. A variable lidar ratio with height was used and a jump in aerosol properties between the first and the second 10 profiles was introduced. In this case, each group has been asked to provide the mean aerosol extinction profile for the 40 minutes time period with an error of less than 10% in the 500-2500 m height range.

3.2.2 Raman intercomparison results

In Table 3.5 the groups which participated in the intercomparison for the extinction retrieval are listed with the indication of the used averaging procedure (the group from Neuchatel joint the activity for cases 2 and 3 only). An additional lidar group, from the Alfred Wegener Institute for Polar and Marine Research in Potsdam (A20 in the table), which is not a member of EARLINET, participated in the Raman algorithm intercomparison as a “guest group”.

Table 3.7: Deviations and quadratic deviations from the solution for the case 1 with 10000 laser shots

10000 laser shots						
	300 - 1500 m		1500-2000 m		2000-2500 m	
Group	dev. from solution [%]	quadr. dev. fr. solution [%]	dev. from solution [%]	quadr. dev. fr. solution [%]	dev. from solution [%]	quadr. dev. fr. solution [%]
A1	1.90	2.75	0.11	3.46	-4.42	8.75
A3	0.36	2.44	-0.22	4.59	-2.08	5.23
A4	-0.12	2.54	-0.04	2.63	-3.90	5.69
A5	-0.33	1.91	-3.14	5.06	-5.00	5.76
A6	2.86	2.91	1.81	3.44	-4.01	5.10
A7	0.46	1.88	-0.26	2.30	-2.43	7.81
A9	0.18	1.89	-0.51	3.98	-2.62	4.18
A11	-3.66	6.31	-2.66	8.27	-4.65	44.29
A12	-0.05	1.77	-0.73	2.30	-4.25	7.81
A16	0.51	2.23	-1.51	5.80	-4.93	7.22
A17	0.08	2.58	-0.68	5.10	-2.33	5.78
A20	5.00	6.20	2.39	5.61	-0.11	38.84
mean values	0.60	2.95	-0.45	4.38	-3.40	12.21

Table 3.8: Deviations and quadratic deviations from the solution for the case 1 with 1000 laser shots

1000 laser shots						
	300 - 1500 m		1500-2000 m		2000-2500 m	
Group	dev. from solution [%]	quadr. dev. fr. solution [%]	dev. from solution [%]	quadr. dev. fr. solution [%]	dev. from solution [%]	quadr. dev. fr. solution [%]
A1	3.55	4.91	-0.66	2.88	-1.80	5.92
A3	0.23	6.41	-1.41	13.52	0.56	14.05
A4	0.26	4.33	-0.33	2.61	-8.58	13.78
A5	-0.42	3.82	-3.93	6.60	-3.75	8.99
A6	3.44	4.27	1.33	3.19	-1.51	1.62
A7	0.59	3.97	-0.56	6.31	-2.99	42.76
A9	0.18	4.26	-1.45	9.44	-0.24	9.76
A11	-3.44	7.16	-3.40	12.87	-7.77	50.07
A12	2.70	4.97	-0.42	2.99	-4.63	5.74
A16	0.84	5.68	0.90	2.86	3.94	10.87
A17	0.63	4.64	-0.81	8.65	-1.01	10.83
A20	5.00	6.38	1.76	6.51	2.01	45.15
mean values	1.13	5.07	-0.75	6.54	-2.15	18.30

Case 1 Figures 3.6 to 3.7 and Tables 3.6 to 3.8 summarise the results of the Raman algorithm intercomparison for case 1. Figure 3.6 shows the comparison between the results obtained by the different groups and the input profile used in the simulation for the signal with a shot noise corresponding to 10000 laser pulses and 1000 laser pulses, respectively. In order to perform a quantitative evaluation of the quality of the different algorithms two different statistical estimators (parameters) have been considered: deviation and quadratic deviation between the input and the retrieved profiles, defined as

$$\text{Deviation} = \frac{< x > -s}{s} \ , \tag{3.1}$$

$$\text{Quadratic deviation} = \frac{1}{s}\sqrt{\frac{\sum_{i=1}^{n}(x_i - s)^2}{n}} \ , \tag{3.2}$$

where x_i are the values of the results for each height z_i, s is the input profile, $< x >$ is the mean value and n the number of considered points:

$$< x >= \frac{\sum_{i=1}^{n} x_i}{n} \ . \tag{3.3}$$

Figure 3.7 reports the deviations of the results, obtained for 10000 and for 1000 laser shots, and the input profile. Three different mean values for height ranges of 300-1500, 1500-2000, and 2000-2500 m, corresponding to the first three steps of the input profile, were calculated. In the case of 10000 laser shots, all deviations are within 5%, in the case of 1000 laser shots the deviations are always within 9%. In the calculations, peak values in the low range (up to 450 m height) obtained by group A20 have been neglected. However, the profiles show large systematic deviations in the lowest range. Table 3.6 reports the altitude resolution for each station for case 1. Calculated deviations together with quadratic deviations are reported in Tables 3.7 and 3.8. In some cases, quadratic deviations reach very high values, but this is strongly dependent on different averaging of data and, consequently, on different

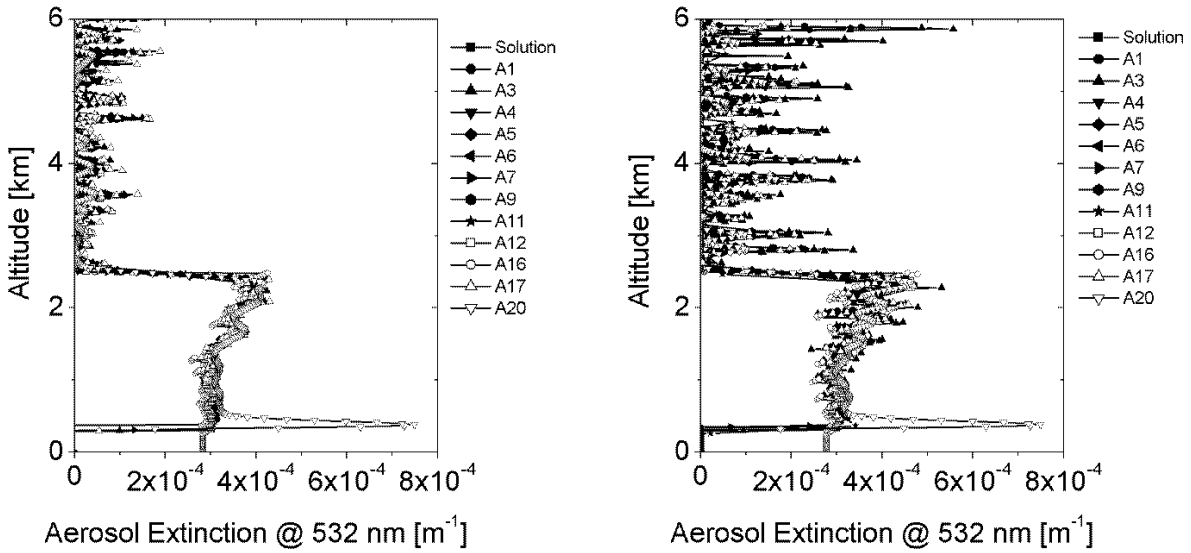

Figure 3.6: Results for case 1 for each lidar station, corresponding to 10000 laser shots (left side) and 1000 laser shots (right side), compared with the given solution.

final altitude resolutions. However, taking into account different averaging and different calculation schemes of the derivative, it is possible to assert that the intercomparison for the 12 participating groups showed good results in case 1 for all used algorithms.

Case 2 Results obtained for case 2 are summarised in Figures 3.8 to 3.9 and Tables 3.9 to 3.12. In Table 3.9, altitude resolutions obtained for time averages of 10, 20, and 30 minutes are listed. Figure 3.8 shows the results of case 2 obtained by each group for 10 minutes (Fig. 3.8(a)), 20 minutes (Fig. 3.8(c)) and 30 minutes average (Fig. 3.8(e)) together with the relative statistical errors (Fig. 3.8(b),(d),(f)). The figure shows a quite good agreement among all groups and demonstrates that each group obtained the extinction coefficient profile with statistical errors below 10% up to 2000 m as requested for case 2.

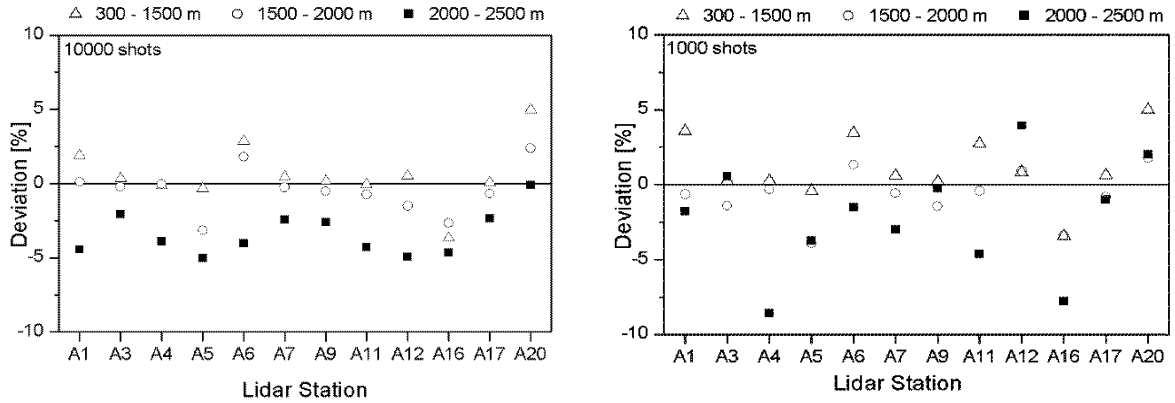

Figure 3.7: Deviations of the results of case 1 from the solution, calculated for 3 different mean values related to three different height ranges (300 - 1500 m, 1500 - 2000 m, 2000 - 2500 m) corresponding to the three steps present in the solution. Averages of 10000 laser shots (left side) and 1000 laser shots (right side) are shown.

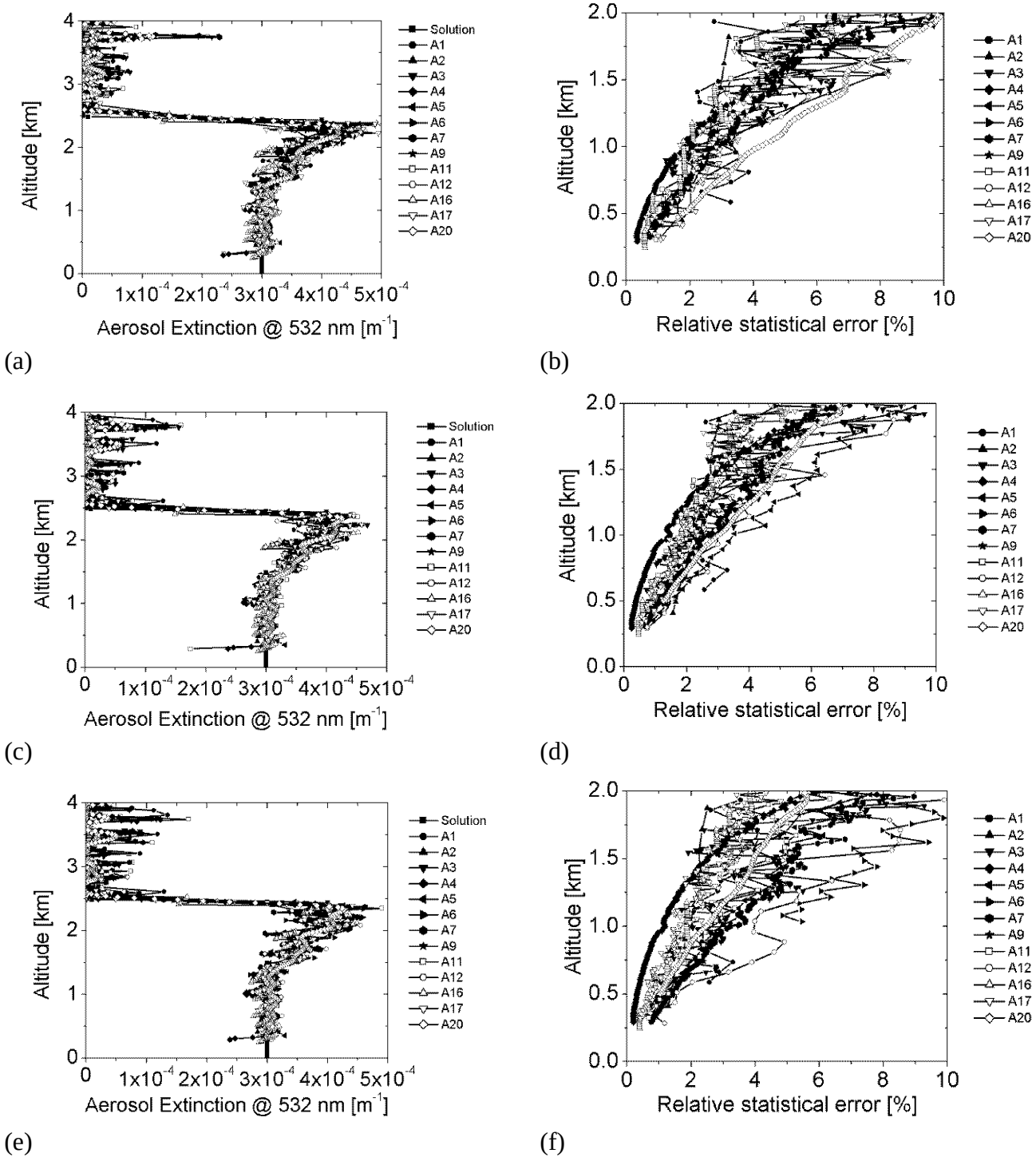

Figure 3.8: Results of case 2 for each lidar station, corresponding to 10 minutes average (18000 laser shots (a) and (b)), 20 minutes average (36000 laser shots, (c) and (d)) and to 30 minutes average (54000 laser shots, (e) and (f)): comparison with the given solution (a), (c), (e), relative statistical error (b), (d), (f).

Table 3.9: Altitude resolution for case 2

Altitude resolution for case 2			
Group	10 min.	20 min.	30 min.
A1	75 m	75 m	75 m
A2	Variable from 100 m to 270 m up to 3500 m and fixed 270 m above	Variable from 80 m to 210 m up to 3375 m and fixed 210 m above	Variable from 80 m to 210 m up to 3375 m and fixed 210 m above
A3	180 m	150 m	120 m
A4	120 m up to 500 m and 950 m up to 9000 m.	120 m up to 500 m and 950 m up to 9000 m.	120 m up to 500 m and 950 m up to 9000 m.
A5	120 m up to 2000 m 510 m above	90 m up to 3000 m 270 m above	90 m up to 2900 m 270 m above
A6	90 m up to 2500 m 495 m above	90 m up to 2500 m 495 m above	45 m up to 2500 m 495 m above
A7	105 m	85 m	65 m
A9	165 m	165 m	135 m
A11	77 m	64 m	55 m
A12	150 m up to 3000 m 450 m above	105 m up to 3000 m 450 m above	75 m up to 3000 m 450 m above
A16	150 m up to 3000 m 600 m above	150 m up to 3000 m 600 m above	150 m up to 3000 m 600 m above
A17	120 m up to 2800 m 330 m above	120 m up to 2800 m 330 m above	120 m up to 2800 m 330 m above
A20	150 m	150 m	150 m

Figure 3.9 reports the deviations and the quadratic deviations of the results, obtained for 10, 20 and 30 minutes average, from the solution for the extinction coefficient, calculated for 3 different mean values related to three different height ranges (250-1500 m, 1500-2000 m, 2000-2500 m) corresponding to the first three steps present in the input extinction profile. The deviations are within 10% for all the lidar stations at each height range for 10, 20 and 30 minutes average. The quadratic deviations are within 15% for almost all stations. When averaging more laser pulses as in the cases with 20 and 30 minutes average, the quadratic deviations are within 10% up to 2 km of height with only few exceptions. This shows that the results obtained by each group are not much spread around the solution with the fixed final altitude resolution in almost all cases.
Calculated deviations together with quadratic deviations are reported in Tables 3.10, 3.11 and 3.12 for each group. Deviations are always within 10% up to 2 km of height and this is consistent with the relative statistical errors obtained by each group. Just in one case, quadratic deviations exceed 20% in the height range 2000 - 2500 m. Taking into account different averaging and different calculation schemes of the derivative, it is possible to assert that this intercomparison between 13 participating groups showed good results for all used algorithms. Each group provided extinction coefficient profiles with a maximum statistical error below 10% up to 2 km of height and the relative deviations from the input extinction profile are always lower than 10% in this height range.

However, discrepancies were found in the determination of the averaging length that is required to achieve results with given statistical error. The groups claimed to have averaged the signals between 55 and 950 m in altitude with similar statistical errors of the derived extinction profile (see Table

Table 3.10: Deviations and quadratic deviations from the solution for the case 2 corresponding to 10 minutes average.

10 min.						
	250 - 1500 m		1500-2000 m		2000-2500 m	
Group	dev. from solution [%]	quadr. dev. fr. solution [%]	dev. from solution [%]	quadr. dev. fr. solution [%]	dev. from solution [%]	quadr. dev. fr. solution [%]
A1	1.22	4.09	-0.85	11.54	-1.76	7.83
A2	-1.58	3.04	-2.08	2.46	-2.95	4.32
A3	2.98	3.45	9.24	10.24	-10.32	13.71
A4	1.65	5.33	0.69	2.10	-2.11	9.23
A5	2.25	4.04	-1.20	1.93	0.65	8.50
A6	0.81	2.26	-0.34	4.36	-1.49	15.04
A7	0.34	2.92	-0.91	5.14	-2.34	11.08
A9	-1.77	3.76	-0.95	4.98	9.57	10.20
A11	0.71	6.96	-1.08	5.70	0.51	8.53
A12	1.89	4.45	1.64	2.64	-10.69	11.77
A16	-0.15	4.34	-7.40	8.97	-0.88	24.51
A17	0.27	4.24	-1.51	2.89	-1.95	15.74
A20	3.34	3.89	1.36	2.34	-0.19	8.37
mean values	0.92	4.06	-0.26	5.02	-1.84	11.45

Table 3.11: Deviations and quadratic deviations from the solution for the case 2 corresponding to 20 minutes average.

20 min.						
	250 - 1500 m		1500-2000 m		2000-2500 m	
Group	dev. from solution [%]	quadr. dev. fr. solution [%]	dev. from solution [%]	quadr. dev. fr. solution [%]	dev. from solution [%]	quadr. dev. fr. solution [%]
A1	0.71	3.48	2.11	8.75	-4.58	8.86
A2	-2.07	3.00	-1.48	2.90	-8.46	13.11
A3	3.02	3.59	10.13	6.39	-6.52	11.15
A4	1.64	5.51	1.21	3.21	-1.54	7.44
A5	1.82	4.91	-1.46	5.90	0.75	7.87
A6	1.41	2.04	0.68	3.57	-1.01	9.26
A7	0.40	3.35	-0.88	5.54	-0.80	8.35
A9	-0.76	2.86	2.07	4.10	6.42	6.89
A11	0.33	9.20	-0.41	5.43	2.00	6.94
A12	1.90	4.37	4.37	9.10	0.31	8.77
A16	0.71	3.76	-3.85	6.83	-5.88	20.31
A17	0.27	3.33	-0.99	2.72	-0.89	7.96
A20	3.44	3.98	1.76	3.29	0.53	7.41
mean values	0.99	4.11	1.02	5.21	-1.51	9.56

Table 3.12: Deviations and quadratic deviations from the solution for the case 2 corresponding to 30 minutes average.

30 min.						
	250 - 1500 m		1500-2000 m		2000-2500 m	
Group	dev. from solution [%]	quadr. dev. fr. solution [%]	dev. from solution [%]	quadr. dev. fr. solution [%]	dev. from solution [%]	quadr. dev. fr. solution [%]
A1	0.71	3.48	2.11	8.75	-4.58	8.86
A2	-2.10	3.26	-1.41	2.72	-8.90	13.37
A3	3.04	4.44	9.10	6.96	-1.86	7.25
A4	1.62	5.46	1.41	2.99	-2.20	7.80
A5	1.70	4.21	-1.04	6.58	0.07	5.84
A6	1.41	7.07	0.25	9.20	1.32	10.58
A7	0.36	3.72	-0.81	6.83	-0.71	8.90
A9	-0.61	2.83	-1.50	5.33	6.80	7.37
A11	2.26	5.02	0.54	6.38	0.97	11.67
A12	2.67	5.13	0.04	9.25	-1.26	9.39
A16	0.19	4.09	-2.42	3.87	-5.08	20.12
A17	0.24	2.88	-0.77	2.25	-1.55	7.26
A20	3.47	4.11	1.96	3.38	-0.10	7.58
mean values	1.15	4.28	0.57	5.73	-1.31	9.69

Table 3.13: Deviations and quadratic deviations from the solution for the case 2 corresponding to 30 minutes average with a fixed altitude resolution of 90 m

30 minutes average and 90 m altitude resolution						
	250 - 1500 m		1500-2000 m		2000-2500 m	
Group	dev. from solution [%]	quadr. dev. fr. solution [%]	dev. from solution [%]	quadr. dev. fr. solution [%]	dev. from solution [%]	quadr. dev. fr. solution [%]
A1	1.91	4.90	0.07	3.98	-6.99	17.46
A2	-2.10	3.26	-1.41	2.72	-8.90	13.37
A3	0.32	3.31	-0.97	7.28	-0.24	8.05
A4	0.16	3.93	-0.42	2.45	-3.24	7.57
A5	1.70	4.21	-1.04	6.58	0.07	5.84
A6	2.09	3.71	0.41	2.83	1.06	1.41
A7	0.37	2.89	-0.67	4.50	-1.45	7.24
A9	0.25	4.29	-0.83	2.59	2.38	13.33
A11	-0.02	2.41	-1.17	3.60	-0.80	1.76
A12	0.31	3.91	-0.72	7.45	-0.98	8.80
A16	-0.56	5.31	-1.19	11.85	-5.81	17.71
A17	0.23	3.70	-0.87	6.80	-0.82	8.91
mean values	0.39	3.82	-0.73	5.22	-2.14	9.29

Table 3.14: Altitude resolution for case 3

Group	**Altitude resolution**
A1	90 m
A2	variable from 30 m at 400 m, 75 m at 3600 m up to 120 m at 10000 m
A3	180 m
A4	100 m up to 500 m and 900 m up to 9000 m
A5	120 m up to 3600 m and 270 m above
A6	90 m up to 3300 m, 300 m up to 3500 m and 600 m above
A7	65 m
A9	165 m
A11	55 m
A12	150 m up to 3700 m and 450 m above
A16	150 m up to 4000 m and 600 m above
A17	120 m

Table 3.15: Deviations and quadratic deviations from the solution for case 3

	400 - 1000 m		1000-3200 m	
Group	dev. from solution [%]	quadr. dev. fr. solution [%]	dev. from solution [%]	quadr. dev. fr. solution [%]
A1	24.56	44.93	-2.35	10.24
A2	5.47	22.01	-1.67	6.00
A3	5.48	20.42	-0.46	6.20
A4	8.12	18.75	-1.22	6.15
A5	7.20	8.29	-0.32	9.03
A6	7.45	10.58	0.97	5.58
A7	5.06	20.70	-0.37	8.65
A9	-1.58	2.38	1.75	4.34
A11	1.54	8.08	0.06	7.89
A12	-0.39	1.44	1.52	5.89
A16	10.47	44.80	0.28	12.19
A17	4.75	20.62	-0.49	8.65
mean values	6.51	18.58	-0.19	7.57

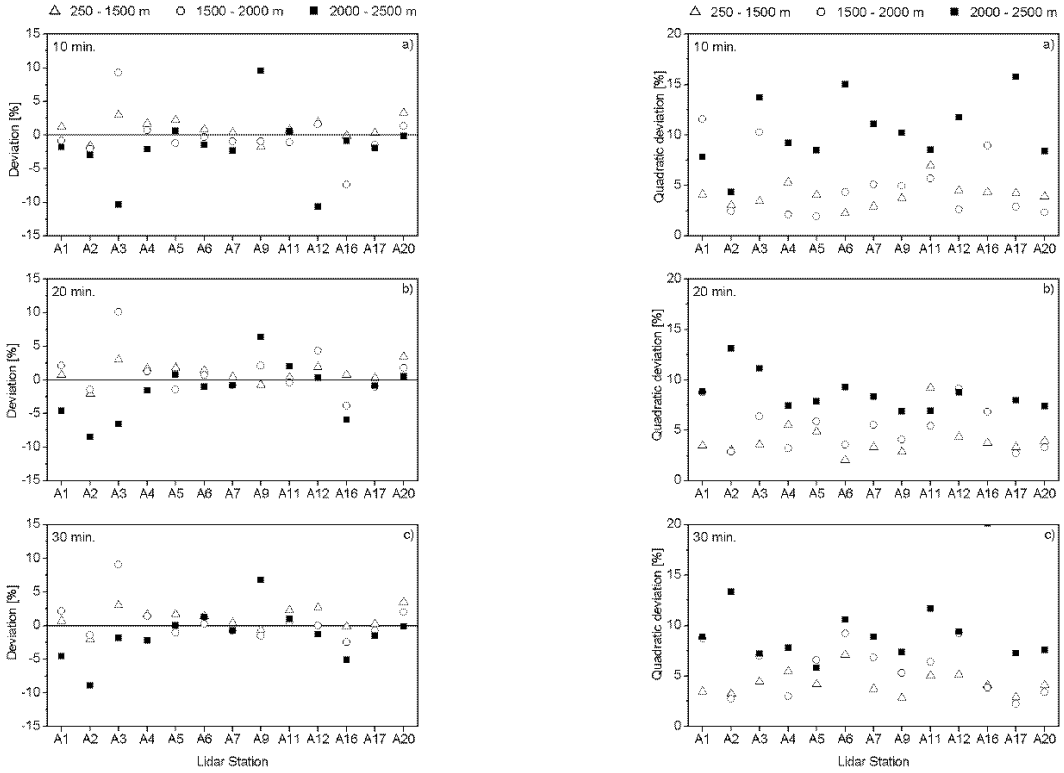

Figure 3.9: Deviations (left side) and quadratic deviations (right side) of the results of case 2 for each lidar station from the solution, calculated for 3 different mean values relating to three different height ranges (250 - 1500 m, 1500 - 2000 m, 2000 - 2500 m) corresponding to the three steps present in the solution for the three different cases: 10 minutes average (a), 20 minutes average (b), 30 minutes average (c).

3.9). For this reason, a resolution test using a stepwise changing aerosol profile without signal noise has been done and each group determined their real averaging length from this test. Afterwards a further intercomparison, where each group has been asked to provide the extinction profile with a fixed altitude resolution of 90 m, has been performed for case 2 (30 minutes average). Figure 3.10 reports the results obtained by each group compared with the solution in this case. It shows a quite good coincidence among all groups. Relative statistical errors are always below 10% up to 2000 m. Figure 3.11 reports the deviations and the quadratic deviations of the results from the solution for the extinction coefficient, calculated for three different mean values which are related to three different ranges of heights (250-1500 m, 1500-2000 m, 2000-2500 m) corresponding to the first three steps present in the input extinction profile.
Calculated deviations together with quadratic deviations are reported in Table 3.13. Mean deviations are always within 5% up to 2000 m and within 10% in the 2000 - 2500 m height range. Mean quadratic deviations are almost always within 10% with few exceptions mostly related to the 2000 - 2500m height range where the presence of a steep step in the input profile between 2400 and 2500m has to be considered.

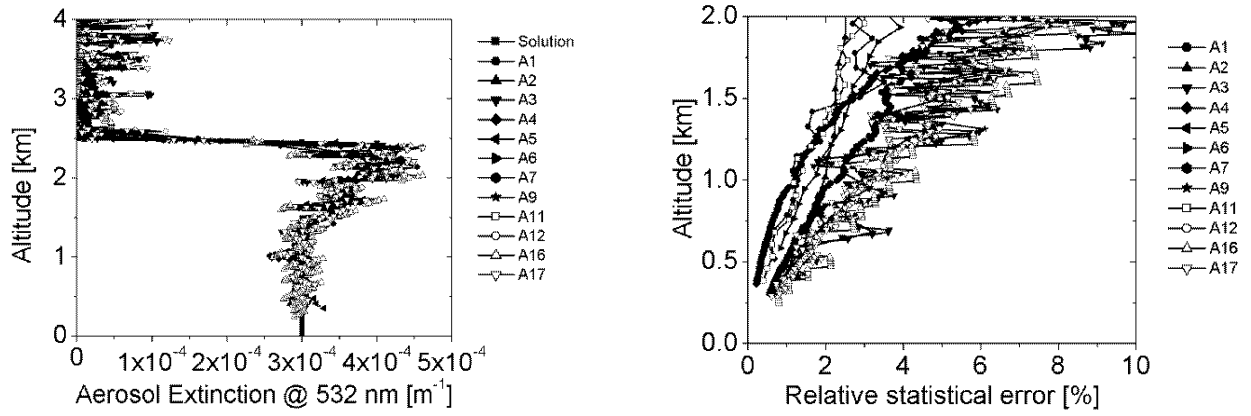

(a) (b)

Figure 3.10: Results of case 2 for each lidar station, 30 minutes average (54000 laser shots) with fixed altitude resolution of 90 m: comparison with the given solution (a) and relative statistical error (b).

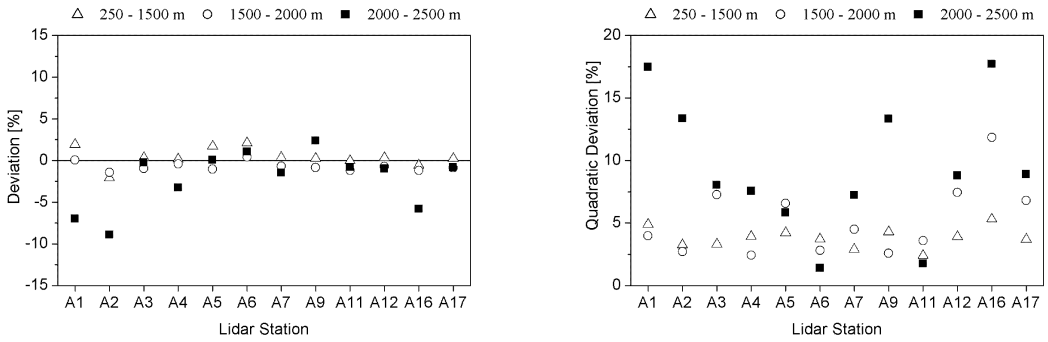

Figure 3.11: Deviations (left side) and quadratic deviations (right side) between the results of case 2 with a fixed altitude resolution of 90 m and the solution. Mean values were calculated for three different height ranges (250-1500 m, 1500-2000 m, 2000-2500 m) corresponding to the three steps present in the solution.

Case 3 In Table 3.14 the final altitude resolutions for case 3 are listed. In this case no solution was provided and the intercomparison was really blind. The given record corresponds to a period of 40 minutes average. In the second 20 minutes a jump in aerosol properties is present. Each group has been asked to provide the mean aerosol extinction profile for the entire time period with an error lower than 10% in the 500-2500 m height range. Because of this quite large and fast jump in the aerosol properties, it is necessary to calculate the extinction profile for the two periods (first 20 minutes and second 20 minutes) separately and then calculate the mean extinction profiles for the 40 minutes period. By this it is possible to take into account the atmospheric variability and to avoid a systematic deviation of about 10-15% due to the change in the extinction properties.

Figure 3.12 shows the results of case 3. Almost all statistical errors are less than 10% up to 2500 m of height and just few points are above this limit. Each group has correctly taken into account the atmospheric variability and a good agreement is present between the solution and each profile. The deviations from the solution are within 10% up to 2.5 km for most groups excluding the height region around 1 km of height where a large stepwise change in the extinction profile is present.

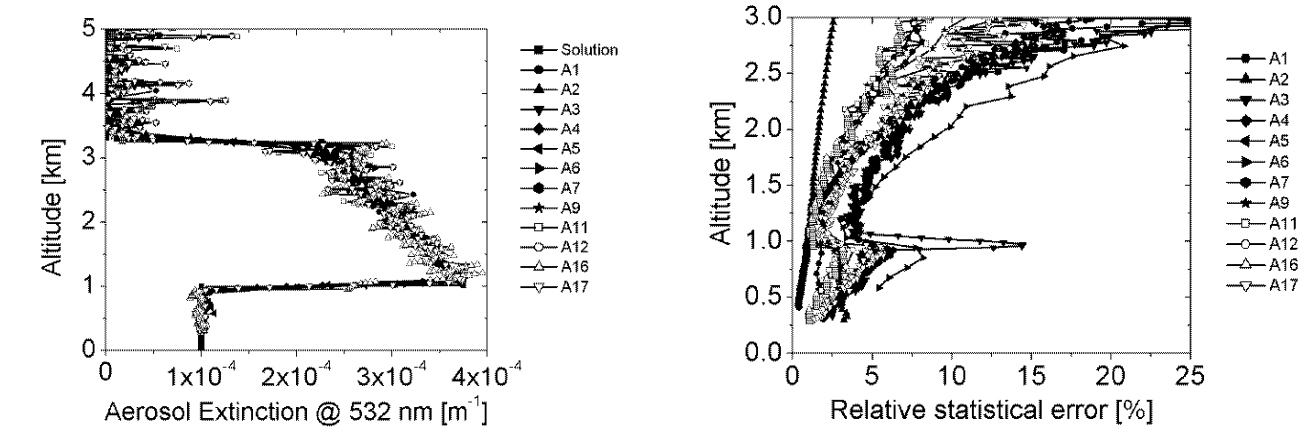

(a) (b)

Figure 3.12: Results of case 3 for each lidar station, corresponding to 40 minutes average (72000 laser shots). Comparison with the given solution (a), relative statistical error (b).

Mean deviations and mean quadratic deviations, calculated in the two height ranges 400-1000 m and 1000 - 3200 m, are reported for each group in Table 3.15. Mean deviations are always within 8% up to 1000 m of height with two exceptions (A1 and A16) and within 7% in the 1000 - 3200 m height range. Mean quadratic deviations are within 22% in the height range 1000 - 3200 m except for groups A1 and A16 and within 15% in the 1000 - 3200 m height range for all groups. Higher values of mean relative deviations and mean quadratic deviations in the 400 - 1000 m height range are due to the

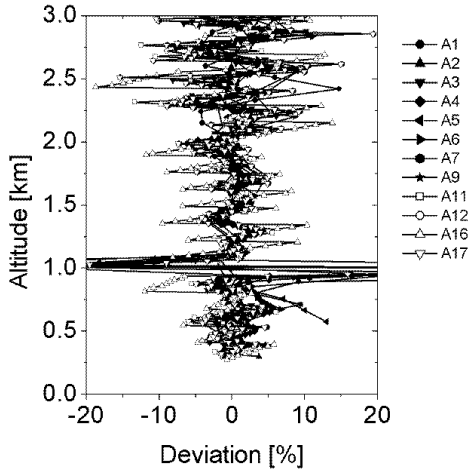

Figure 3.13: Deviations of the results of case 3 for each lidar station from the solution.

lower absolute values.
Also for case 3, considering the blind intercomparison and the jump in the aerosol properties, it is possible to state that the intercomparison gives good results. With respect to the last case, it may be pointed out that it refers to simulated data characterised by a very high signal-to-noise ratio, larger than real cases. For this reason, it is correct to calculate extinction separately for each 10 records and then average the results. While in the present case this is the right approach, in real cases Raman signals are often too noisy to derive sufficiently accurate profiles already from part of the whole measurement. Thus it is more useful to average all records first and then calculate the extinction from the averaged signal. Although the extinction profiles changed dramatically in the simulation case, the systematic error due to different averaging procedures stayed in the order of 10-15%, which is comparable with typical statistical errors. Therefore the procedure of averaging signals first can be applied even under conditions of changing aerosol properties without introducing too large systematic errors.
Summarizing, it can be stated that the extinction determination can be done with good accuracy, in most cases the mean deviations were not larger than the statistical error. Additional simulations for the determination of aerosol backscatter from Raman and elastic measurements as well as for a different wavelength (355 nm) are planned in the next future.

Chapter 4

System intercomparisons

edited by V. Matthias (MPI)

with contributions from V. Freudenthaler (MIM), J. Bösenberg (MPI), A. Amodeo (IMAA-CNR), D. Balis (AUTH), A. Chaykovski (IPNANB), G. Chourdakis (NTUA), A. Comeron (UPC), A. Delaval (LMD), F. de Tomasi (INFM(L)), R. Eixmann (IAP), A. Hågård (FOA), L. Konguem (UABER), S. Kreipl (IFU), R. Matthey (OCN), I. Mattis (IFT), V. Rizi (ULAQ), J. Rodriguez (IST), V. Simeonov (EPFL) and X. Wang (INFM(N))

4.1 Lidar systems

Lidar systems are rather complex, involving several subsystems, and their performance is critically dependent on a number of adjustments that are not easily standardised. To achieve comparable performance at many stations which are widely spread over Europe it is therefore mandatory to perform direct intercomparisons at system level. For EARLINET these intercomparisons required a rather big effort because many of the systems are not transportable, so that it was impossible to organise a single central intercomparison campaign. To keep the effort manageable for the participating groups the main part of the intercomparisons were made against the two transportable systems of the Meteorologisches Institut der Ludwig-Maximilians-Universität München (MIM), and the Max-Planck-Institut für Meteorologie Hamburg (MPI). Both systems emit three laser wavelengths in the ultraviolet (355 nm), green (532 nm) and infrared (1064 nm). The MIM system additionally has scanning capability, the MPI system is additionally equipped with a Raman channel at 387 nm.
For the five German stations intercomparisons at system level had already been performed successfully in the frame of the German Aerosol Lidar Network as documented in Bösenberg et al. (2001). It was not considered necessary to repeat these measurements.
Intercomparisons between the EARLINET lidars have been performed at system level between September 2000 and August 2001. The largest experiment involving five systems in September 2000 in Palaiseau (France), was the starting point for several intercomparisons of two systems at a time at different sites. Most of them have been completed in October 2000 with the Munich system travelling to Italy and Greece. The other experiments followed in spring and summer 2001.
Each system that has been successfully compared to a quality controlled system has been regarded as quality controlled itself and could therefore be compared to another system. This has been used for the intercomparisons in Neuchâtel and on Jungfraujoch.
Unfortunately we had to recognise that customs and other logistical problems made it virtually impossible to perform intercomparisons with foreign systems at Minsk. Therefore in Minsk internal

Table 4.1: Brief description of the lidar systems participating in the EARLINET intercomparison experiments. UV: 355 nm, GR: 532 nm, IR: 1064 nm. $^{(1)}$: emitted wavelength is 351 nm, $^{(2)}$: emitted wavelength is 353 nm, $^{(3)}$: transportable system only was used for the intercomparisons and has been compared to a stationary system used for the routine observations.

Intercomparison experiments: participating lidars						
Group	elastic ch.			Raman ch.	Transp.	Intercomparison with
	UV	GR	IR	UV		
MPI	x	x	x	x	x	MIM, IFT, UPC, OCN, UABER, FOA, LMD, IST
MIM	x	x	x		x	MPI, IFT, IAP, AUTH, INFM(P), INFM(N), INFM(L), ULAQ, NTUA, IFU
UABER	x			x		MPI
NTUA	x	x				MIM
UPC			x		x	MPI, IST
IFU	x	x	x		x	MIM
EPFL	x	x	x	x		OCN
IAP	x	x	x	x		MIM
ULAQ	x$^{(1)}$			x		MIM
INFM(L)	x$^{(1)}$			x		MIM
IFT	x	x	x	x	x$^{(3)}$	MIM, MPI
IST			x		x	MPI, UPC (planned)
FOA	x				x	MPI
IPNANB	x$^{(2)}$	x	x	x		internal
INFM(N)	x$^{(1)}$			x		MIM
OCN	x	x	x		x$^{(3)}$	MPI, OCN(internal), EPFL
LMD		x	x			MPI, OCN (planned)
INFM(P)	x	x		x		MIM
AUTH	x	x				MIM

intercomparisons with two of their systems at 532 nm have been made. In the course of the project the group of IPNANB had also managed to operate another system at Belsk, Poland. At that time this system could not be included in the plans for the intercomparisons, so it had to remain untested. However, because of the close cooperation between Belsk and Minsk and because of the long experience of the Minsk group with several lidar systems it is very likely that the system performance is sufficiently good.

Some systems had to repeat the intercomparison experiment because major technical problems were detected that could not be solved within a few days during the measurement campaign. For one system these measurements have been done in summer 2001, for another two they will be performed in spring 2002. Table 4.1 gives a brief overview over the participating systems and to which other system they have been compared. A list of time and place of the experiments is given in Table 4.2. Figure 4.1 visualizes the intercomparison procedure.

Table 4.2: Date and place of the EARLINET intercomparison experiments.

Intercomparison experiments: date and time of the individual intercomparisons				
Group	Intercomparison with	Date	Place	Comments
UABER	MPI	5/2001	Aberystwyth	incl. extinction
NTUA	MIM	9/2000	Athens	
UPC	MPI	9/2000	Palaiseau	
IFU	MIM	7/2001	Munich	
EPFL	OCN	5/2001	Jungraujoch	with OCN microlidar
IAP	MIM	8/1998	Kühlungsborn	within the German Lidar Network
ULAQ	MIM	10/2000	L'Aquila	
INFM(L)	MIM	10/2000	Lecce	
IFT	MIM, MPI	8/1998	Lindenberg	within the German Lidar Network
IST	MPI	9/2000	Palaiseau	new intercomparisons with UPC in 2002
FOA	MPI	8/2001	Hamburg	
IPNANB	internal	4-6/2000	Minsk	using two systems from IPNANB
INFM(N)	MIM	10/2000	Napoli	
OCN	MPI	9/2000	Palaiseau	with OCN microlidar
OCN	internal	4-5/2001	Neuchâtel	OCN stationary with OCN microlidar
LMD	MPI	9/2000	Palaiseau	new intercomparisons with OCN in 2002
INFM(P)	MIM	10/2000	Potenza	
AUTH	MIM	9/2000	Thessaloniki	

4.2 Quality Criteria

The quality criteria had been fixed in advance. Experimentally derived deviations between the MPI, MIM and IFT lidar systems during the intercomparison in 1998 (Bösenberg et al., 2001) have been taken into account together with results from the algorithm intercomparison to define upper limits for the mean and standard deviations at the different wavelengths. All groups agreed on reaching these values during the intercomparisons.
The measurement strategy had been defined in a planning document. The goal of each intercomparison experiment was to derive several aerosol extinction and backscatter profiles from all participating lidar systems under different meteorological conditions. It was aimed to have an optimum of four different episodes under conditions without low clouds on at least two different days. The lidar systems were located very close together with a horizontal distance less than 500 m. Each compared profile was averaged over typically 15 - 30 minutes in time and 50 - 300 m in space. Comparisons best could be made if the amount of aerosol in the atmosphere was moderate or high to make sure that the measured values are above the detection limit. The specifications for high aerosol load were $\beta_{\max} > 3 \cdot 10^{-6}(\mathrm{m} \cdot \mathrm{sr})^{-1}$ at 355 nm and $\alpha_{\max} > 2 \cdot 10^{-4}\mathrm{m}^{-1}$ at 355 nm. These values can be scaled down to the longer wavelengths assuming an $\alpha, \beta \propto \lambda^{-1}$-dependence. This included that all systems were able to measure within the planetary boundary layer, where the highest aerosol load can be expected. Both nighttime and daytime measurements have been compared, especially during situations in which significant differences in daytime and nighttime performance could be expected.

4.2.1 Compared quantities

Compared quantities were (if measured):

- aerosol backscatter at 355 nm, 532 nm and 1064 nm
- aerosol extinction at 355 nm
- aerosol optical depth (in comparison with sun photometer)
- PBL-height
- cloud-base-height

To compare aerosol backscatter profiles calculated with an inversion algorithm (Klett, 1981; Fernald, 1984)), equal lidar ratio profiles and aerosol calibration values have been used. For extinction profiles derived with the Raman method, all corrections to the measured signals (e.g. dead time correction, overlap correction) have been applied by the individual groups before the intercomparison, and the same Ångstrøm coefficients have been assumed for the evaluations. For the determination of optical depth from aerosol extinction profiles, the profiles have been linearly extrapolated to ground and then integrated over the whole height range. To compare these Raman extinction profiles measured at nighttime with daytime sun photometer measurements, time differences up to 3 hours have been allowed. This is justified if a stable meteorological situation during this time can be assumed with no horizontal advection of a different air mass. This was verified by inspecting the temporal development of the lidar signals. PBL-height and cloud-base-height have been defined as the height above ground

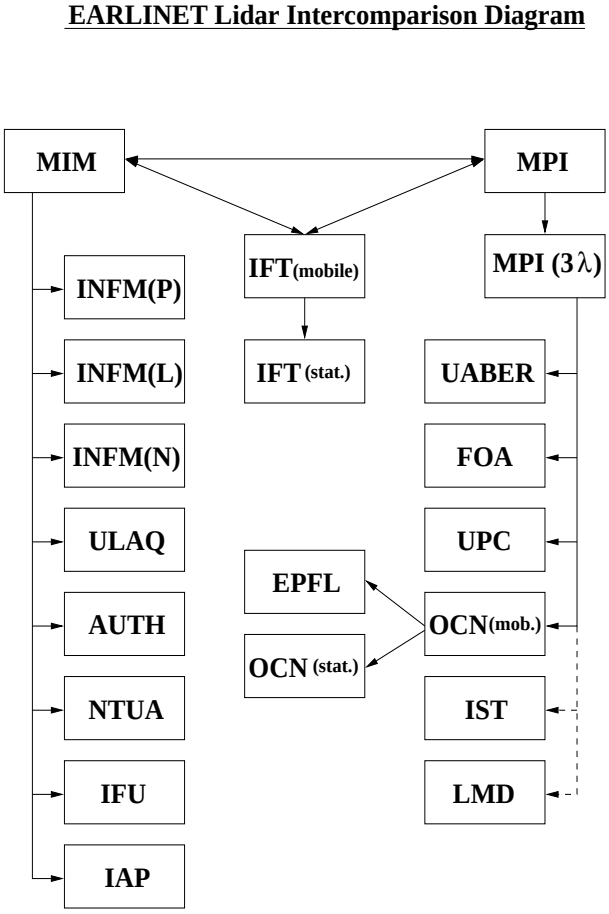

Figure 4.1: Diagram of intercomparison experiments performed for the EARLINET quality assurance.

quantity	mean deviation	std. deviation	min. height interval
aerosol extinction (355 nm)	$< 20\%$ / $5 \cdot 10^{-5}\mathrm{m}^{-1}$	$< 25\%$ / $1 \cdot 10^{-4}\mathrm{m}^{-1}$	1000 m
aerosol extinction (532 nm)	$< 20\%$ / $5 \cdot 10^{-5}\mathrm{m}^{-1}$	$< 30\%$ / $1 \cdot 10^{-4}\mathrm{m}^{-1}$	500 m
aerosol backscatter (355 nm)	$< 20\%$ / $5 \cdot 10^{-7}(\mathrm{m} \cdot \mathrm{sr})^{-1}$	$< 25\%$ / $5 \cdot 10^{-7}(\mathrm{m} \cdot \mathrm{sr})^{-1}$	2000 m
aerosol backscatter (532 nm)	$< 20\%$ / $5 \cdot 10^{-7}(\mathrm{m} \cdot \mathrm{sr})^{-1}$	$< 25\%$ / $5 \cdot 10^{-7}(\mathrm{m} \cdot \mathrm{sr})^{-1}$	2000 m
aerosol backscatter (1064 nm)	$< 30\%$ / $5 \cdot 10^{-7}(\mathrm{m} \cdot \mathrm{sr})^{-1}$	$< 30\%$ / $5 \cdot 10^{-7}(\mathrm{m} \cdot \mathrm{sr})^{-1}$	2000 m
aerosol optical depth (355 nm)	$< 30\%$ / 0.1	$< 30\%$ / 0.1	2000 m
PBL-height	$< 100\,\mathrm{m}$	–	–
cloud-base-height	$< 100\,\mathrm{m}$	–	–

Table 4.3: Maximum deviations allowed for the different compared quantities during the lidar intercomparison experiments.

with the (locally) steepest gradient (either positive or negative) in the logarithm of the range corrected signal. All range corrected signals had the full resolution of the data acquisition system and have not been averaged over more than 100 m in height.

4.2.2 Maximum deviations

The intercomparisons have been treated as successful if the deviations between all systems were in a given interval below one of the values specified in Table 4.3. Profiles have been split into regions with high aerosol load (usually the PBL) and low aerosol load (usually the free troposphere (FT)) to fit the requirements for each interval separately. For regions with moderate to high aerosol load (mostly within the PBL) deviations and standard deviations are given in %. For regions with low aerosol load they are given in $(\mathrm{m} \cdot \mathrm{sr})^{-1}$ and m^{-1}, respectively.

4.3 Results

Although each intercomparison experiment has been scheduled for 3-5 days of measurements, not in each case the above mentioned criteria on the number of intercomparison episodes under different meteorological conditions and on the minimum aerosol backscatter and extinction values could be reached. Sometimes bad weather prevented extended measurements and in some cases technical problems had to be solved before further measurements could be taken. Therefore most of the intercomparisons have been restricted to three cases with at least one with high aerosol load.

4.3.1 Intercomparison between lidar systems

During the experiments several systems immediately showed problems to reach the quality criteria. Especially in the near range below 1000 m remarkable deviations among the measurements have been found. These effects were mainly due to incomplete overlap between emitted laser beam and receiving telescope field of view and due to detector saturation from too large near range signals. Since the reasons for the deviations could always be detected, measures have been taken by those groups to avoid the problems in the future. In those cases, where a main reconstruction of the system would be necessary to reach the goals of the quality assurance, the limits of the current system have been fixed and the groups installed additional or new hardware after the experiment to perform the EARLINET routine measurements. The intercomparisons will be repeated with the improved systems.

Lidar intercomparisons: IFT/MIM/MPI, results in regions with high aerosol					
Date [UT]	Quantity	height range	IFT/MIM	MIM/MPI	MPI/IFT
9.8.98 22:30 - 23:00	355 nm bsc.[1)]	600 -1300	–	–	-39.0 ± 53.0
	532 nm bsc.	600 -1300	-7.7 ± 27.1	–	–
9.8.98 22:30 - 23:00	355 nm bsc.[1)]	3300 -4200	–	–	-37.7 ± 52.9
	532 nm bsc.	3300 -4200	4.1 ± 44.7	–	–
11.8.98 12:07 - 12:12	355 nm bsc.[1)]	500 - 3200	–	-16.1 ± 19.7	–
	532 nm bsc.	500 - 3200	8.6 ± 12.6	–	–
11.8.98 21:15 - 21:45	355 nm bsc.[2)]	600 -2000	11.3 ± 18.5	1.5 ± 7.5	-12.9 ± 16.2
	532 nm bsc.	600 -2000	2.9 ± 17.2	–	–
	1064 nm bsc.	600 -2000	5.6 ± 9.3	–	–
	355 nm ext.[2)]	600 -2000	–	–	4.7 ± 11.9
Lidar intercomparisons: IFT/MIM/MPI, results in regions with low aerosol					
Date [UT]	Quantity	height range	IFT/MIM	MIM/MPI	MPI/IFT
9.8.98 22:30 - 23:00	355 nm bsc.[1)]	1500 -3000	–	–	$-1.3 \pm 1.4 \cdot 10^{-7}$
	532 nm bsc.	1500 -3000	$-0.25 \pm 0.87 \cdot 10^{-7}$	–	–
11.8.98 21:15 - 21:45	355 nm bsc.[2)]	2400 - 3800	$-0.6 \pm 2.2 \cdot 10^{-7}$	$-0.4 \pm 2.0 \cdot 10^{-7}$	$1.5 \pm 3.2 \cdot 10^{-7}$
	532 nm bsc.	2400 -3800	$-0.6 \pm 1.2 \cdot 10^{-7}$	–	–
	1064 nm bsc.	2400 -4300	$-0.9 \pm 1.0 \cdot 10^{-7}$	–	–
	355 nm ext.[2)]	2400 -3800	–	–	$1.7 \pm 2.5 \cdot 10^{-5}$

Table 4.4: Mean deviations for different measured quantities during the LACE experiment. Units are $(\mathrm{m} \cdot \mathrm{sr})^{-1}$ for backscatter values and m^{-1} for extinction values in regions with low aerosol, in % in regions with high aerosol. [1)] MPI 320 nm, [2)] MPI 351 nm.

IFT/MIM/MPI

The measurements between these three German groups already have been performed in August 1998 and are documented in Bösenberg et al. (2001). The main results are given in table 4.4.

At that time the MPI system was based on an excimer laser emitting at 351 nm with a XeF-filling. During the experiment it was also running at 320 nm. This wavelength is generated via stimulated Raman scattering on Deuterium using an emission wavelength of 248 nm (KrF-filling).

Three different days, one with low aerosol load and two with high aerosol load have been chosen for the intercomparisons between IFT, MIM and MPI. The deviations stay within the limits except for the relative deviations on August 9, but this was a case with low aerosol load where the aerosol backscatter was lower than $1.0 \cdot 10^{-6}(\mathrm{m} \cdot \mathrm{sr})^{-1}$, so the absolute deviations stay well below the

Lidar intercomparisons: MPI internal				
Date [UT]	Quantity	height range [m]	mean dev. $[(\mathrm{m} \cdot \mathrm{sr})^{-1}]$	standard dev. $[(\mathrm{m} \cdot \mathrm{sr})^{-1}]$
2000/07/31 14:53 - 15:03 UT	351/355 nm bsc.	400 - 1300	$-1.8 \cdot 10^{-7}$ / 11.0%	$2.4 \cdot 10^{-7}$ / 14.5 %
	351/355 nm bsc.	1500 - 4800	$0.1 \cdot 10^{-7}$	$0.1 \cdot 10^{-7}$
2001/04/05 17:41 - 17:48 UT	351/355 nm bsc.	400 - 3200	$0.1 \cdot 10^{-7}$ / 3.8 %	$0.4 \cdot 10^{-7}$ / 10.6 %
	351/355 nm bsc.	4000 - 7000	$-0.2 \cdot 10^{-7}$	$0.3 \cdot 10^{-7}$

Table 4.5: Mean deviations and standard deviations for the internal intercomparison of the MPI excimer laser based UV Raman lidar and the Nd:YAG laser based three wavelengths aerosol Raman lidar.

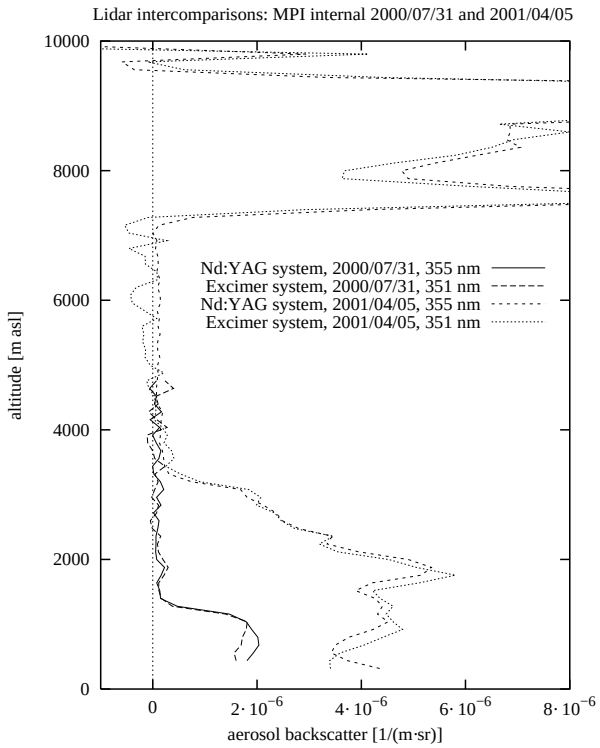

Figure 4.2: Intercomparison of aerosol backscatter profiles at 351 nm and 355 nm for the MPI internal lidar intercomparison. Measurements were taken on July 31, 2000 and April 5, 2001.

$5 \cdot 10^{-7}(\mathrm{m} \cdot \mathrm{sr})^{-1}$ which is the maximum allowed absolute deviation.
The three wavelength Nd:YAG laser system which the MPI uses during EARLINET has been compared to the Excimer (XeF) system at Hamburg. The measurements have been performed before the system has been transported to Palaiseau in September 2000 and to Aberystwyth in May 2001. Aerosol profiles and the corresponding deviations are given in Figure 4.2 and Table 4.5, respectively.

MIM/IAP

The measurements between MIM and IAP have also already been made in August 1998. Although only two cases on one day were available for the intercomparison, it was decided not to repeat the experiment. Aerosol backscatter values were quite high and the deviations were within the limits (see table 4.6). Problems occured only at 1064 nm, where good agreement could be achieved only in a limited range of 1100 - 1700 m. These problems are connected with the high sensitivity of the resulting aerosol backscatter profile on the calibration value which is due to the very low Rayleigh backscattering at 1064 nm.

MIM/AUTH

The intercomparisons have been restricted to 532 nm, because instabilities in the AUTH-system made reliable measurements at 355 nm impossible. Thermal drifts of the alignment have also been detected at 532 nm. This led to changing overlap functions and three of the four intercomparisons that are shown here are at altitudes above 2000 m asl. However, on September 22, the lowest compared altitude was 1200 m.

Lidar intercomparisons: MIM/IAP					
Date [UT]	Quantity	height range	high aerosol	height range	low aerosol
16.8.98 18:41 - 19:01	355 nm bsc.	850 -1800	11.8 ± 18.2	2200 - 3600	$2.9 \pm 3.7 \cdot 10^{-7}$
	532 nm bsc.	850 -1800	5.0 ± 17.7	2200 - 3600	$0.04 \pm 0.4 \cdot 10^{-7}$
16.8.98 20:51 - 21:22	355 nm bsc.	850 -1800	1.6 ± 10.6	2200 - 3600	$2.8 \pm 3.6 \cdot 10^{-7}$
	532 nm bsc.	850 -1800	16.8 ± 22.8	2200 - 3600	$1.8 \pm 1.9 \cdot 10^{-7}$
	1064 nm bsc.	1050 -1650	-3.5 ± 16.2	–	–

Table 4.6: Mean deviations (in $(\mathrm{m} \cdot \mathrm{sr})^{-1}$ for backscatter values in regions with low aerosol, in % in regions with high aerosol) between the IAP and the MIM lidar for three different wavelengths.

Generally, the deviations are small and stay well below the given limits (see Table 4.7). On September 22, 18:10 - 18:15 and on September 23, 9:40 - 9:45, differences of ca. 30 m in the observed height of the aerosol layer can be seen in parts of the profiles. These differences are most likely due to inhomogeneities in the aerosol distribution. On September 23 this can be shown by looking at the temporal development of the aerosol distribution. On September 22 it remains a speculation, but the differences are that small that they don't affect the measurement accuracy at all.
Currently nighttime measurements at 355 nm and 387 nm (nitrogen Raman channel) are performed, which are checked one by one for the stability of the alignment.

MIM/NTUA

The measurements from the University of Athens have been made with their new powerful Nd:YAG laser. This laser permits much better aerosol backscatter and will in the future also allow the detection of Raman backscatted signals. However, because the laser was just built in the lidar system, the intercomparisons revealed several diffculties operating this new system. The much higher signal caused detector saturation effects in the near range so the lowest measurement height was in the order of 1400 m. Additional trigger problems made a height correction of the NTUA data necessary. The trigger delay has been determined after the measurement campaign and the profiles have been corrected accordingly. It had to be concluded that the measurements at 532 nm could not be used at all due to a non-correct alignment of the 532 nm laser beam to the receiving telescope axis and therefore the intercomparisons were restricted to 355 nm.
These measurements from September 28 and 29 show fairly good agreement, especially in the far

Lidar intercomparisons: MIM/AUTH				
Date [UT]	Quantity	height range [m]	mean dev. $[(\mathrm{m} \cdot \mathrm{sr})^{-1}]$	standard dev. $[(\mathrm{m} \cdot \mathrm{sr})^{-1}]$
2000/09/22 18:10 - 18:15 UT	532 nm bsc.	1200 - 4000	$0.5 \cdot 10^{-7}$ / 2.2%	$2.1 \cdot 10^{-7}$ / 9.5 %
	532 nm bsc.	4300 - 7000	$0.2 \cdot 10^{-7}$	$0.4 \cdot 10^{-7}$
2000/09/23 9:40 - 9:45 UT	532 nm bsc.	2000 - 3200	$0.1 \cdot 10^{-7}$ / 0.3%	$3.6 \cdot 10^{-7}$ / 19.2 %
	532 nm bsc.	3400 - 6500	$0.2 \cdot 10^{-7}$	$0.4 \cdot 10^{-7}$
2000/09/23 10:05 - 10:25 UT	532 nm bsc.	2000 - 3300	$1.8 \cdot 10^{-7}$ / 10.6%	$2.4 \cdot 10^{-7}$ / 13.8 %
	532 nm bsc.	3400 - 7000	$0.0 \cdot 10^{-7}$	$0.3 \cdot 10^{-7}$
2000/09/23 11:20 - 11:50 UT	532 nm bsc.	2000 - 3000	$1.4 \cdot 10^{-7}$ / 8.9%	$1.6 \cdot 10^{-7}$ / 10.5 %
	532 nm bsc.	3300 - 7000	$0.3 \cdot 10^{-7}$	$0.4 \cdot 10^{-7}$

Table 4.7: Mean deviations and standard deviations for four intercomparisons between the MIM and the AUTH lidar at 532 nm.

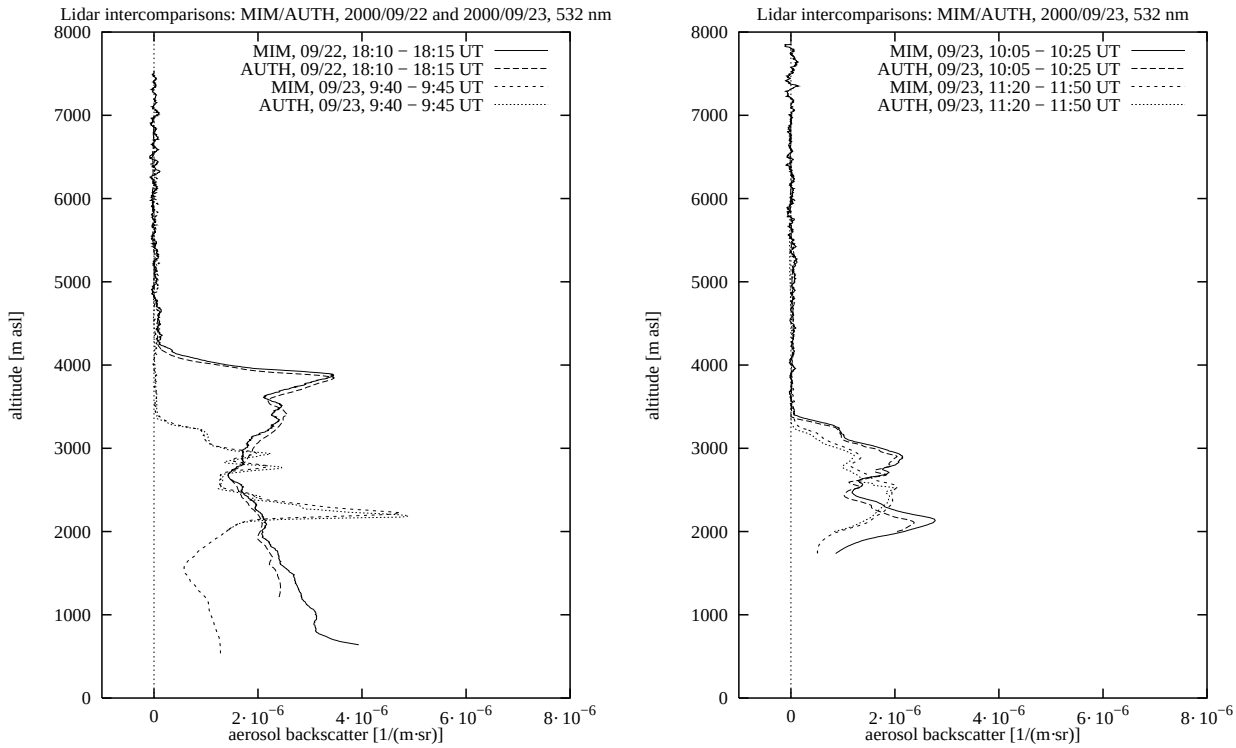

Figure 4.3: Intercomparison of aerosol backscatter profiles at 532 nm between MIM and AUTH perfomed on September 22 and 23, 2000.

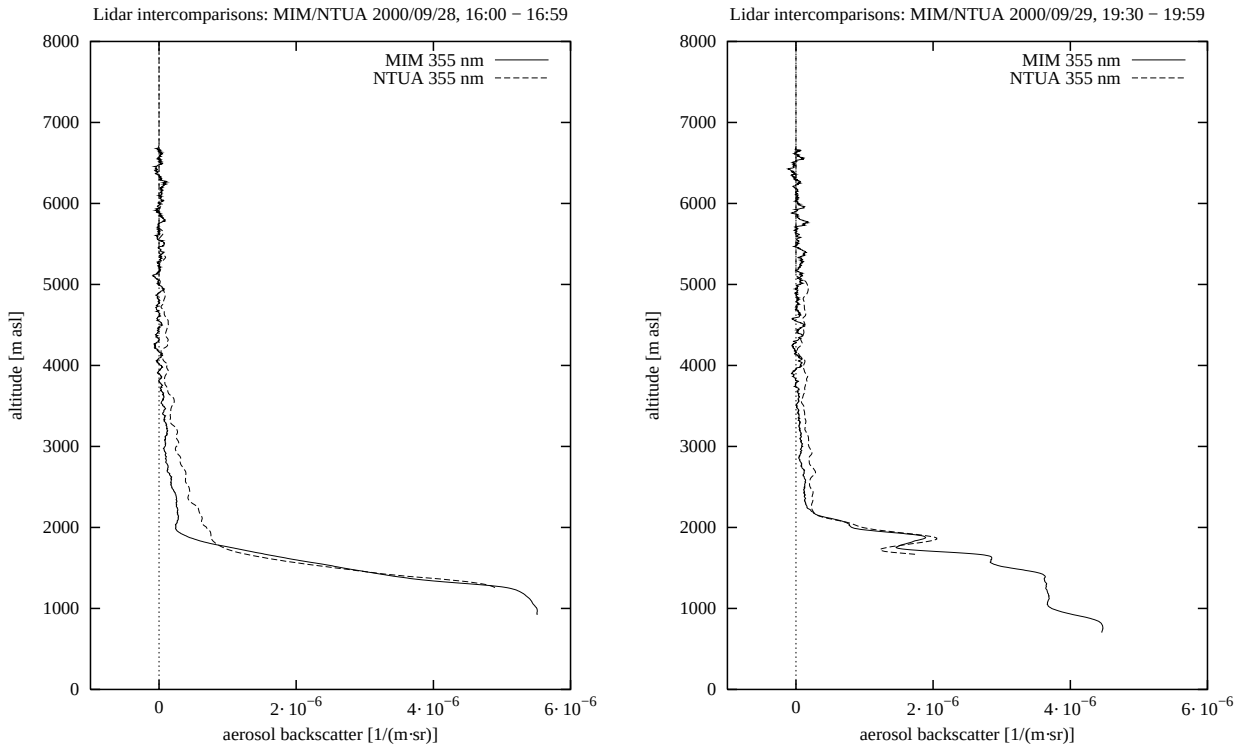

Figure 4.4: Intercomparison of aerosol backscatter profiles at 355 nm between MIM and NTUA performed on September 28 and 29, 2000.

Lidar intercomparisons: MIM/NTUA				
Date [UT]	Quantity	height range [m]	mean dev. $[(\mathrm{m}\cdot\mathrm{sr})^{-1}]$	standard dev. $[(\mathrm{m}\cdot\mathrm{sr})^{-1}]$
2000/09/28	355 nm bsc.	1250 - 1800	$0.6\cdot10^{-7}$ / 2.1%	$2.2\cdot10^{-7}$ / 8.4 %
16:00 - 16:59 UT	355 nm bsc.	2000- 6700	$1.0\cdot10^{-7}$	$1.4\cdot10^{-7}$
2000/09/29	355 nm bsc.	1700 - 2100	$0.2\cdot10^{-7}$ / 1.8%	$2.2\cdot10^{-7}$ / 16.1 %
19:30 - 19:59 UT	355 nm bsc.	2300 - 5000	$1.0\cdot10^{-7}$	$1.1\cdot10^{-7}$

Table 4.8: Mean deviations and standard deviations for two intercomparisons between the MIM and the NTUA lidar at 355 nm (note a 27° difference between the pointing angles of the lidar systems). Measurements are from September 28 and 29, 2000.

Lidar intercomparisons: MIM/INFM(L)				
Date [UT]	Quantity	height range [m]	mean dev. $[(\mathrm{m}\cdot\mathrm{sr})^{-1}]$	standard dev. $[(\mathrm{m}\cdot\mathrm{sr})^{-1}]$
2000/10/05	351/355 nm bsc.	400 - 3100	$0.4\cdot10^{-7}$ / 2.5%	$3.5\cdot10^{-7}$ / 23.7 %
14:58 - 15:07 UT	351/355 nm bsc.	3500 - 6500	$-1.9\cdot10^{-7}$	$5.0\cdot10^{-7}$
2000/10/05 15:57 - 16:08 UT	351/355 nm bsc.	350 - 3100	$0.3\cdot10^{-7}$ / 1.6 %	$2.7\cdot10^{-7}$ / 15.4 %
2000/10/05	351/355 nm bsc.	400 - 2200	$-3.0\cdot10^{-7}$ / -13.1%	$4.9\cdot10^{-7}$ / 21.4 %
23:43 - 23:46 UT	351/355 nm bsc.	3000 - 8500	$-0.7\cdot10^{-7}$	$5.0\cdot10^{-7}$

Table 4.9: Mean deviations and standard deviations for three intercomparisons between the MIM and the INFM(L) lidar at 355 nm and 351 nm, respectively.

range, taking into account a 27° difference in the pointing angle between the two lidar systems (see Fig. 4.4 and Table 4.8). Since the PBL was rather low at Athens those days, only few points with higher aerosol backscatter could be compared.
The mentioned problems are typical for a situation where major changes in a lidar system are made. They have been solved in the meantime (i.e. correct trigger set-up, insertion of neutral density filters, telescope fiber realignment) and the lidar is fully operable now. The intercomparisons helped much at this point to determine and solve all problems quickly.

MIM/INFM(L)

Due to bad weather conditions, all measurements shown here were performed on a single day. However, there was some change of the aerosol load in the atmosphere especially between 1000 m and 3000 m and the absolute values were sufficiently high to have good intercomparisons.
In all cases the mean deviations are quite small, although the standard deviations reach the limits in some cases (Fig. 4.5 and 4.6 and Table 4.9). This is caused by the statistical errors of the INFM(L) system, which especially in altitudes above ca. 2000 m, are significantly higher than those of the MIM system. In high altitudes, the Italian system switches from analog to photon counting detection, which allows to cover a large range of signal dynamics but reduces the possible temporal and spatial resolution. Since the profiles shown here are averaged over 10 minutes and 60 m only, there is still room for an improvement of the statistical error. Routine measurements are usually averaged over 30 minutes in time. The cirrus case on October 5, 23:43 - 23:46 UT (Fig. 4.6) demonstrates good agreement in height determination although the absolute backscatter values in the cirrus cloud have significant differences. This is believed to be caused by specular reflections of the ice crystals which can be of substantial effect if the lidar systems have slightly different observation angles.

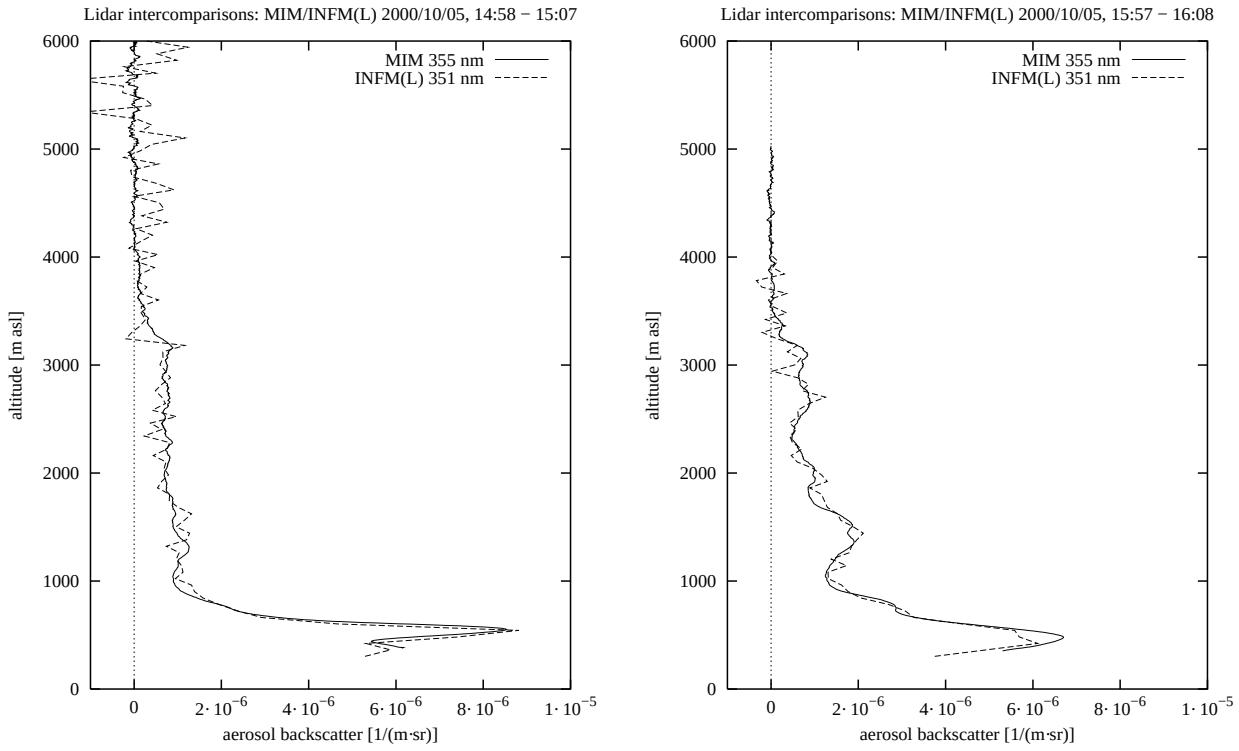

Figure 4.5: Intercomparison of aerosol backscatter profiles at 351 nm and 355 nm, respectively, between MIM and INFM(L) on October 5, 2000, 14:58 - 15:07 and 15:57 - 16:08 UT.

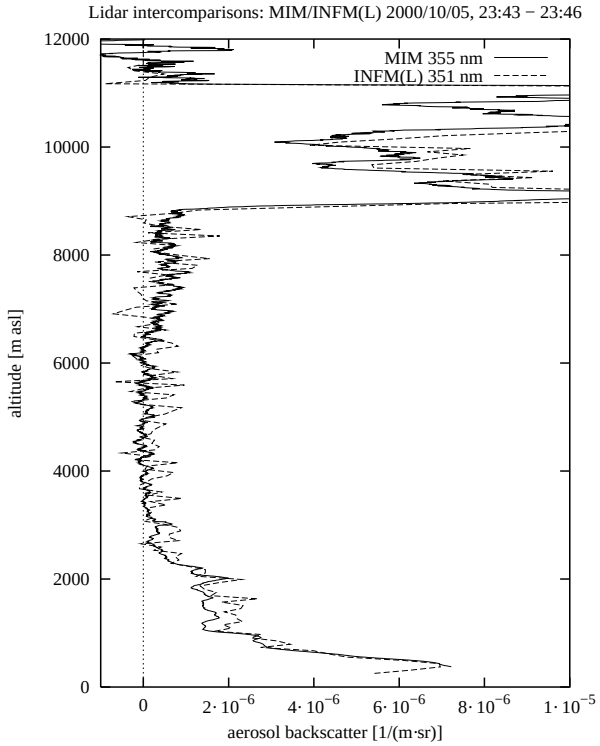

Figure 4.6: Intercomparison of aerosol backscatter profiles at 351 nm and 355 nm, respectively, between MIM and INFM(L) on October 15, 2000.

Lidar intercomparisons: MIM/INFM(P)				
Date [UT]	Quantity	height range [m]	mean dev. $[(\mathrm{m}\cdot\mathrm{sr})^{-1}]$	standard dev. $[(\mathrm{m}\cdot\mathrm{sr})^{-1}]$
2000/10/10 16:20 - 17:02 UT	355 nm bsc.	1800 - 2500	$-2.1\cdot10^{-7}$ / -14.1%	$2.8\cdot10^{-7}$ / 19.0 %
	355 nm bsc.	3000 - 7000	$-0.2\cdot10^{-7}$	$0.7\cdot10^{-7}$
2000/10/10 16:20 - 17:02 UT	532 nm bsc.	1800 - 2500	$-0.3\cdot10^{-7}$ / -3.2%	$-0.7\cdot10^{-7}$ / 8.3 %
	532 nm bsc.	3000 - 7000	$0.1\cdot10^{-7}$	$0.3\cdot10^{-7}$
2000/10/11 10:21 - 10:28 UT	355 nm bsc.	1800 - 3500	$-0.6\cdot10^{-7}$ / -3.8%	$2.0\cdot10^{-7}$ / 12.7 %
	355 nm bsc.	4000 - 5500	$0.3\cdot10^{-7}$	$2.2\cdot10^{-7}$
2000/10/11 10:21 - 10:28 UT	532 nm bsc.	1800 - 3500	$-0.2\cdot10^{-7}$ / -2.7%	$0.7\cdot10^{-7}$ / 8.1 %
	532 nm bsc.	4000 - 9000	$-0.1\cdot10^{-7}$	$0.8\cdot10^{-7}$
2000/10/11 11:58 - 12:02 UT	355 nm bsc.	1700 - 3500	$-0.3\cdot10^{-7}$ / -1.8%	$1.4\cdot10^{-7}$ / 8.0 %
	355 nm bsc.	4000 - 5000	$0.3\cdot10^{-7}$	$3.0\cdot10^{-7}$
2000/10/11 11:58 - 12:02 UT	532 nm bsc.	1700 - 3500	$-0.4\cdot10^{-7}$ / -4.1%	$1.1\cdot10^{-7}$ / 12.5 %
	532 nm bsc.	4000 - 7500	$-0.1\cdot10^{-7}$	$1.4\cdot10^{-7}$

Table 4.10: Mean deviations and standard deviations for three intercomparisons between the MIM and the INFM(P) lidar at 355 nm and 532 nm.

MIM/INFM(P)

Three intercomparisons from two days in October 2000 are shown here. The measurements suffered from bad weather conditions, therefore only on October 10 a 40 minutes average could be taken. The following day, only shorter periods in cloud gaps were used for the intercomparisons. Potenza is in 820 m above sea level (asl), the lowest point with full overlap was in ca. 1000 m above ground level, so the measurements have been compared at altitudes above ca. 1800 m asl.
At both wavelengths only minor deviations between the systems have been detected (Fig. 4.7 and 4.8 and Table 4.10). The lowest measurement heights were mostly affected by some smaller differences which could be due to overlap effects or due to detector non-linearities. However, they remain small and don't affect the good performance both systems showed during this intercomparison.

MIM/INFM(N)

Three days with quite different weather conditions could be used for the intercomparisons between MIM and INFM(N). Both systems usually have full overlap at altitudes around 400 m, but on October

Lidar intercomparisons: MIM/INFM(N)				
Date [UT]	Quantity	height range [m]	mean dev. $[(\mathrm{m}\cdot\mathrm{sr})^{-1}]$	standard dev. $[(\mathrm{m}\cdot\mathrm{sr})^{-1}]$
2000/10/13 14:12 - 14:26 UT	351/355 nm bsc.	1100 - 5000	$-0.3\cdot10^{-7}$ / -1.1%	$2.2\cdot10^{-7}$ / 7.3 %
2000/10/14 11:02 - 11:12 UT	351/355 nm bsc.	550 - 4700	$0.4\cdot10^{-7}$ / 4.8 %	$2.0\cdot10^{-7}$ / 24.4 %
	351/355 nm bsc.	5000 -9400	$1.9\cdot10^{-7}$	$6.6\cdot10^{-7}$
2000/10/16 8:20 - 8:30 UT	351/355 nm bsc.	450 - 2600	$0.8\cdot10^{-7}$ / 6.5%	$1.3\cdot10^{-7}$ / 10.4 %
	351/355 nm bsc.	2800 - 3500	$0.0\cdot10^{-7}$	$1.0\cdot10^{-7}$

Table 4.11: Mean deviations and standard deviations for three intercomparisons between the MIM and the INFM(N) lidar at 355 nm and 351 nm, respectively.

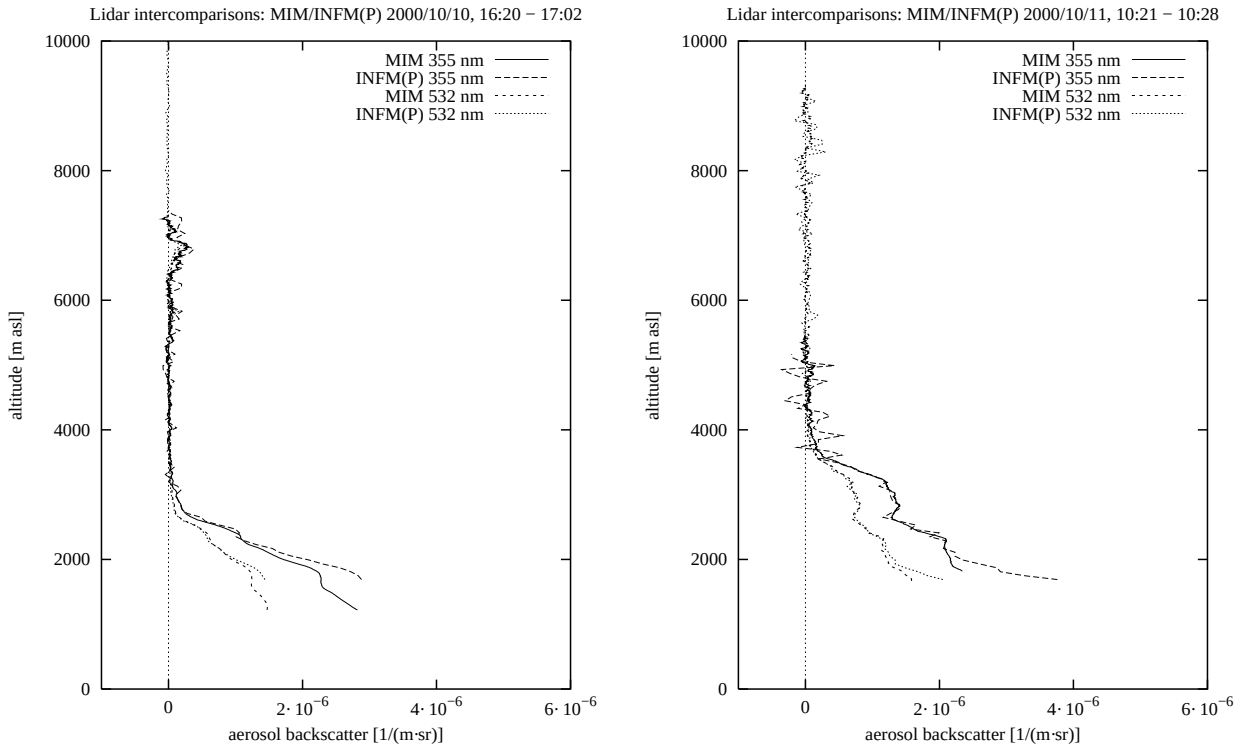

Figure 4.7: Intercomparison of aerosol backscatter profiles at 355 nm and 532 nm between MIM and INFM(P) on October 10 and 11, 2000.

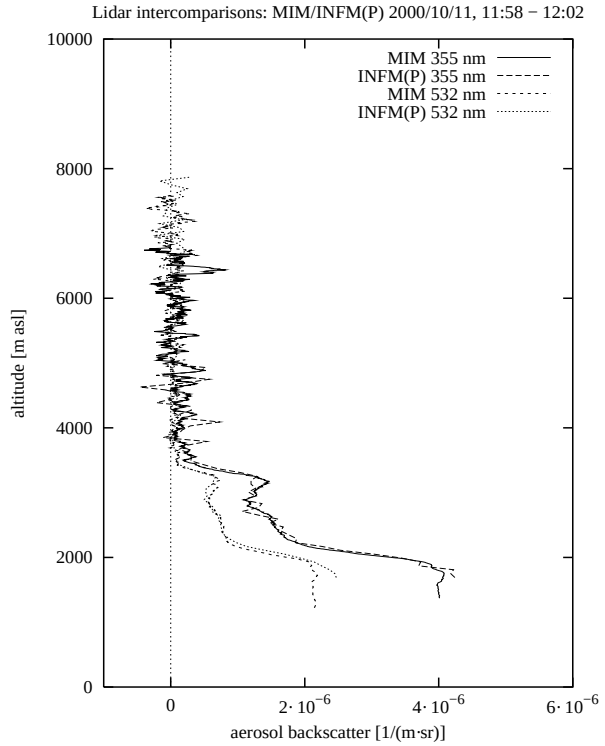

Figure 4.8: Intercomparison of aerosol backscatter profiles at 355 nm and 532 nm between MIM and INFM(P) on October 11, 2000.

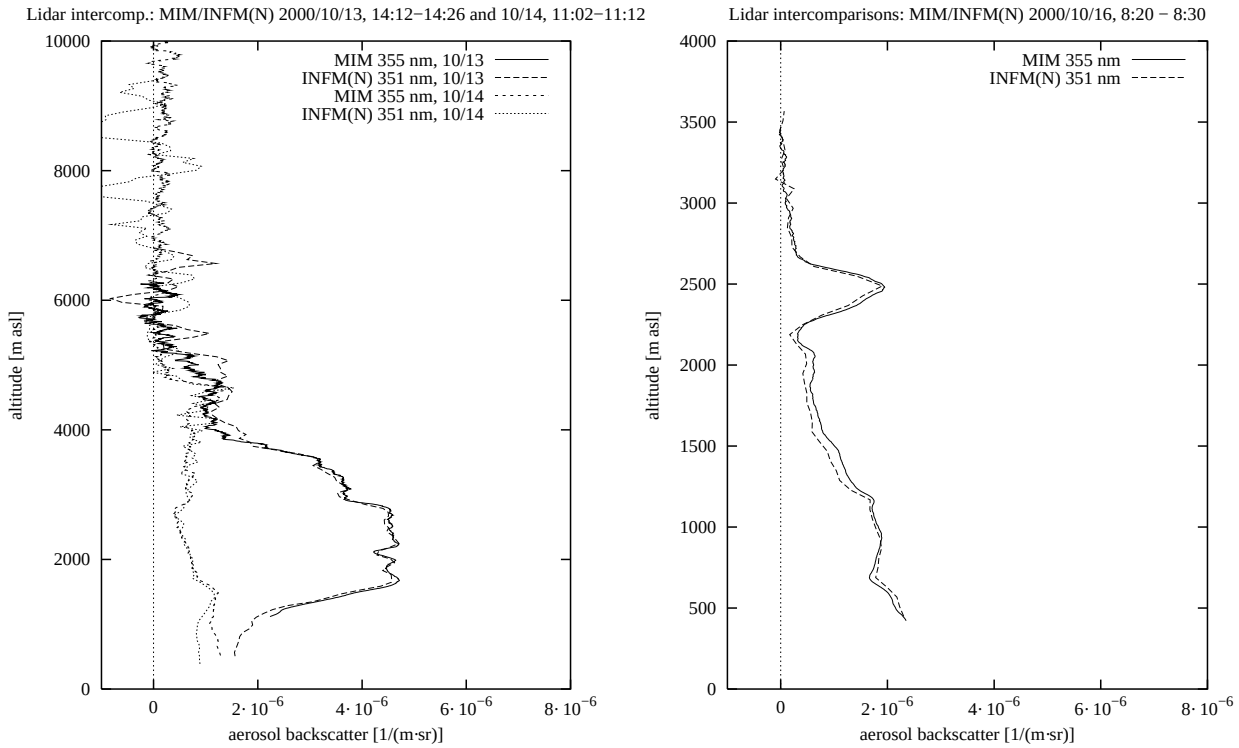

Figure 4.9: Intercomparison of aerosol backscatter profiles at 351 nm and 355 nm, respectively, between MIM and INFM(N) on October 13, 14 and 16, 2000.

13 the Munich system delivered data at altitudes above 1000 m only due to a small misalignment of the photomultiplier used at 355 nm. The differences between the measured aerosol profiles are very small (Fig. 4.9 and Table 4.11). The high standard deviation within the boundary layer on October 14 is due to the low backscatter values (less than $1 \cdot 10^{-6}(\mathrm{m} \cdot \mathrm{sr})^{-1}$), the absolute deviation stays well below the limits. At high altitudes the signal statistics of the INFM(N) system leads to a high standard deviation. Again appropriate averaging can improve those results.

Lidar intercomparisons: MIM/ULAQ				
Date [UT]	Quantity	height range [m]	mean dev. $[(\mathrm{m} \cdot \mathrm{sr})^{-1}]$	standard dev. $[(\mathrm{m} \cdot \mathrm{sr})^{-1}]$
2000/10/17	351/355 nm bsc.	1500 - 3000	$-1.0 \cdot 10^{-7}$ / -14.0%	$2.3 \cdot 10^{-7}$ / 32.6 %
21:13 - 21:19 UT	351/355 nm bsc.	3000 - 5000	$-1.2 \cdot 10^{-7}$	$3.1 \cdot 10^{-7}$
2000/10/18	351/355 nm bsc.	1000 - 3000	$1.7 \cdot 10^{-7}$ / 12.3%	$4.2 \cdot 10^{-7}$ / 31.1 %
20:29 - 21:23 UT	351/355 nm bsc.	3200 - 5000	$0.2 \cdot 10^{-7}$	$1.1 \cdot 10^{-7}$
2000/10/19	351/355 nm bsc.	1000 - 2500	$-1.7 \cdot 10^{-7}$ / -5.1%	$4.0 \cdot 10^{-7}$ / 11.6 %
18:41 - 19:12 UT	351/355 nm bsc.	2700 - 7400	$-1.7 \cdot 10^{-7}$	$4.2 \cdot 10^{-7}$
	351/355 nm bsc.	7600 - 11700	$-19.7 \cdot 10^{-7}$ / -48.1 %	$31.0 \cdot 10^{-7}$ / 75.6 %

Table 4.12: Mean deviations and standard deviations for three intercomparisons between the MIM at 355 nm and the ULAQ lidar at 351 nm.

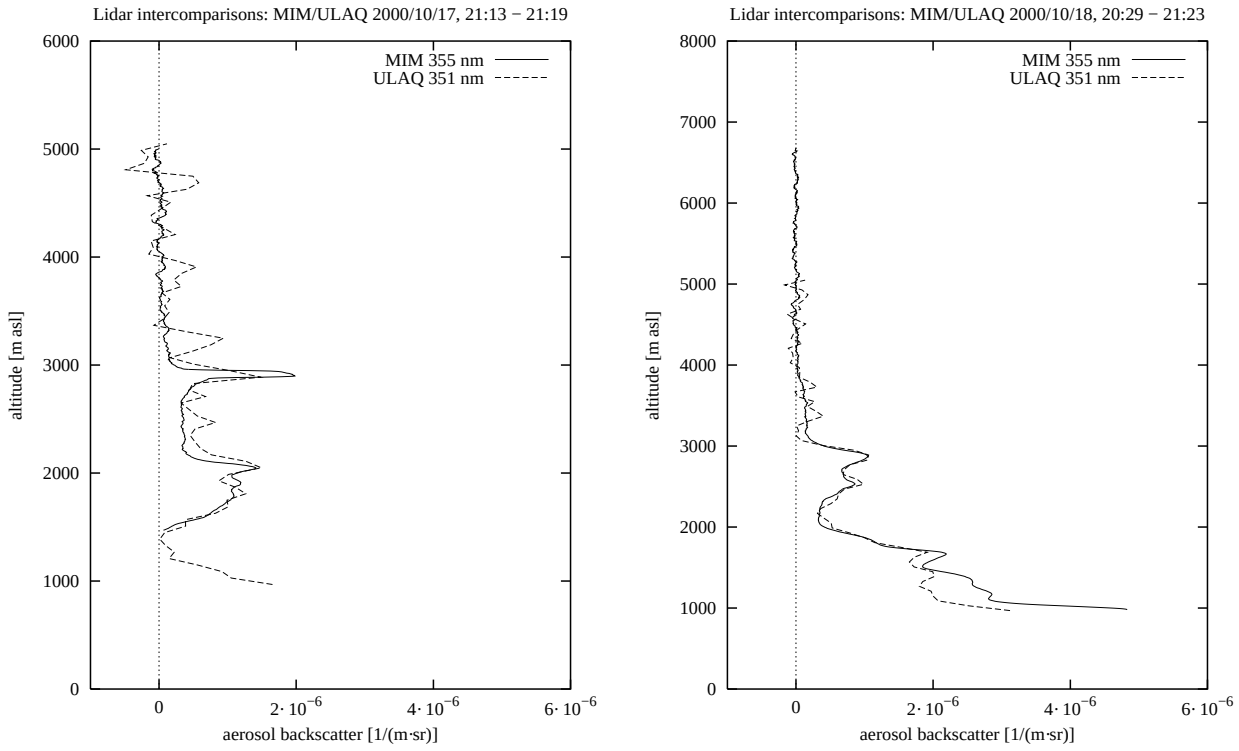

Figure 4.10: Intercomparison of aerosol backscatter profiles at 351 nm and 355 nm, respectively, between MIM and ULAQ on October 17 and 18, 2000.

MIM/ULAQ

The main difference between the systems of Munich and the University of L'Aquila is that the Italian system is designed for the upper troposphere. Aerosol backscatter profiles down to altitudes within the planetary boundary layer can only be derived by using the additional Raman channel. Using equation 2.9 for the determination of the aerosol backscatter profiles out of simultaneous elastic and Raman measurements, the overlap function cancels in the equations and the backscatter profile can be derived also in regions of incomplete overlap.
However, this restricts measurements to nighttime and makes intercomparisons with a pure elastic lidar system difficult. The lidar ratio, which has to be assumed in the calculation of aerosol backscatter profiles from elastic lidar returns, is included in the quotient of elastic and Raman signals and can only be derived for altitudes with full overlap. In this case full overlap is only given at altitudes above 4000 m. Additionally, the lidar ratio is usually chosen constant with height for the evaluation of the pure elastic backcatter with the Klett-algorithm since no information on the lidar ratio is available, while the implicit lidar ratio will in almost all cases be changing with height. The given numbers for the calculated deviations are in this case just a more or less accurate estimate (Table 4.12).
Due to the low Raman signal, high statistical errors in the upper range can be seen in the aerosol profile from ULAQ if the averaged episode is relatively short like on October 17, where only 6 minutes are available between 21:13 and 21:19 UT (Fig. 4.10, left side). This is improved in the other examples from the two following days (Fig. 4.10, right side, and Fig. 4.11). On October 19, the low cloud in the aerosol profile has been skipped for the intercomparison. In the cirrus clouds, the deviations have been calculated, however, these values are not comparable with the demands on aerosol profiles, because cirrus can be fairly inhomogeneous even for two lidar systems located very close together.

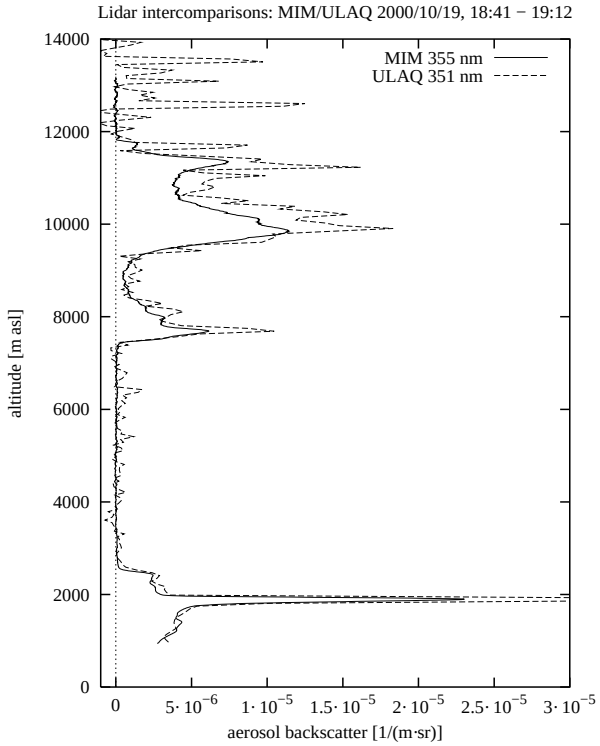

Figure 4.11: Intercomparison of aerosol backscatter profiles at 351 nm and 355 nm, respectively, between MIM and ULAQ on October 19, 2000.

MIM/IFU

Both systems operate at the three wavelengths 355 nm, 532 nm and 1064. Because Garmisch is not very far from Munich and both systems are mobile, the Garmisch system travelled two times to Munich to perform simultaneous measurements with the MIM system. The first two intercomparisons took place in winter and were characterized by low aerosol backscatter coefficients, so they couldn't fulfill the requirement of having at least moderate aerosol content in the planetary boundary layer (see chapter 4.2). Enhanced aerosol was present during the third day (July 6) which was, therefore, used for the final evaluation. The Garmisch system stored data every 7 minutes. Here, profiles for 355 nm and 532 nm are shown (Fig. 4.13). The agreement at 532 nm is excellent, at 355 nm the measurements also agree well but suffered a little from having taken place during the brightest period

Lidar intercomparisons: MIM/IFU				
Date [UT]	Quantity	height range [m]	mean dev. $[(\mathrm{m}\cdot\mathrm{sr})^{-1}]$	standard dev. $[(\mathrm{m}\cdot\mathrm{sr})^{-1}]$
2001/07/06	355 nm bsc.	1000 - 5000	$-0.2\cdot10^{-7}$ / -1.0%	$4.9\cdot10^{-7}$ / 23.0 %
14:04 - 14:11 UT	355 nm bsc.	5300 - 6200	$-0.4\cdot10^{-7}$	$-13.0\cdot10^{-7}$
2001/07/06	532 nm bsc.	800 - 5000	$-0.1\cdot10^{-7}$ / -1.6%	$0.8\cdot10^{-7}$ / 10.8 %
12:07 - 12:13 UT	532 nm bsc.	5500 - 6400	$-0.4\cdot10^{-7}$	$-2.2\cdot10^{-7}$
2001/07/06	532 nm bsc.	800 - 5000	$0.1\cdot10^{-7}$ / 1.2%	$0.9\cdot10^{-7}$ / 8.9 %
13:20 - 13:27 UT	532 nm bsc.	5500 - 7000	$0.2\cdot10^{-7}$	$1.9\cdot10^{-7}$

Table 4.13: Mean deviations and standard deviations for three intercomparisons between the MIM and the IFU lidar at 355 nm and 532 nm.

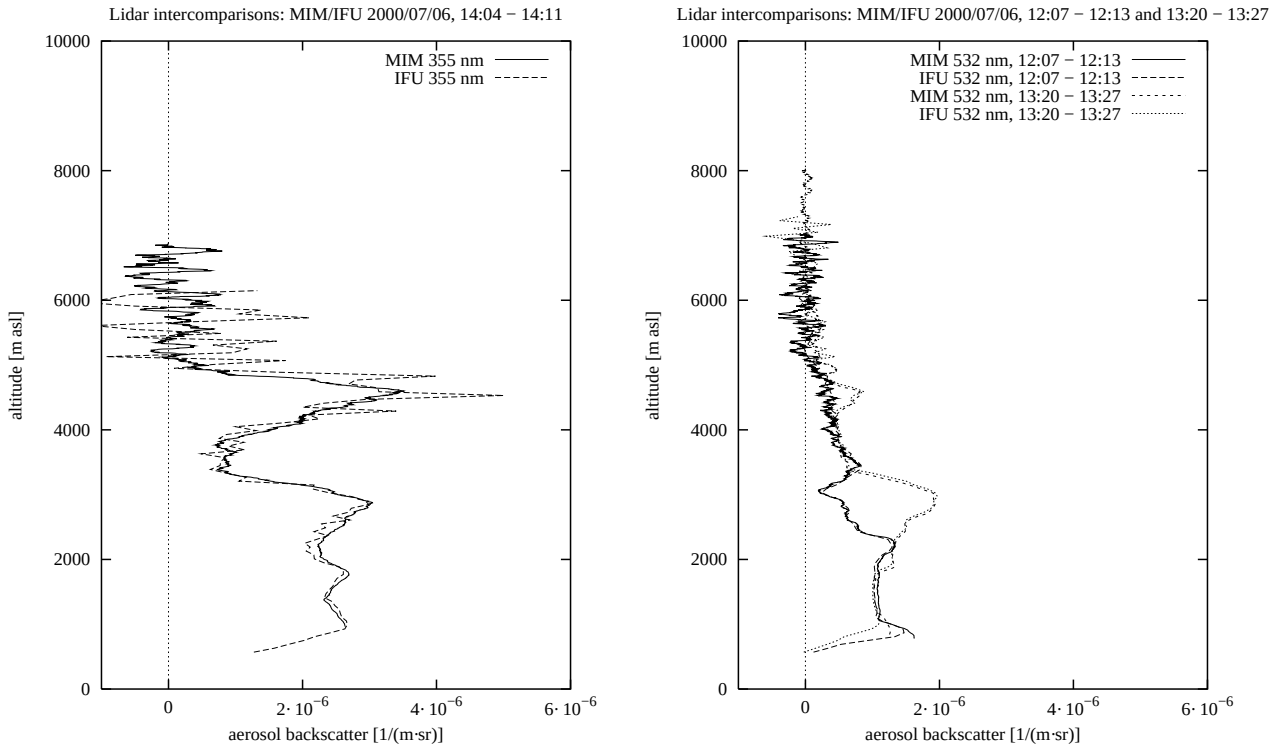

Figure 4.12: Intercomparison of aerosol backscatter profiles at 355 nm and 532 nm between MIM and IFU.

of that summer day, resulting in enhanced noise due to background light. At that wavelength a rather broadband interference filter is still used. The implementation of better spectral filtering is under way and is expected to improve the signal-to-noise ratio substantially. However, with appropriate averaging in time and space the present statistical errors can also be reduced significantly.

MPI/OCN

The three wavelength aerosol Raman lidar of the MPI Hamburg has been compared to the micro lidar of the Observatoire Cantonal Neuchatel (OCN) in September 2000 in Palaiseau. The micro lidar is emitting at very high repetition rates (11 kHz) and very low pulse energy ($\approx 1\mu$J) at 532 nm. Due to this low pulse energy it is limited in range at daytime. Two of the intercomparison episodes are at

Lidar intercomparisons: MPI/OCN				
Date [UT]	Quantity	height range [m]	mean dev. $[(\mathrm{m}\cdot\mathrm{sr})^{-1}]$	standard dev. $[(\mathrm{m}\cdot\mathrm{sr})^{-1}]$
2000/09/11	532 nm bsc.	400 - 1300	$3.4\cdot10^{-7}$ / 33.3%	$3.7\cdot10^{-7}$ / 36.9 %
19:40 - 20:00 UT	532 nm bsc.	2000 - 9800	$0.2\cdot10^{-7}$	$0.5\cdot10^{-7}$
2000/09/13	532 nm bsc.	300 - 2400	$0.2\cdot10^{-7}$ / 1.5 %	$3.6\cdot10^{-7}$ / 21.9 %
14:51 - 15:08 UT	532 nm bsc.	2500 - 4700	$0.3\cdot10^{-7}$	$2.9\cdot10^{-7}$
2000/09/14	532 nm bsc.	300 - 1300	$-3.7\cdot10^{-7}$ / -17.9 %	$4.0\cdot10^{-7}$ / 19.3 %
20:30 - 21:00 UT	532 nm bsc.	1500 - 9000	$0.3\cdot10^{-7}$	$0.5\cdot10^{-7}$

Table 4.14: Mean deviations and standard deviations for three intercomparisons between the MPI and the OCN lidar at 532 nm.

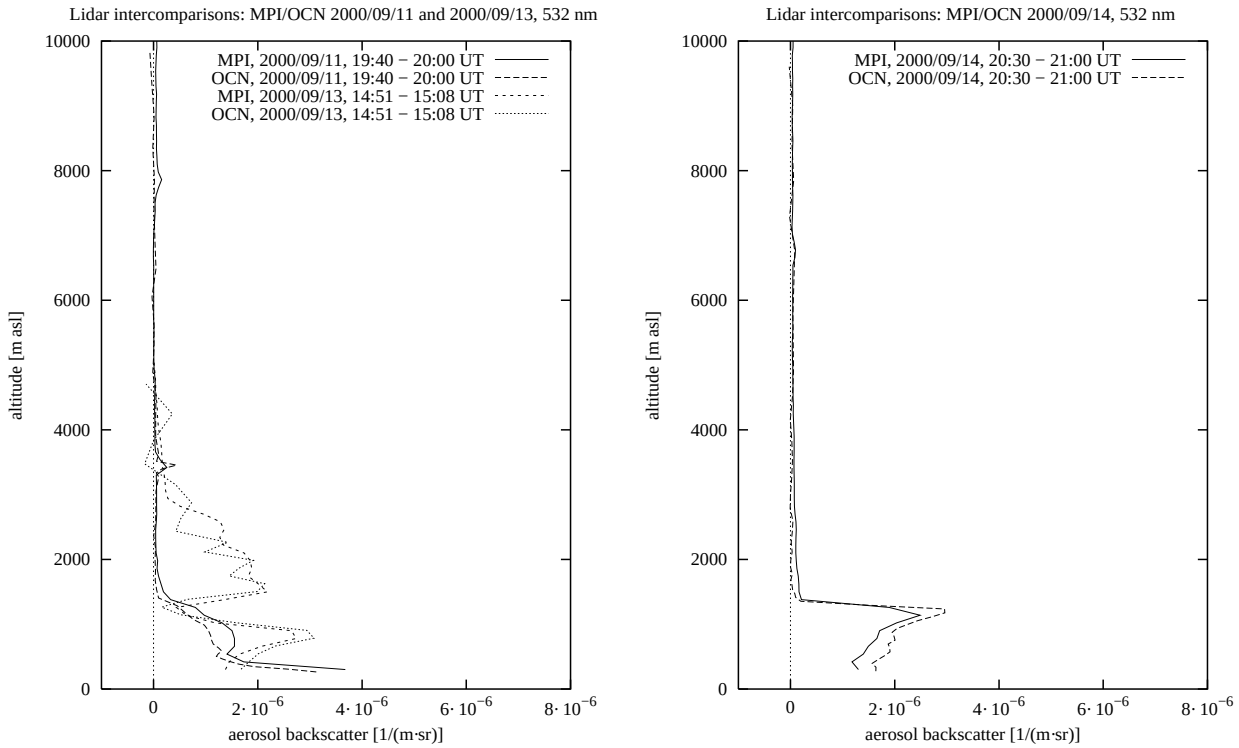

Figure 4.13: Intercomparison of aerosol backscatter profiles at 532 nm between MPI and OCN.

nighttime when profiles can be measured up to more than 9000 m. At daytime the micro lidar data can only be used with good accuracy up to 4000 - 5000 m. All absolute deviations are within the allowed limits, only on September 11 the relative error of the aerosol backscatter exceeds the limits because of the prevailing low backscatter (Fig. 4.13 and Table 4.14).

MPI/UPC

The lidar system of the Universidad Polytecnica de Catalunya, Barcelona, is operated as a backscatter lidar at 1064 nm. It also has been compared to the MPI system at Palaiseau. The measurement range is between 200 and 10000 m, however, in the far range the signal is getting weak due to the large dynamic range and the relatively small receiving telescope. This is the main reason for the deviations in the far range on September 11, but they still remain within the limits. On September 12 and 13, the intercomparison is restricted to the aerosol layer because the common calibration value had to be

Lidar intercomparisons: MPI/UPC				
Date [UT]	Quantity	height range [m]	mean dev. $[(\mathrm{m}\cdot\mathrm{sr})^{-1}]$	standard dev. $[(\mathrm{m}\cdot\mathrm{sr})^{-1}]$
2000/09/11	1064 nm bsc.	400 - 1300	$-0.3\cdot10^{-7}$ / -6.0%	$0.9\cdot10^{-7}$ / 22.2 %
20:05 - 20:20 UT	1064 nm bsc.	2000 - 9800	$-0.3\cdot10^{-7}$	$1.3\cdot10^{-7}$
2000/09/12 19:22 - 19:37 UT	1064 nm bsc.	900 - 4200	$-0.2\cdot10^{-7}$ / -8.3%	$0.7\cdot10^{-7}$ / 24.9 %
2000/09/13 14:51 - 15:08 UT	1064 nm bsc.	300 - 2500	$-0.4\cdot10^{-7}$ / -4.7%	$1.4\cdot10^{-7}$ / 17.3 %

Table 4.15: Mean deviations and standard deviations for three intercomparisons between the MPI and the UPC lidar at 1064 nm.

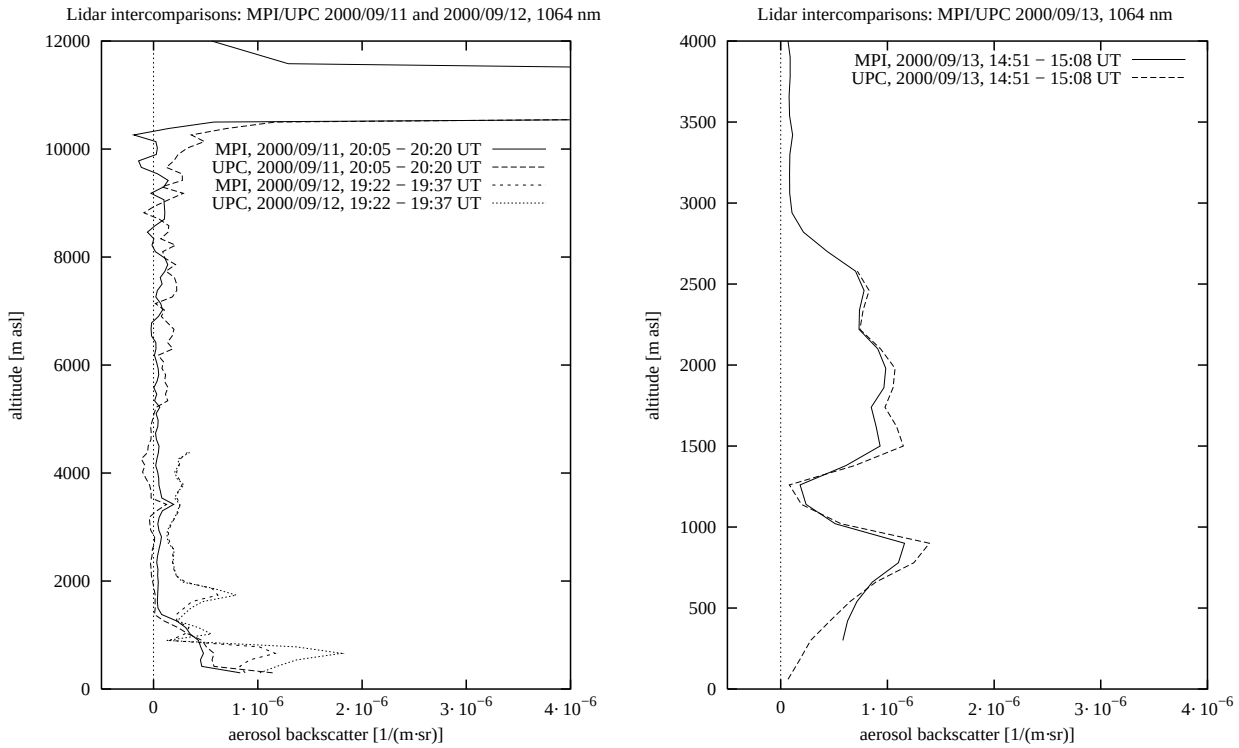

Figure 4.14: Intercomparison of aerosol backscatter profiles at 1064 nm between MPI and UPC.

chosen on top of this layer, where enough backscattered signal is detected. In the free troposphere the backscattered signal at 1064 nm is too weak to be distinguished from the background and high errors can be introduced when calibrating in that part of the atmosphere (see Fig. 4.14 and Table 4.15). The algorithm used by the UPC is only capable of iterating downward from the calibration point and therefore backscatter values are only given below the calibration height.
On September 12, additionally, values below 900 m have been skipped for the calculation of the deviations. Small parts of clouds influenced the signal at ca. 600 - 800 m, so the data in those heights could not be used. The unstable weather situation also was the main reason why only episodes of 15 minutes have been compared here, but this doesn't affect the results.

MPI/UABER

Both systems operate the 355 nm elastic channel as well as a nitrogen Raman channel at 387 nm, so aerosol extinction profiles could also be determined and compared. During this intercomparison, measurements have mostly been restricted to nighttime, because the Raman channels can only be operated with very low background light. Additionally, the elastic channels of the UABER lidar operate only in photon counting mode and therefore give best results during nighttime. Both systems had to deal with problems concerning data from their large far range telescope at 355 nm, so most of the profiles shown here are measured with a small near range telescope and limited in range. High standard deviations in the upper heights are due to the low signal level achieved with the small telescope.
On May 8, 2001, misalignment of the small telescope of UABER prevented comparisons in the range below 800 m. Above that height the standard deviation slightly exceeds the limits. Good agreement can be found for the average values of the extinction profiles in the PBL. The standard deviation shows high relative deviations of up to 35 %, but they stay within the predefined maximum absolute deviation of $1.0 \cdot 10^{-4}\mathrm{m}^{-1}$ (Fig. 4.15 and 4.15 and Table 4.16).

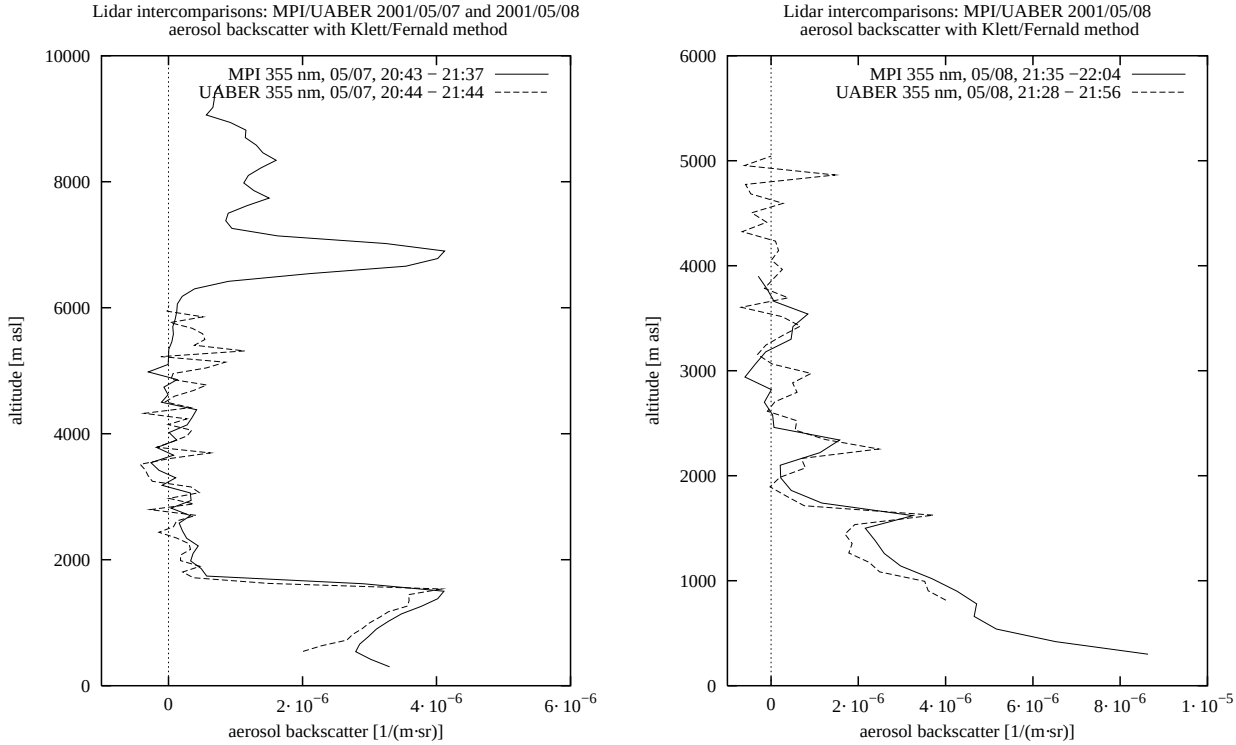

Figure 4.15: Intercomparison of aerosol backscatter profiles at 355 nm between MPI and UABER on May 6 and 7, 2001.

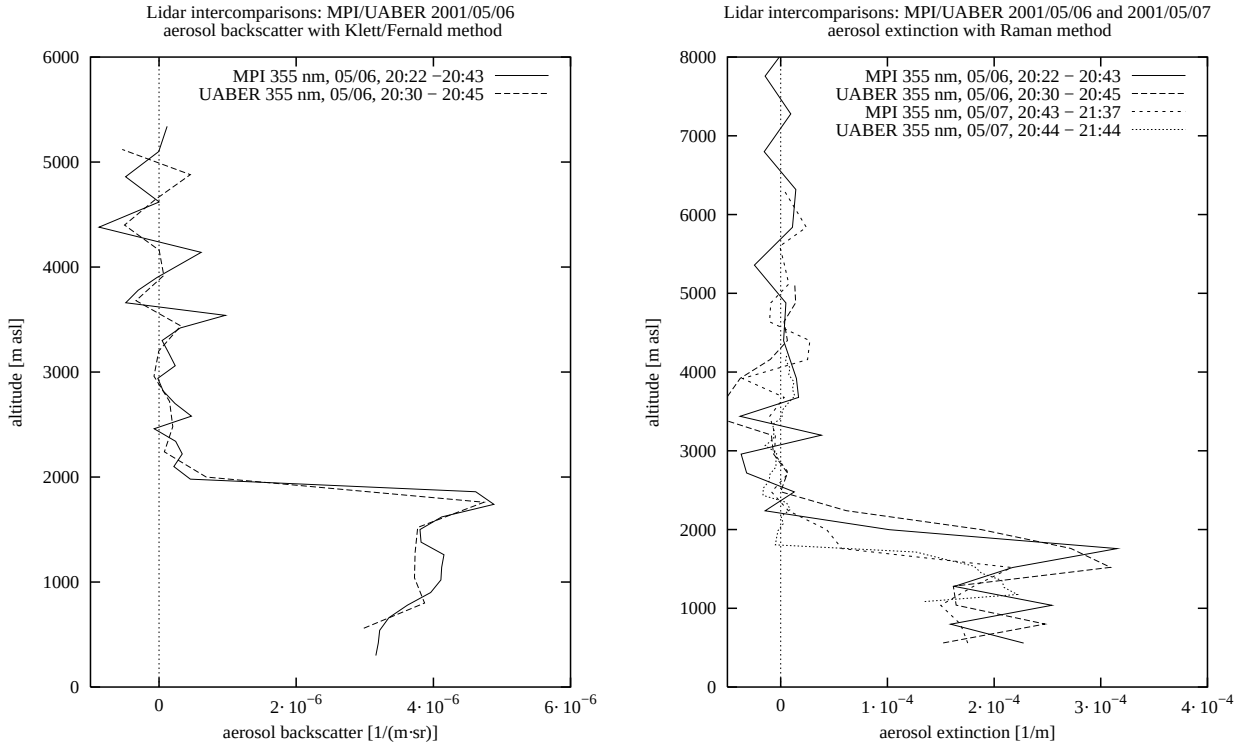

Figure 4.16: Intercomparison of aerosol backscatter profiles at 355 nm between MPI and UABER on May 8, 2001 and of aerosol extinction profiles on May 6 and 7, 2001.

Lidar intercomparisons: MPI/UABER				
Date [UT]	Quantity	height range [m]	mean dev. $[(\mathrm{m}\cdot\mathrm{sr})^{-1}]$	standard dev. $[(\mathrm{m}\cdot\mathrm{sr})^{-1}]$
2001/05/06	355 nm bsc.	500 - 1900	$1.7\cdot10^{-7}$ / 4.2%	$2.8\cdot10^{-7}$ / 7.2 %
20:30 - 20:45 UT	355 nm bsc.	2300 - 5000	$0.6\cdot10^{-7}$	$3.5\cdot10^{-7}$
2001/05/07	355 nm bsc.	500 - 1600	$3.0\cdot10^{-7}$ / 8.9 %	$4.1\cdot10^{-7}$ / 12.1 %
20:44 - 21:44 UT	355 nm bsc.	1800 -6000	$0.7\cdot10^{-7}$	$3.6\cdot10^{-7}$
2001/05/08	355 nm bsc.	800 - 1700	$4.9\cdot10^{-7}$ / 15.4%	$6.5\cdot10^{-7}$ / 20.4 %
21:28 - 21:56 UT	355 nm bsc.	2700 - 3900	$1.4\cdot10^{-7}$	$6.4\cdot10^{-7}$
Date [UT]	Quantity	height range [m]	mean dev. $[\mathrm{m}^{-1}]$	standard dev. $[\mathrm{m}^{-1}]$
2001/05/06	355 nm ext.	500 - 1800	$0.5\cdot10^{-5}$ / 2.1%	$7.9\cdot10^{-5}$ / 35.5 %
20:30 - 20:45 UT	355 nm ext.	2400 - 5000	$1.3\cdot10^{-5}$	$3.6\cdot10^{-5}$
2001/05/07	355 nm ext.	1100 - 1800	$-0.04\cdot10^{-5}$ / -0.2%	$3.2\cdot10^{-5}$ / 20.8 %
20:44 - 21:44 UT	355 nm ext.	2400 - 4000	$-0.6\cdot10^{-5}$	$2.1\cdot10^{-5}$

Table 4.16: Mean deviations and standard deviations for the intercomparison of aerosol backscatter and extinction profiles between the MPI and the UABER lidar at 355 nm.

Besides the good agreement of the measured profiles, the intercomparison was also successful in determining an adjustment error of the big telescope of UABER which could be corrected after the experiment. The delivered data from this station are now expected to be improved.

MPI/FOA

The experiment has been done with a new setup of the FOA lidar system. The beam/telescope configuration has been changed from a coaxial to a biaxial system. First measurements on August 20, 2001 showed a full overlap of the FOA lidar in ca. 1200 m. The agreement with the MPI lidar was good, only a small difference in height has been found (Fig. 4.17). The deviations between the profiles would be significantly lower when shifting the FOA profile ca. 50 m in height. The reason for the height difference could be determined later (the heightscale has been shifted after averaging), but the data have not been changed here (Table 4.17).

For the measurements on August 22 and August 23 the field of view of the FOA telescope has been increased from 0.7 mrad to 1.0 mrad. Now the lowest usable altitude was ca. 1000 m. The measured profiles agreed well also under changed conditions with aerosols up to 4000 m asl. Because the FOA algorithm is still under development, the FOA data has been evaluated with a MPI algorithm using same lidar ratio and calibration values.

Lidar intercomparisons: MPI/FOA				
Date [UT]	Quantity	height range [m]	mean dev. $[(\mathrm{m}\cdot\mathrm{sr})^{-1}]$	standard dev. $[(\mathrm{m}\cdot\mathrm{sr})^{-1}]$
2001/08/20	355 nm bsc.	1200 - 2400	$1.2\cdot10^{-7}$ / 10.7%	$3.0\cdot10^{-7}$ / 26.5 %
15:27 - 15:38 UT	355 nm bsc.	2800 - 5000	$-0.7\cdot10^{-7}$	$1.3\cdot10^{-7}$
2000/08/22	355 nm bsc.	1000 - 2300	$2.3\cdot10^{-7}$ / 9.2 %	$4.8\cdot10^{-7}$ / 19.0 %
18:31 - 18:36 UT	355 nm bsc.	2800 -5500	$1.4\cdot10^{-7}$	$1.9\cdot10^{-7}$
2001/08/23	355 nm bsc.	1000 - 3800	$0.8\cdot10^{-7}$ / 4.0%	$3.2\cdot10^{-7}$ / 16.1 %
9:39 - 10:07 UT	355 nm bsc.	4200 - 5500	$0.5\cdot10^{-7}$	$0.6\cdot10^{-7}$

Table 4.17: Mean deviations and standard deviations for the intercomparison of aerosol backscatter profiles between the MPI and the FOA lidar at 355 nm.

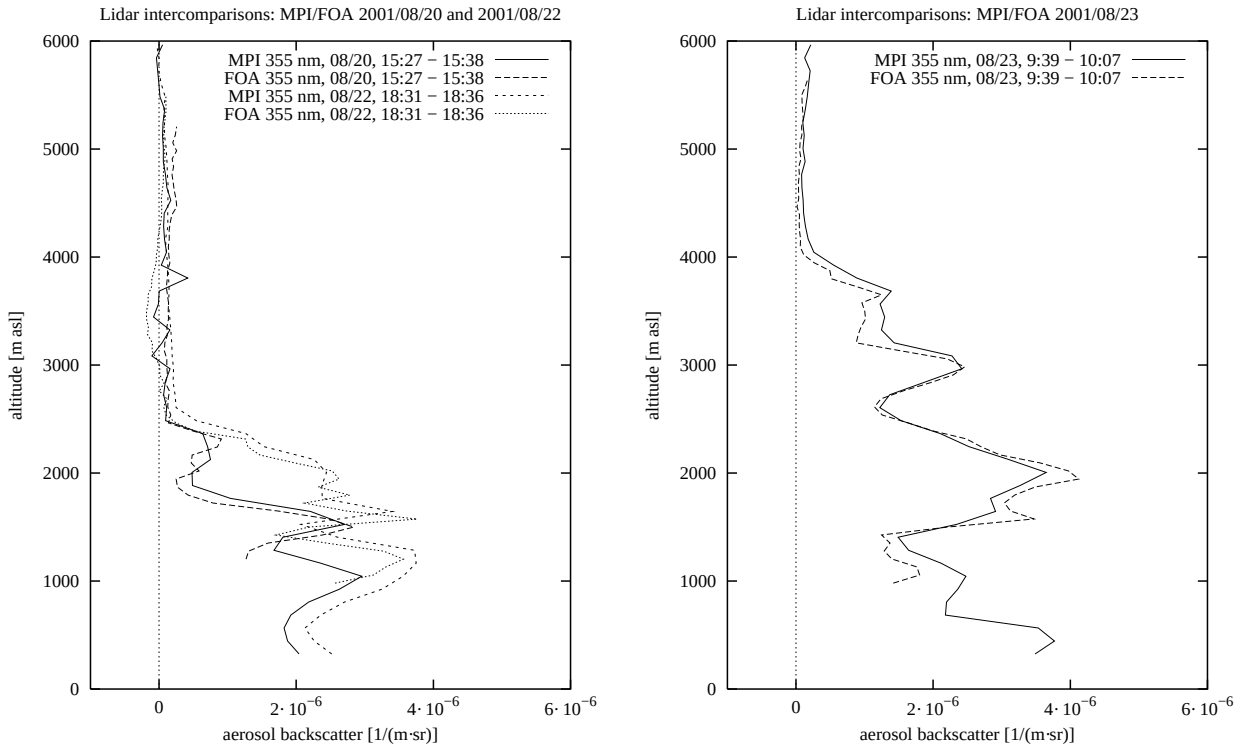

Figure 4.17: Intercomparison of aerosol backscatter profiles at 355 nm between MPI and FOA on August, 20, August 22 and August 23, 2001.

As a result of the experiment some changes in the configuration of the FOA system have been suggested. This includes the use of a larger field of view and a smaller distance between the transmitted beam and the telescope to achieve full overlap at lower range. This will be useful to get better coverage of the boundary layer which often extends to a few hundred meters only, in particular in winter. However, a tradeoff has to be made between the desired lower minimum range and the increased dynamic range of the signal and the increased noise due to background light.

OCN/EPFL

The lidar group of the Ecole Polytechnique Fédérale de Lausanne is running a three wavelength lidar system on top of the Jungfraujoch in 3580 m above sea level. This lidar system is installed for investigations of aerosol in the free troposphere and the stratosphere. Here usually very low aerosol extinction and backscatter is present, so most aerosol profiles will be very close to zero. The elastic channel at 532 nm is equipped with analog detection and photon counting detection to measure also very weak signals from the stratosophere. Both data acquisitions are running simultaneously and the signals can be compared to each other.

The top of the Jungfraujoch is difficult to reach with lots of equipment. Therefore it was decided to do the intercomparisons with the most compact system available within the EARLINET. The micro lidar of the Observatoire Cantonal de Neuchâtel is very small and can be easily transported. It has been compared to the MPI system in September 2000 with good results. Especially at nighttime the performance of the system is comparable to lidars with much more powerful lasers. However, the intercomparisons are restricted to elastic detection at 532 nm.

Measurements have been taken on May 7 and 8, 2001, all measurements were at nighttime to extend the intercomparison range to higher altitudes. Although the measured aerosol backscatter was quite

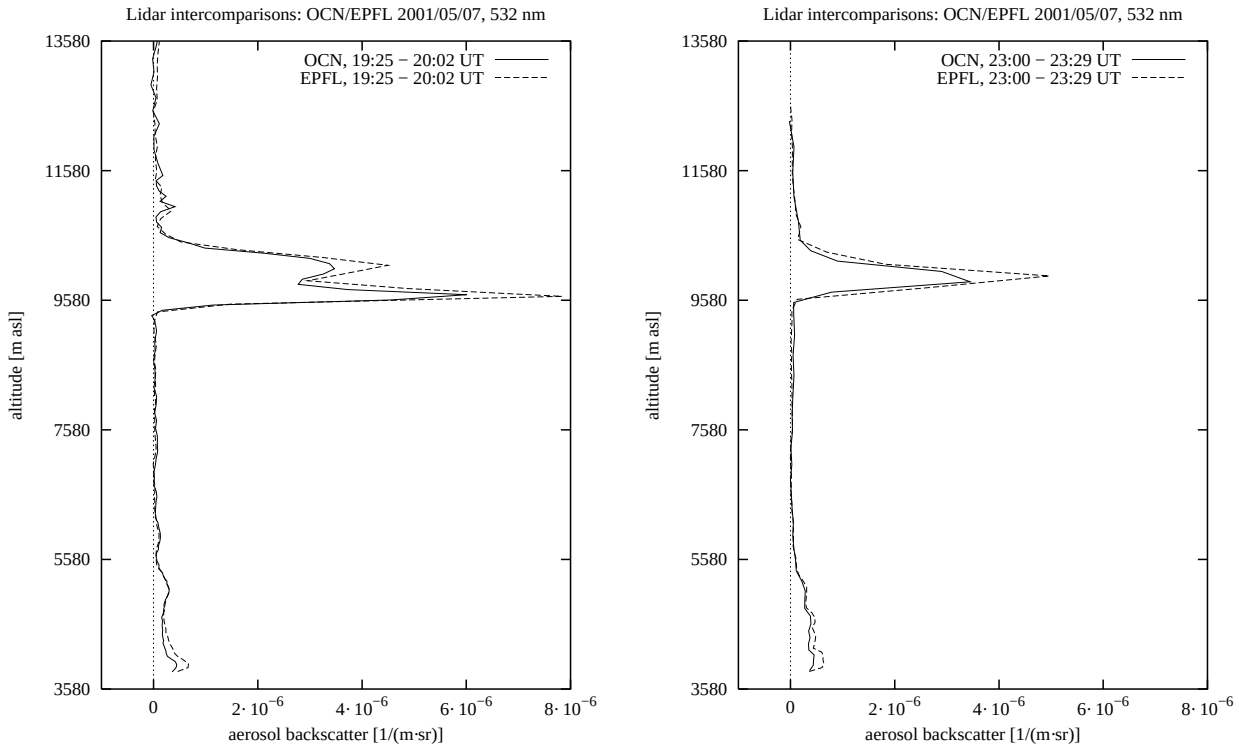

Figure 4.18: Intercomparison of aerosol backscatter profiles at 532 nm between OCN and EPFL in presence of aerosol and cirrus clouds. Measurements were taken on May 7, 2001.

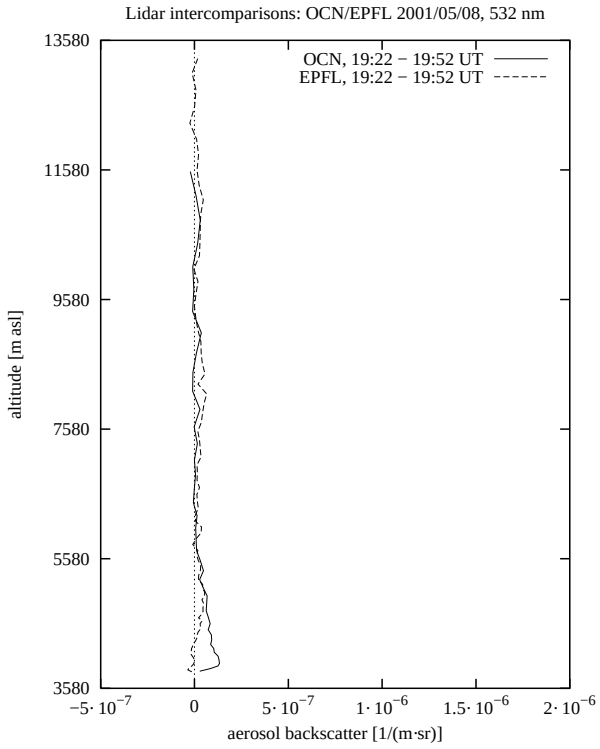

Figure 4.19: Intercomparison of aerosol backscatter profiles at 532 nm between OCN and EPFL under low aerosol conditions. Measurements were taken on May 8, 2001.

Lidar intercomparisons: OCN/EPFL				
Date [UT]	Quantity	height range [m asl]	mean dev. $[(\mathrm{m}\cdot\mathrm{sr})^{-1}]$	standard dev. $[(\mathrm{m}\cdot\mathrm{sr})^{-1}]$
2001/05/07 19:25 - 20:02 UT	532 nm bsc.	4000 - 5400	$-0.6\cdot10^{-7}$ / -20.9%	$0.9\cdot10^{-7}$ / 32.5 %
	532 nm bsc.	5600 - 9000	$0.1\cdot10^{-7}$	$0.3\cdot10^{-7}$ / 22.0%
	532 nm bsc.	9600 - 10600 (Ci)	$-5.7\cdot10^{-7}$ / -16.6%	$7.5\cdot10^{-7}$ / 22.0 %
2001/05/07 23:00 - 23:29 UT	532 nm bsc.	4000 - 5200	$-0.9\cdot10^{-7}$ / -21.1%	$1.1\cdot10^{-7}$ / 25.4%
	532 nm bsc.	5700 - 9100	$0.1\cdot10^{-7}$	$0.2\cdot10^{-7}$
	532 nm bsc.	9700 - 10400 (Ci)	$-5.9\cdot10^{-7}$ / -25.9 %	$7.2\cdot10^{-7}$ / 31.5 %
2001/05/08 19:22 - 19:52 UT	532 nm bsc.	4000 - 11600	$-0.15\cdot10^{-7}$	$0.5\cdot10^{-7}$

Table 4.18: Mean deviations and standard deviations for three intercomparisons between the OCN and the EPFL lidar at 532 nm.

small, as expected, on May 7 some aerosol has been detected up to altitudes of 5000 m above sea level. (Fig. 4.18) Additionally, cirrus clouds were present and they can be regarded as "aerosol" for the purpose of this study. But cirrus is usually much more inhomogeneous than other aerosol layers, so one has to be very careful when comparing cirrus backscatter from different lidar systems against each other. They have different field of views and point to different parts of the atmosphere, which can lead to higher deviations between the measured profiles than expected. On May 8 the atmosphere was very clean and the whole measurement range can be regarded as within the free troposphere (see also the changed scale for aerosol backscatter in Figure 4.19). For the calculation of the deviations, from the EPFL only the analog channel has been chosen. Photon counting and analog channel generally showed very good agreement, only in the near range the photon counting channel was saturated and could not be used for the calculation of aerosol backscatter profiles. Cases with moderate or high aerosol load have not been required at this site because of the high altitude of the station. All deviations between the profiles are much below the $5\cdot10^{-7}(\mathrm{m}\cdot\mathrm{sr})^{-1}$ margin, within the aerosol layer detected on May 7 they even are in the range of the allowed relative values (Table 4.18). In the cirrus clouds the deviations are little higher than they would be allowed for aerosol layers. Considering the difficulties that are connected with the inhomogeneity of cirrus clouds, this result can be regarded as sufficiently accurate to prove the quality of the systems also under conditions of high aerosol backscatter.

Lidar intercomparisons: OCN internal				
Date [UT]	Quantity	height range [m]	mean dev. $[(\mathrm{m}\cdot\mathrm{sr})^{-1}]$	standard dev. $[(\mathrm{m}\cdot\mathrm{sr})^{-1}]$
2001/04/30 19:00 - 19:30 UT	532 nm bsc.	500 - 1100	$0.3\cdot10^{-7}$ / 1.4%	$2.1\cdot10^{-7}$ / 10.9 %
	532 nm bsc.	1500 - 8000	$0.1\cdot10^{-7}$	$0.8\cdot10^{-7}$
2001/05/02 18:35 - 19:05 UT	532 nm bsc.	1000 - 4200	$0.4\cdot10^{-7}$ / 3.7%	$0.7\cdot10^{-7}$ / 6.9%
	532 nm bsc.	5000 - 8000	$0.6\cdot10^{-7}$	$1.5\cdot10^{-7}$
2001/05/02 20:10 - 20:40 UT	532 nm bsc.	700 - 1400	$1.4\cdot10^{-7}$ / 13.9%	$1.6\cdot10^{-7}$ / 16.8 %
	532 nm bsc.	1500 - 6000	$0.0\cdot10^{-7}$	$0.5\cdot10^{-7}$

Table 4.19: Mean deviations and standard deviations for three intercomparisons between the OCN transportable Micro lidar and the OCN stationary three wavelengths lidar at 532 nm.

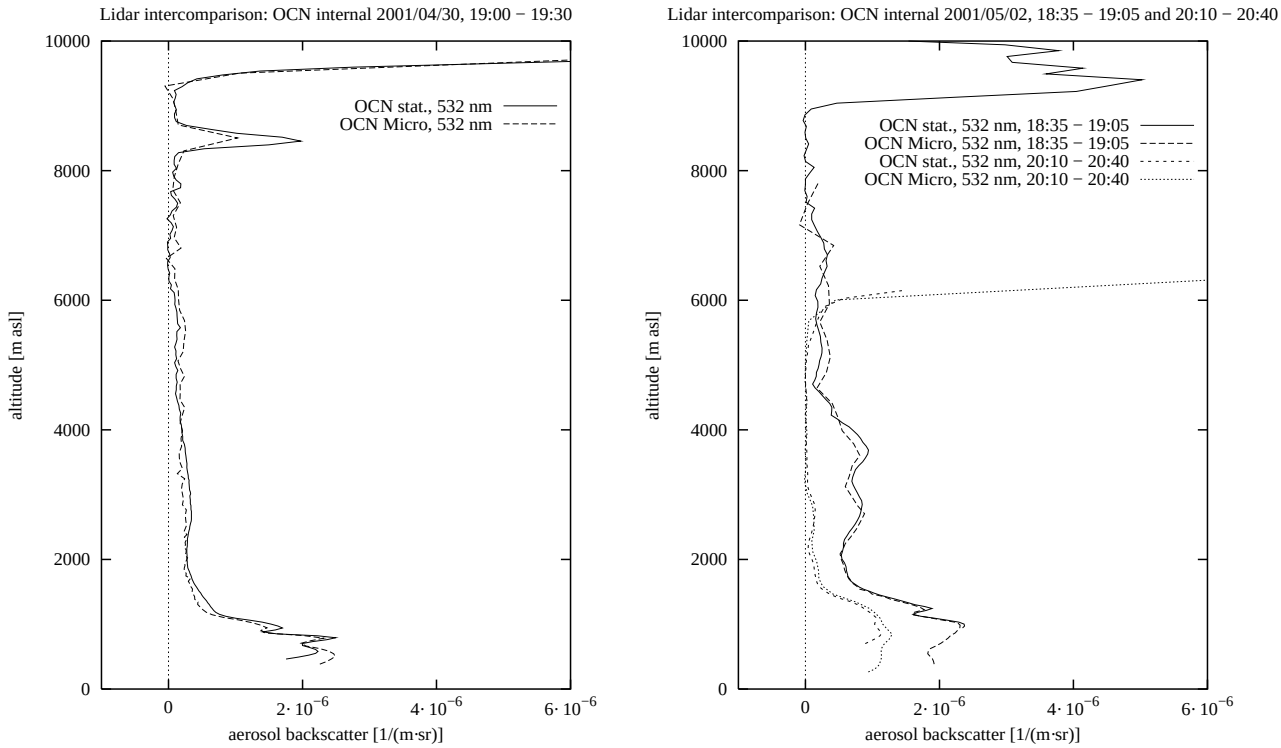

Figure 4.20: Intercomparison of aerosol backscatter profiles at 532 nm between the OCN transportable Micro lidar and the OCN stationary three wavelengths lidar.

OCN internal

For performing the routine measurements within the EARLINET, the OCN is operating a stationary three wavelengths lidar. For the intercomparisons to MPI and EPFL the easily transportable micro lidar was used and this system has therefore also been compared to the stationary one. The measurements shown here are from two different days in spring 2001 and have been performed at nighttime when the micro lidar can deliver much better results than at daytime (Fig. 4.20). The intercomparisons covered a height range from 500 m to 10000 m. The calculated deviations are small with mean deviations smaller than 15% and standard deviations not exceeding 17 % in the dust layer. In the free troposphere the deviations stay well below $2 \cdot 10^{-7}(\mathrm{m} \cdot \mathrm{sr})^{-1}$ (Table 4.19).

IPNANB internal

The Institute of Physics of the National Academy of Sciences of Belarus is the only non-EU-participant in the EARLINET project. Because it is still difficult to travel to countries of the former Soviet Union, especially with modern technical equipment, the quality control of the Minsk lidar systems has been made by internal intercomparisons of the stratospheric lidar and the boundary layer lidar, both emitting at 532 nm. However, there are main differences between the systems. The stratospheric lidar uses photon counting for signal detection while the boundary layer system is equipped with analog channels. Additionally, the lowest usable altitude for the stratosphere system is ca. 1800 m, so all intercomparisons are restricted to altitudes above that height.

Four days between April 5, 2000 and June 1, 2000 have been chosen for the intercomparisons. On those days, the aerosol layer reached altitudes well above 1800 m, so the system performance under high aerosol load could also be tested. The profiles agree quite well and all absolute deviations stay

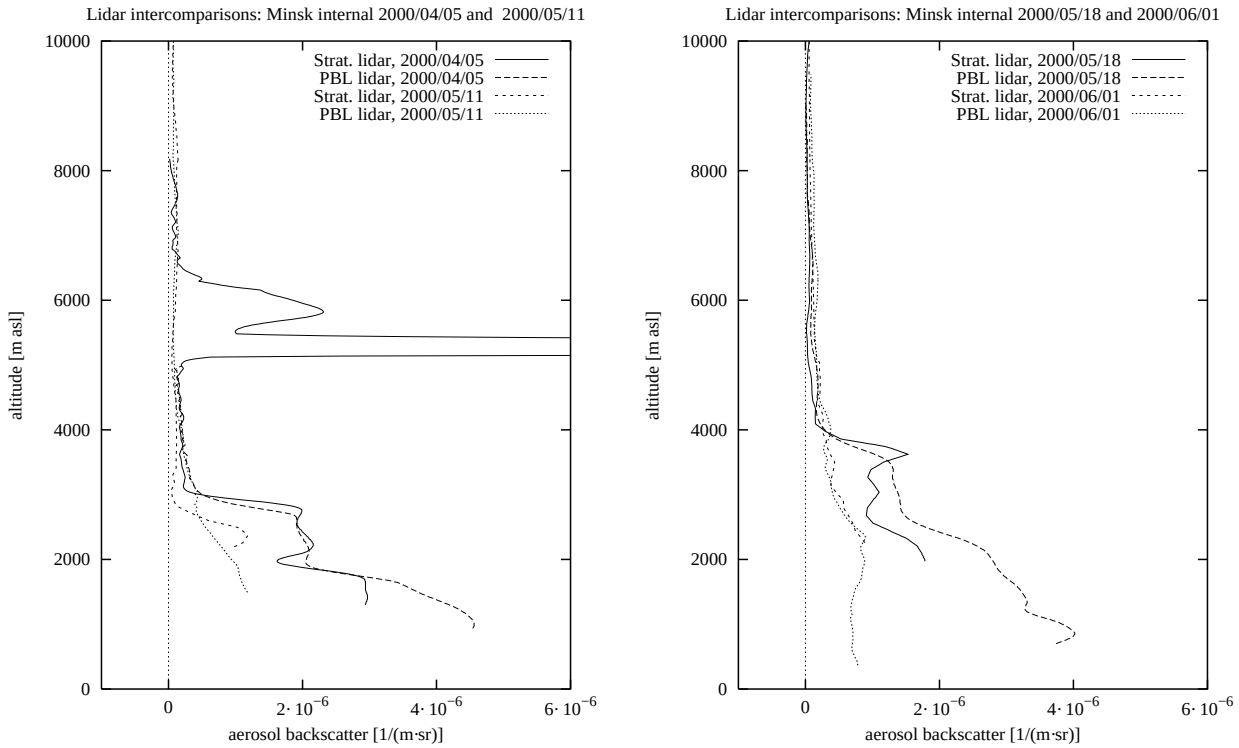

Figure 4.21: Intercomparison of aerosol backscatter profiles at 532 nm between the boundary layer lidar and the stratospheric lidar of IPNANB.

below the allowed limits (Fig. 4.21 and Table 4.20). Some of the deviations can be attributed to the changing atmosphere because not all measurements could be taken simultaneously and differences up to 70 minutes between the measurements are possible.

MPI/LMD

Simultaneous measurements with the French system from LMD have been performed during the experiment in Palaiseau/France in September 2000. These measurements showed that the LMD system is well suited for upper tropospheric measurements, but no results could be achieved below ca. 3000 m. The attempt to correct the measured profiles by determining an overlap function was

Lidar intercomparisons: IPNANB internal				
Date [UT]	Quantity	height range [m]	mean dev. $[(\mathrm{m}\cdot\mathrm{sr})^{-1}]$	standard dev. $[(\mathrm{m}\cdot\mathrm{sr})^{-1}]$
2000/04/05	532 nm bsc.	1800 - 2800	$0.04\cdot10^{-7}$ / -0.2%	$2.2\cdot10^{-7}$ / 11.2 %
18:03 - 18:19 UT	532 nm bsc.	3200 - 5000	$0.2\cdot10^{-7}$	$0.5\cdot10^{-7}$
2000/05/11	532 nm bsc.	2300 - 2700	$-3.3\cdot10^{-7}$ / -37.3%	$4.0\cdot10^{-7}$ / 44.5%
18:00 - 19:16 UT	532 nm bsc.	3500 - 14000	$0.0\cdot10^{-7}$	$0.3\cdot10^{-7}$
2000/05/18	532 nm bsc.	2700 - 3800	$1.6\cdot10^{-7}$ / 15.2%	$3.8\cdot10^{-7}$ / 34.7 %
19:17 - 19:43 UT	532 nm bsc.	4200 - 9000	$0.4\cdot10^{-7}$	$0.5\cdot10^{-7}$
2000/06/01	532 nm bsc.	2300 - 4500	$-0.1\cdot10^{-7}$ / -2.2%	$0.7\cdot10^{-7}$ / 16.9 %
19:15 - 20:31 UT	532 nm bsc.	5000 - 9500	$0.3\cdot10^{-7}$	$0.4\cdot10^{-7}$

Table 4.20: Mean deviations and standard deviations for four intercomparisons between the IPNANB boundary layer lidar and the IPNANB stratospheric lidar at 532 nm.

made, but the results showed still too high deviations from the measurements performed by the MPI system.
As a consequence, the LMD installed a new system for the PBL which performed measurements between December 2000 and April 2001. In the meantime, changes in the configuration of the large system have been made and measurements could be used beginning in ca. 800 m above ground afterwards.
It was decided to do intercomparison measurements with the micro lidar of the LMD which then can be compared to a quality assured system of the EARLINET later on. First measurements have been taken in winter 2001/2002 with good results comparing the Pr^2 of both systems. However, more measurements have to be made under conditions with sufficiently high aerosol which is scheduled for spring 2002.

MPI/IST

Intercomparison measurements have already been done in September 2000 in Palaiseau, however, they were not successful. In the beginning, hardware problems of the Portuguese system prevented intercomparisons. After they had been solved, only one day was left for simultaneous measurements during the experiment. It was obvious from these measurements that the field of view of the Lisbon system was much too narrow and that the whole system was fairly difficult to operate due to thermal instabilities. Therefore a complete new build-up including a second wavelength at 532 nm has been done between October 2000 and May 2001. New intercomparison measurements were scheduled for summer 2001 in Barcelona. Unfortunately, these measurements had to be further delayed and cannot be reported here. They are now scheduled for early summer 2002 when the UPC in Barcelona will have upgraded their system with a second wavelength at 532 nm and an additional Raman channel at 607 nm.

4.3.2 Intercomparison between lidar and sunphotometer

During nighttime Raman lidar can deliver aerosol extinction profiles with high accuracy. If the measurements cover a significant part of the planetary boundary layer, the aerosol optical depth (AOD) can be derived by integrating the extinction over the whole height range from ground to the top of the profile. Assuming that the planetary boundary layer is one or two hours after sunset still well mixed, the extinction profile can be extrapolated to ground without large errors using constant extinction values.
These measurements can best be compared to star photometer measurements which can be performed simultaneously, however, this instrument is not very frequently operated on a routine basis. In contrast to that, automatically operating sun photometers are in the meantime quite often available, and lidar systems can be compared to those instruments. The comparisons are not easy because a time delay of ca. 2 - 3 hours between the last measurement of the sunphotometer at daytime and the first Raman lidar measurement at nighttime cannot be avoided. Additionally, cirrus clouds can prevent accurate sun photometer measurements and therefore great care must be taken when comparing those instruments. However, from continuous lidar measurements, the development of the aerosol distribution and the presence of cirrus clouds can be observed which enables in some situations intercomparisons without large errors.

During the intercomparison experiment in Palaiseau, the MPI Raman lidar could be compared to the automatic sunphotometer from LMD on two different days. In Figure 4.22 the optical depth measurements from the sunphotometer are plotted at the four measured wavelengths between 440 nm and

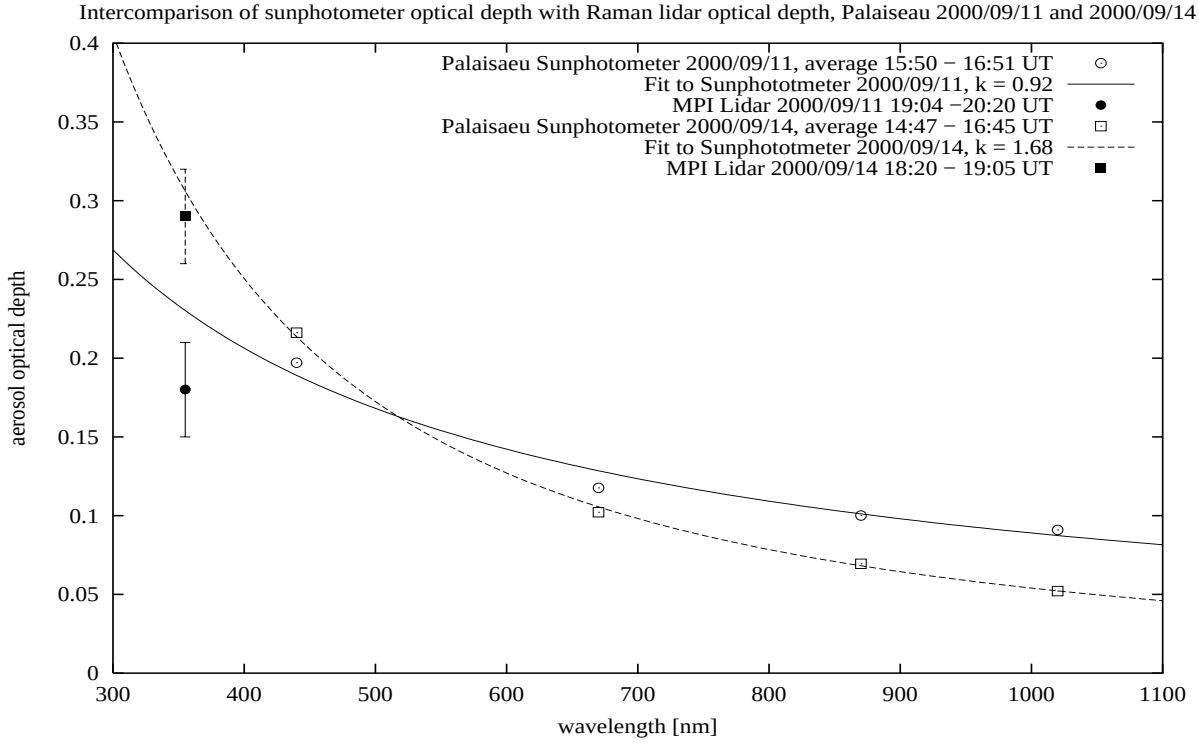

Figure 4.22: Intercomparison of aerosol optical depth measurements with the MPI Raman lidar and the sunphotometer from LMD Palaiseau.

1020 nm. Assuming that the optical depth follows an Ångstrøm law ($\mathrm{AOD} \propto \lambda^{-\mathrm{k}}$), the measurements have been extrapolated to lower wavelengths although this is connected with additional errors due to the insufficient knowledge about the wavelength dependence of the aerosol optical depth at wavelengths below 400 nm. The given error of the lidar data contains the statistical measurement error and the error in the optical depth of the lowest part of the atmosphere where the lidar can't deliver extinction values. This error has been estimated to 25 % of the assumed optical depth. The accuracy of the sunphotometer optical depth data is usually in the order of 0.02.
Having in mind the above mentioned potential error sources, the presented measurements of September 11 and 14, 2000, show good agreement. For the sunphotometer, late afternoon periods with fairly constant optical depth have been averaged. The lidar data have been taken after sunset and 45 to 70 minutes averages have been used to derive the aerosol extinction profile. This leads to small statistical errors of the extinction, the largest error comes from the unknown extinction values in the lowest part of the boundary layer.

4.3.3 Summary of measurements

The whole set of intercomparison experiments turned out to be a good and hard test for all systems. In several cases improvements of the systems could be done after the measurements. Many of the existing problems certainly would not have been detected without the intercomparison measurements. Besides that, in almost all cases a high quality of the measurements could be stated and the predefined goals could be reached. Figure 4.23 gives the deviations and standard deviations in the PBL for all aerosol backscatter intercomparisons reported here. Almost all values are well within the 20 % limits, most of them even within $\pm 10\%$. Only two cases have significantly higher deviations in the atmospheric dust layer. However, those cases are connected with low aerosol load and the absolute

deviations stay well below the allowed value of $5 \cdot 10^{-7}(\mathrm{m} \cdot \mathrm{sr})^{-1}$.
The standard deviations exceed in some cases the 25 % margin. Again these cases generally are connected with low aerosol load and the absolute deviations are still acceptable. Overestimation of the errors sometimes occurs if small differences in height have been detected. The used point to point calculation of the differences can lead to quite high differences if strong gradients occur in the aerosol profile.
The absolute deviations of all compared profiles in regions with low aerosol are displayed in Figure 4.24. Here mean deviations stay in almost all cases below $2 \cdot 10^{-7}(\mathrm{m} \cdot \mathrm{sr})^{-1}$ and this value holds for the standard deviation, too. In those cases where higher standard deviations have been detected, higher averaging, especially in height, would lead to smaller fluctuations. Since usually no aerosol structures have to be resolved in the free troposphere, this is an appropriate procedure to increase the data quality in higher altitudes.
Intercomparisons of aerosol extinction profiles could only be done in one case because only the MPI lidar is transportable *and* equipped with Raman channels. The second transportable Raman lidar, belonging to IFT Leipzig, was not available for intercomparison experiments within EARLINET. The effort to move the MPI system is much higher than for the one from Munich, therefore the MIM system, although not equipped with Raman channels, was chosen to travel to Italy and Greece. In Italy all systems have Raman channels but none of them is transportable. The extinction profiles measured by MPI and UABER in May 2001 showed good agreement although the calculated standard deviation is 35 % in one case. The allowed absolute limits nevertheless were not exceeded.
Additionally, the MPI system has been compared to sunphotometer measurements in Palaiseau. De-

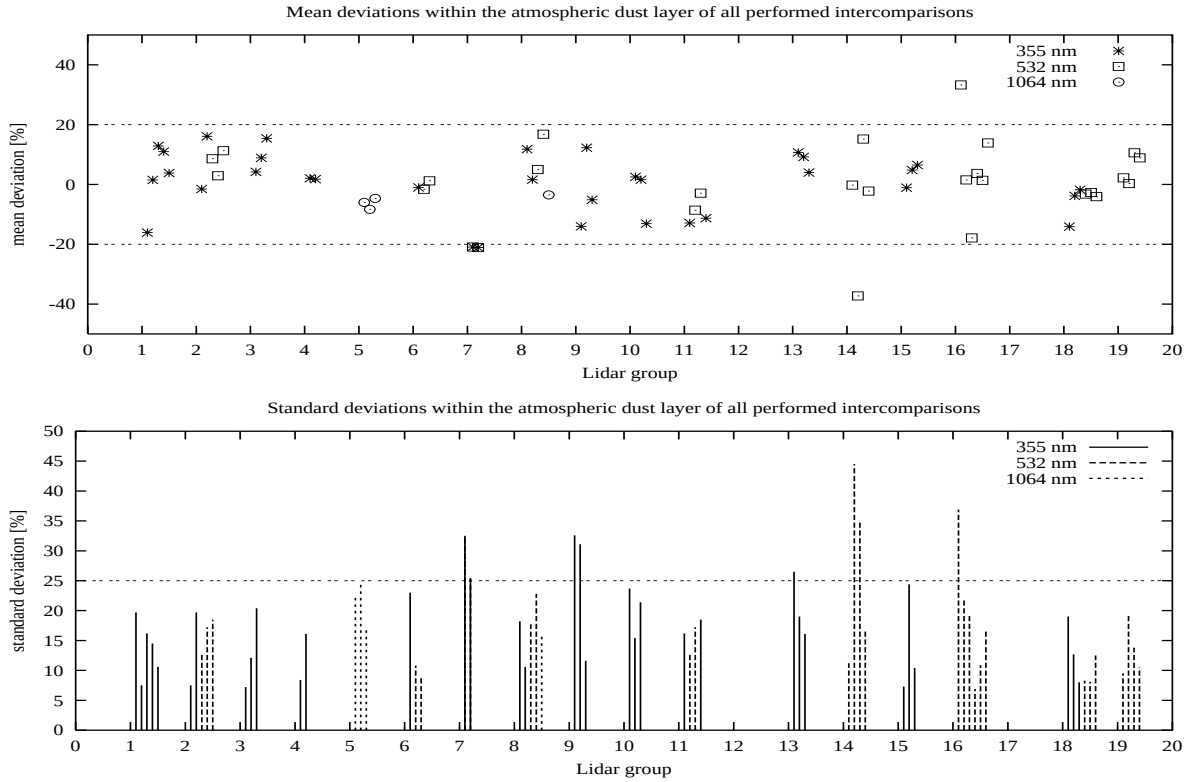

Figure 4.23: Mean deviations and standard deviations of all aerosol backscatter intercomparisons in the dust layer. 1: MPI, 2: MIM, 3: UABER, 4: NTUA, 5: UPC, 6: IFU, 7: EPFL, 8: IAP, 9: ULAQ, 10: INFM(L), 11: IFT, 12: IST, 13: FOA, 14: IPNANB, 15: INFM(N), 16: OCN, 17: LMD, 18: INFM(P), 19: AUTH.

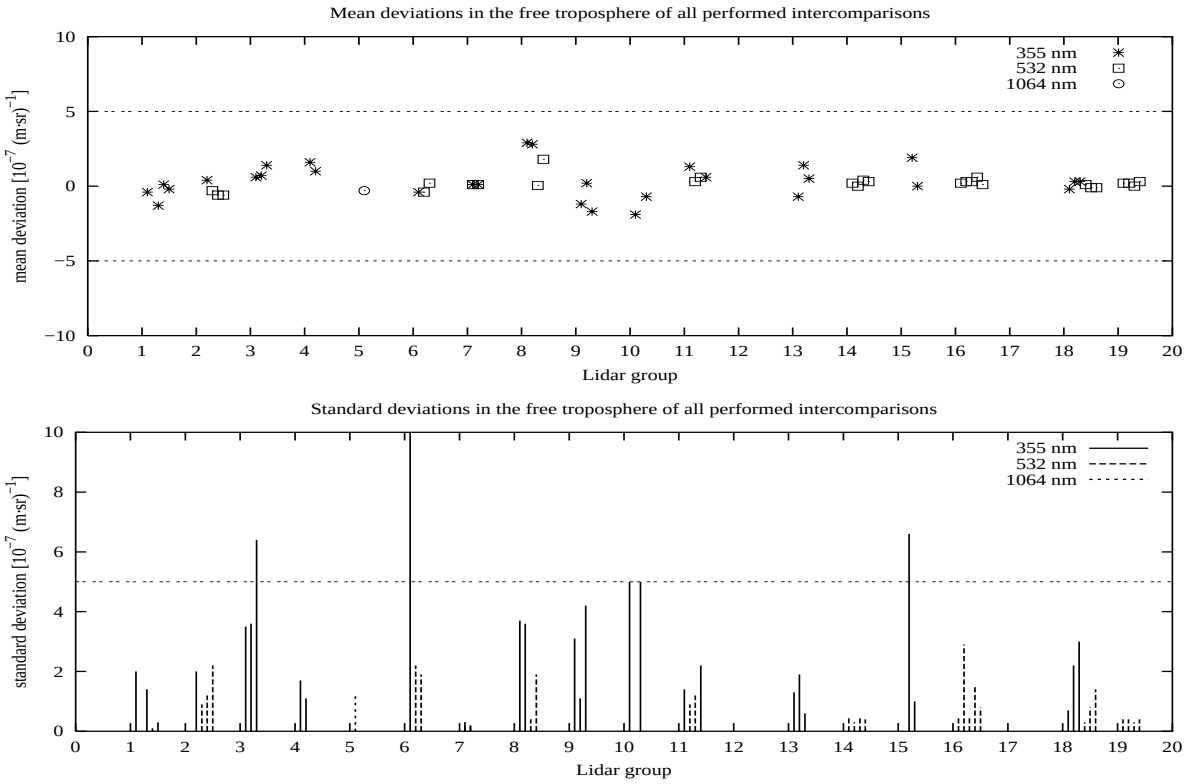

Figure 4.24: Mean deviations and standard deviations of all aerosol backscatter intercomparisons in the free troposphere. 1: MPI, 2: MIM, 3: UABER, 4: NTUA, 5: UPC, 6: IFU, 7: EPFL, 8: IAP, 9: ULAQ, 10: INFM(L), 11: IFT, 12: IST, 13: FOA, 14: IPNANB, 15: INFM(N), 16: OCN, 17: LMD, 18: INFM(P), 19: AUTH.

spite the difficulties connected with the comparison of these very different instruments, the agreement is good and demonstrates the high quality of the lidar data.
The maximum allowed deviation of 100 m in height determination has never been exceeded in these experiments. Sometimes deviations in the order of 10 - 50 m occured, which could not be explained immediately. However, the aerosol distribution in the boundary layer can be quite inhomogeneous and this also can lead to some differences in the measured profiles.

Chapter 5

Summary

To achieve the goals of EARLINET, it is essential to provide aerosol backscatter and extinction profiles on a quantitative basis. To derive those quantities, 19 European lidar groups operate aerosol lidar systems which are quite different in detail. To come to a homogeneous data set, and to make sure that all systems and the algorithms used for the evaluation work well, a large number of intercomparison experiments have been performed, testing at least two systems at a time at one place. Algorithms have been tested separately by using synthetic lidar data as input and recalculating the assumed aerosol distribution.
The backscatter algorithm intercomparison has been performed in three stages with increasing knowlegde on the necessary input parameters. In stage one neither the necessary reference value nor the height dependent lidar ratio was given. In stage two the prescribed lidar ratio was provided and in stage 3 also the reference value was given. It became again clear that the estimation of the lidar ratio which is required for real measurements has a large effect on the calculated aerosol backscatter profile. The calculated profiles can differ by more than 50 % if no information on the lidar ratio is available. This effect decreases with increasing wavelength. The effect of the reference value was rather small in the chosen examples, however, at 1064 nm the result can depend strongly on this value which also has to be estimated for real measurements. The errors of the algorithms themselves have been tested in stage 3 with knowledge of all input parameters. The remaining calculation errors stay in the order of 2-4 % and can be regarded as negligible when compared to the uncertainties caused by wrong estimation of the input parameters lidar ratio and reference value.
During the intercomparison, some groups detected errors in their algorithm. Those errors could be eliminated and in stage 3 only the algorithms of two groups showed errors larger than 10 %. At the end 17 different algorithms from 18 lidar groups have been tested successfully. One group is still working on its algorithms which will be tested with the same instruments after the implementation.
The Raman algorithm intercomparison has been done in a similar way, but with additional noise on the simulated profiles and the error estimation also has been tested. Three cases have been calculated. The first was a test case with known solution and two different noise levels. The second was also with known solution but divided into 15 time steps to test also the averaging methods. The third case had 20 time steps with changing aerosol properties after 10 time steps. Only information on the used atmospheric density and the wavelength dependence of the aerosol extinction was provided. All involved groups achieved good results for the extinction calculation from the simulated signals, also in case 3, the totally blind intercomparison. The deviations of the calculated profiles from the solution were in almost all cases within the given statistical errors of the signals. However, discrepancies have been found in the error calculation. Although all groups supplied similar statistical errors for their solution in case 2, the used vertical averaging lengths were very different. Therefore a test with fixed altitude resolution has been made, showing good results but different error estimations. Here further

work is necessary and will be done in the next future.
The instrument intercomparison included all lidar groups with 19 lidar systems. 18 groups have compared their systems to quality assured lidar systems, one (the Minsk system) did internal intercomparisons with two of their lidar systems operating at the same place and the same wavelength and one system (in Belsk/Poland, operated by the group from Minsk) had to remain untested. In 16 cases the measurements showed deviations less than 20 % in the aerosol backscatter profile, in most cases the mean errors in the atmospheric dust layer were even less than 10 %. The standard deviations were with a few exceptions below 25 %. Higher deviations were always connected with low aerosol load and had not been exceeded the maximum allowed absolute deviation in those cases. Therefore the system accuracy, including algorithms can be estimated to be better than 20 %, in many cases even better than 10 % in the atmospheric dust layer. Above that layer, absolute deviations are typically in the order of $10^{-7}(\mathrm{m} \cdot \mathrm{sr})^{-1}$or better which is less than 10 % of low aerosol values in the dust layer. Having in mind that errors in the aerosol backscatter profile determination using pure elastic backscatter at 355 nm can be as large as 50 % if no information about the lidar ratio can be provided from Raman measurements, these errors are quite small.
Intercomparison of Raman extinction measurements only could be done in one case. This is due to the fact that most systems which are equipped with Raman channels are rather large (container size) or not transportable. In fact at present only the MPI Hamburg and the IfT Leipzig operate transportable Raman lidar systems and the system from Leipzig was not available for intercomparisons in EARLINET.
The compared measurements by MPI and UABER, performed in May 2001, showed good agreement of the extinction profiles although the standard deviation of the measured extinction can be rather large for Raman measurements due to the weak backscattered signal. Mean deviations were well below 10 % in both analyzed cases, a result which permits an accurate determination of the optical depth, too.
This quantity has been compared in two cases to sunphotometer measurements during the intercomparison campaign in Palaiseau. The agreement was good (within 0.05 aerosol optical depth) if one considers the difficulties of such intercomparisons beginning with the time difference of 2-3 hours, the different optical path and the unknown wavelength dependence in the ultraviolet. This result shows that optical depth measurements can be done with lidar systems and vertically resolved profiles can be derived also in presence of high level clouds.
Although good intercomparison results could be achieved, some of the tested systems had to be improved before. The detected errors were mainly due to detector saturation, overlap problems or thermal instabilities. The problems have been solved in most cases, however, in some cases the lidar groups have to determine the validity range of their data very carefully and apply further improvements (e.g. to thermal stabilization) to their systems. In this sense the intercomparisons showed that good agreement can be achieved but great care also has to be taken to maintain this quality during the routine operation of the lidar systems.
In two cases the system intercomparisons failed in the first attempt. Major system reconstructions have been recommended in these cases and they have been completed in spring 2001. However, new intercomparison experiments could not be done up to now but are scheduled for 2002. They will complete the set of measurements that proves a high quality of the lidar systems participating in EARLINET.

Acknowledgement

The financial support of this work by the European Commission under grant EVR1-CT-1999-40003 is gratefully acknowledged. The Swiss Federal Office for Education and Sciences is acknowledged for the support of Observatoire Cantonal Neuchâtel (contract no. 99.0650-1) and of Ecole Polytechnique Fédérale de Lausanne (contract no. 582.607).
We thank the scientific and technical staff of the Meteorological Observatory Lindenberg for the very good support during the LACE 98 campaign when the intercomparisons of the German aerosol lidar systems have been made. That campaign has been funded by the German Federal Minister for Research and Education within the “Atmospheric Aerosol Research” program.
We are grateful to AERONET and Bernadette Chatenet for providing sunphotometer data from Palaiseau for the intercomparison of the optical depth.

Bibliography

Ansmann, A., Riebesell, M., and Weitkamp, C. (1990). Measurement of atmospheric aerosol extinction profiles with a Raman lidar. *Optics Letters*, 15.

Ansmann, A., Wandinger, U., Riebesell, M., Weitkamp, C., and Michaelis, W. (1992). Independent measurement of extinction and backscatter profiles in cirrus clouds by using a combined Raman elastic-backscatter lidar. *Applied Optics*, 31:7113–7131.

Bodhaine, B., Wood, N., Dutton, E., and Slusser, J. (1999). On Rayleigh Optical Depth Calculations. *J. Atmospheric and Oceanic Technol.*, 16:1854–1861.

Bösenberg, J. (1998). Ground-based differential absorption lidar for water vapor and temperature profiling: methodology. *Applied Optics*, 37:3845 – 3860.

Bösenberg, J., Alpers, M., Althausen, D., Ansmann, A., Böckmann, C., Eixmann, R., Franke, A., Freudenthaler, V., Giehl, H., Jäger, H., Kreipl, S., Linné, H., Matthias, V., Mattis, I., Müller, D., Sarközi, J., Schneidenbach, L., Schneider, J., Trickl, T., Vorobieva, E., Wandinger, U., and Wiegner, M. (2001). The German Aerosol Lidar Network: Methodology, Data, Analysis. MPI-Report 317, Max-Planck-Institut für Meteorologie, Hamburg.

Bösenberg, J. and Theopold, F. (1988). Evaluation of DIAL measurements in presence of signal noise. In *Proceedings of the 14^{th} International Laser Radar Conference, San Condilo, Italy*, pages 209–211.

Bösenberg, J., Timm, R., and Wulfmeyer, V. (1997). Study on retrieval algorithms for a backscatter lidar. Final report. MPI-Report 226, Max-Planck-Institut für Meteorologie, Hamburg.

Edlen, B. (1953). The dispersion of standard air. *Journal of the Optical Society of America*, 43:339.

Elterman, L. (1968). UV, visible, and IR attenuation for altitudes to 50 km, 1968. Environmental Research Papers 285, AFCRL-68-0153, Air Force Cambridge.

Fernald, F. G. (1984). Analysis of atmospheric lidar observations: Some comments. *Applied Optics*, 23:652–653.

Fernald, F. G., Herman, B. M., and Reagan, J. A. (1972). Determination of aerosol height distributions by lidar . *Journal of Applied Meteorology*, 11:482–489.

Godin, S., Carswell, A., Donovan, D., Claude, H., Steinbrecht, W., Mcdermid, I., McGee, T., Gross, M., Nakane, H., Swart, D., Bergwerff, H., Uchino, O., von der Gathen, P., and Neuber, R. (1999). Ozone differential absorption lidar algorithm intercomparison. *Applied Optics*, 38:6225–6236.

Gutkowicz-Krusin, D. (1993). Multiangle lidar performance in the presence of horizontal inhomogeneities in atmospheric extinction and scattering. *Applied Optics*, 32:3266–3272.

Klett, J. D. (1981). Stable analytical inversion solution for processing lidar returns. *Applied Optics*, 20:211–220.

Klett, J. D. (1985). Lidar inversion with variable backscatter/extinction ratios. *Applied Optics*, 24:1638–1643.

Kovalev, V. A. and Moosmüller, H. (1994). Distortion of particulate extinction profiles measured with lidar in a two-component atmosphere. *Applied Optics*, 33:6499–6507.

Matsumoto, M. and Takeuchi, N. (1994). Effects of misestimated far-end boundary values on two common lidar inversion solutions. *Applied Optics*, 33:6451–6456.

Sasano, Y., Browell, E. V., and Ismail, S. (1985). Error caused by using a constant extinction/backscattering ratio in the lidar solution. *Applied Optics*, 24:3929–3932.

Shipley, S. T., Tracy, D. H., Eloranta, E. W., Trauger, J. T., Sroga, J. T., Roesler, F. L., and Weinman, J. A. (1983). High spectral resolution lidar to measure optical scattering properties of atmospheric aerosols. 1: Theory and instrumentation. *Applied Optics*, 22:3716–3732.

Steinbrecht, W., Jäger, H., Adriani, A., di Donfrancesco, G., Barnes, J., Beyerle, G., Neuber, R., David, C., Godin, S., Donovan, D., Carswell, A., Gross, M., McGee, T., Masci, F., D'Altorio, A., Rizi, V., Visconti, G., McDermid, I., Megie, G., Mielke, A., Stein, B., Wedekind, C., Nagai, T., Uchino, O., Nakane, H., Osborn, M., and Winkler, D. (1996). NDSC Intercomparison of Stratospheric Aerosol Processing Algorithms. In Ansmann, A., Neuber, R., Rairoux, P., and Wandinger, U., editors, *Advances in Atmospheric Remote Sensing with Lidar*, pages 501–504.

United States Committee on Extension to the Standard Atmosphere (1976). *U. S. Standard Atmosphere, 1976*. Washington: National Oceanic and Amospheric Administration.

Wandinger, U. (1998). Multiple-scattering influence on extinction-and backscatter-coefficient measurements with Raman and high-spectral-resolution lidars. *Applied Optics*, 37:417–427.

Whiteman, D. (1999). Application of statistical methods to the determination of slope in lidar data. *Applied Optics*, 38, 15:3360 – 3369.

Wiegner, M. and Freudenthaler, V. (1998). Two approaches to derive aerosol extinction coefficient profiles from backscatter lidar measurements. In *19th International Laser Radar Conference, Annapolis, USA*, pages 127 – 129.

MPI-Report-Reference: *Reprinted in

Report 1 - 289 Please order the reference list from MPI for Meteorology, Hamburg

Report No. 290
June 1999
A nonlinear impulse response model of the coupled carbon cycle-ocean-atmosphere climate system
Georg Hooss, Reinhard Voss, Klaus Hasselmann, Ernst Maier-Reimer, Fortunat Joos

Report No. 291
June 1999
Rapid algorithms for plane-parallel radiative transfer calculations
Vassili Prigarin

Report No. 292
June 1999
Oceanic Control of Decadal North Atlantic Sea Level Pressure Variability in Winter
Mojib Latif, Klaus Arpe, Erich Roeckner
* Geophysical Research Letters, 1999 (submitted)

Report No. 293
July 1999
A process-based, climate-sensitive model to derive methane emissions from natural wetlands:
Application to 5 wetland sites, sensitivity to model parameters and climate
Bernadette P. Walter, Martin Heimann
* Global Biogeochemical Cycles, 1999 (submitted)

Report No. 294
August 1999
Possible Changes of $\delta^{18}O$ in Precipitation Caused by a Meltwater Event in the North Atlantic
Martin Werner, Uwe Mikolajewicz, Georg Hoffmann, Martin Heimann
* Journal of Geophysical Research - Atmospheres, 105, D8, 10161-10167, 2000

Report No. 295
August 1999
Borehole versus Isotope Temperatures on Greenland:
Seasonality Does Matter
Martin Werner, Uwe Mikolajewicz, Martin Heimann, Georg Hoffmann
* Geophysical Research Letters, 27, 5, 723-726, 2000

Report No. 296
August 1999
Numerical Modelling of Regional Scale Transport and Photochemistry directly together with Meteorological Processes
Bärbel Langmann
* Atmospheric Environment, 34, 3585-3598, 2000

Report No. 297
August 1999
The impact of two different land-surface coupling techniques in a single column version of the ECHAM4 atmospheric model
Jan-Peter Schulz, Lydia Dümenil, Jan Polcher
* Journal of Applied Meteorology, 40, 642-663, 2001

Report No. 298
September 1999
Long-term climate changes due to increased CO_2 concentration in the coupled atmosphere-ocean general circulation model ECHAM3/LSG
Reinhard Voss, Uwe Mikolajewicz
* Climate Dynamics, 17, 45-60, 2001

Report No. 299
October 1999
Tropical Stabilisation of the Thermohaline Circulation in a Greenhouse Warming Simulation
Mojib Latif, Erich Roeckner
* Journal of Climate, 1999 (submitted)

Report No. 300
October 1999
Impact of Global Warming on the Asian Winter Monsoon in a Coupled GCM
Zeng-Zhen Hu, Lennart Bengtsson, Klaus Arpe
* Journal of Geophysical Research-Atmosphere, 105, D4, 4607-4624, 2000

Report No. 301
December 1999
Impacts of Deforestation and Afforestation in the Mediterranean Region as Simulated by the MPI Atmospheric GCM
Lydia Dümenil Gates, Stefan Ließ

Report No. 302
December 1999
Dynamical and Cloud-Radiation Feedbacks in El Niño and Greenhouse Warming
Fei-Fei Jin, Zeng-Zhen Hu, Mojib Latif, Lennart Bengtsson, Erich Roeckner
* Geophysical Research Letter, 28, 8, 1539-1542, 2001

MPI-Report-Reference: *Reprinted in

Report 1 - 289 Please order the reference list from MPI for Meteorology, Hamburg

Report No. 303
December 1999
The leading variability mode of the coupled troposphere-stratosphere winter circulation in different climate regimes
Judith Perlwitz, Hans-F. Graf, Reinhard Voss
* Journal of Geophysical Research, 105, 6915-6926, 2000

Report No. 304
January 2000
Generation of SST anomalies in the midlatitudes
Dietmar Dommenget, Mojib Latif
* Journal of Climate, 1999 (submitted)

Report No. 305
June 2000
Tropical Pacific/Atlantic Ocean Interactions at Multi-Decadal Time Scales
Mojib Latif
* Geophysical Research Letters, 28,3,539-542,2001

Report No. 306
June 2000
On the Interpretation of Climate Change in the Tropical Pacific
Mojib Latif
* Journal of Climate, 2000 (submitted)

Report No. 307
June 2000
Observed historical discharge data from major rivers for climate model validation
Lydia Dümenil Gates, Stefan Hagemann, Claudia Golz

Report No. 308
July 2000
Atmospheric Correction of Colour Images of Case I Waters - a Review of Case II Waters - a Review
D. Pozdnyakov, S. Bakan, H. Grassl
* Remote Sensing of Environment, 2000 (submitted)

Report No. 309
August 2000
A Cautionary Note on the Interpretation of EOFs
Dietmar Dommenget, Mojib Latif
* Journal of Climate, 2000 (submitted)

Report No. 310
September 2000
Midlatitude Forcing Mechanisms for Glacier Mass Balance Investigated Using General Circulation Models
Bernhard K. Reichert, Lennart Bengtsson, Johannes Oerlemans
* Journal of Climate, 2000 (accepted)

Report No. 311
October 2000
The impact of a downslope water-transport parameterization in a global ocean general circulation model
Stephanie Legutke, Ernst Maier-Reimer

Report No. 312
November 2000
The Hamburg Ocean-Atmosphere Parameters and Fluxes from Satellite Data (HOAPS): A Climatological Atlas of Satellite-Derived Air-Sea-Interaction Parameters over the Oceans
Hartmut Graßl, Volker Jost, Ramesh Kumar, Jörg Schulz, Peter Bauer, Peter Schlüssel

Report No. 313
December 2000
Secular trends in daily precipitation characteristics: greenhouse gas simulation with a coupled AOGCM
Vladimir Semenov, Lennart Bengtsson

Report No. 314
December 2000
Estimation of the error due to operator splitting for micro-physical-multiphase chemical systems in meso-scale air quality models
Frank Müller
* Atmospheric Environment, 2000 (submitted)

Report No. 315
January 2001
Sensitivity of global climate to the detrimental impact of smoke on rain clouds (only available as pdf-file on the web)
Hans-F. Graf, Daniel Rosenfeld, Frank J. Nober

Report No. 316
March 2001
Lake Parameterization for Climate Models
Ben-Jei Tsuang, Chia-Ying Tu, Klaus Arpe

MPI-Report-Reference: *Reprinted in

Report 1 - 289 Please order the reference list from MPI for Meteorology, Hamburg

Report No 317
March 2001
The German Aerosol Lidar Network: Methodology, Data, Analysis
J. Bösenberg, M. Alpers, D. Althausen, A. Ansmann, C. Böckmann, R. Eixmann, A. Franke, V. Freudenthaler, H. Giehl, H. Jäger, S. Kreipl, H. Linné, V. Matthias, I. Mattis, D. Müller, J. Sarközi, L. Schneidenbach, J. Schneider, T. Trickl, E. Vorobieva, U. Wandinger, M. Wiegner

Report No. 318
March 2001
On North Pacific Climate Variability
Mojib Latif
* Journal of Climate, 2001 (submitted)

Report No. 319
March 2001
The Madden-Julian Oscillation in the ECHAM4 / OPYC3 CGCM
Stefan Liess, Lennart Bengtsson, Klaus Arpe
* Climate Dynamics, 2001 (submitted)

Report No. 320
May 2001
Simulated Warm Polar Currents during the Middle Permian
A. M. E. Winguth, C. Heinze, J. E. Kutzbach, E. Maier-Reimer, U. Mikolajewicz, D. Rowley, A. Rees, A. M. Ziegler
* Paleoceanography, 2001 (submitted)

Report No. 321
June 2001
Impact of the Vertical Resolution on the Transport of Passive Tracers in the ECHAM4 Model
Christine Land, Johann Feichter, Robert Sausen
* Tellus, 2001 (submitted)

Report No. 322
August 2001
Summer Session 2000
Beyond Kyoto: Achieving Sustainable Development
Edited by Hartmut Graßl and Jacques Léonardi

Report No. 323
July 2001
An atlas of surface fluxes based on the ECMWF Re-Analysis- a climatological dataset to force global ocean general circulation models
Frank Röske

Report No. 324
August 2001
Long-range transport and multimedia partitioning of semivolatile organic compounds:
A case study on two modern agrochemicals
Gerhard Lammel, Johann Feichter, Adrian Leip
* Journal of Geophysical Research-Atmospheres, 2001 (submitted)

Report No. 325
August 2001
A High Resolution AGCM Study of the El Niño Impact on the North Atlantic / European Sector
Ute Merkel, Mojib Latif
* Geophysical Research Letters, 2001 (submitted)

Report No. 326
August 2001
On dipole-like varibility in the tropical Indian Ocean
Astrid Baquero-Bernal, Mojib Latif
* Journal of Climate, 2001 (submitted)

Report No. 327
August 2001
Global ocean warming tied to anthropogenic forcing
Berhard K. Reichert, Reiner Schnur, Lennart Bengtsson
* Geophysical Research Letters, 2001 (submitted)

Report No. 328
August 2001
Natural Climate Variability as Indicated by Glaciers and Implications for Climate Change: A Modeling Study
Bernhard K. Reichert, Lennart Bengtsson, Johannes Oerlemans
* Journal of Climate, 2001 (submitted)

Report No. 329
August 2001
Vegetation Feedback on Sahelian Rainfall Variability in a Coupled Climate Land-Vegetation Model
K.-G. Schnitzler, W. Knorr, M. Latif, J.Bader, N.Zeng
Geophysical Research Letters, 2001 (submitted)

MPI-Report-Reference: *Reprinted in

Report 1 - 289 Please order the reference list from MPI for Meteorology, Hamburg

Report No. 330
August 2001
Structural Changes of Climate Variability **(only available as pdf-file on the web)**
H.-F.Graf, J. M. Castanheira
Journal of Geophysical Research -Atmospheres, 2001 (submitted)

Report No. 331
August 2001
North Pacific - North Atlantic relationships under stratospheric control? (only available as pdf-file on the web)
H.-F.Graf, J. M. Castanheira
Journal of Geophysical Research -Atmospheres, 2001 (submitted)

Report No. 332
September 2001
Using a Physical Reference Frame to study Global Circulation Variability (only available as pdf-file on the web)
H.-F.Graf, J. M. Castanheira, C.C. DaCamara, A.Rocha
Journal of Atmospheric Sciences, 2001 (in press)

Report No. 333
November 2001
Stratospheric Response to Global Warming in the Northern Hemisphere Winter
Zeng-Zhen Hu

Report No. 334
October 2001
On the Role of European and Non-European Emission Sources for the Budgets of Trace Compounds over Europe
Martin G. Schultz, Johann Feichter, Stefan Bauer, Andreas Volz-Thomas

Report No. 335
November 2001
Slowly Degradable Organics in the Atmospheric Environment and Air-Sea Exchange
Gerhard Lammel

Report No. 336
January 2002
An Improved Land Surface Parameter Dataset for Global and Regional Climate Models
Stefan Hagemann

ISSN 0937 - 1060